ACQUISITION OF ANOIKIS RESISTANCE BY ATTENUATION OF MITOCHONDRIAL RESPIRATION AND REACTIVE OXYGEN SPECIES

By

SUSHAMA KAMARAJUGADDA

A DISSERTATION PRESENTED TO THE GRADUATE SCHOOL
OF THE UNIVERSITY OF FLORIDA IN PARTIAL FULFILLMENT
OF THE REQUIREMENTS FOR THE DEGREE OF
DOCTOR OF PHILOSOPHY

UNIVERSITY OF FLORIDA

2011

To my parents and my husband for their unconditional love and support

ACKNOWLEDGMENTS

Firstly, I would like to thank my advisor Dr. Jianrong Lu for giving me an opportunity to work in his lab. He is a great scientist and has exceptional intellectual ability. His guidance and technical expertise have helped me achieve my research goals. His enthusiasm and ardent zeal for science keeps all of our lab members motivated. I sincerely thank him for his support and encouragement during my Ph.D. program.

Next, I would like to thank my committee members; Dr. Kevin Brown, Dr. Jorg Bungert, Dr. Susan Frost, and Dr. Lizi Wu. They have been very supportive of my research project. Their insight has always helped my project go in the right direction. I thank them for their valuable comments, guidance and critical evaluation of my work.

I would like to Dr. Brown for his advice and guidance all through my Ph.D. He has always been my second mentor in giving both personal and professional advices. I am very thankful to him for all his help at every step of my Ph.D. program. I would like to thank Dr. Susan Frost for her valuable advice during my Medical guild research competition. She is an amazing teacher and has always made sure to correct my mistakes. I thank Dr. Frost for all her guidance. I would like to thank Dr. Jorg Bungert for providing me with his input for my qualifying proposal. I thank him for all his help and support.

Next, I would like to thank Dr. Nicholas Simpson for teaching me NMR technique. He is a great teacher. I admire his enthusiasm, patience and perseverance. I had a great time working with him and thank him very much for all his help. I would like to thank Dr. Anna Maria from Christiaan Leeuwenburgh's lab for her advice and technical assistance.

Next, I would like to thank all current and past lab members for all their help and advice. I would like to thank my undergraduate Ms. Lauren Stemboroski for helping me with my experiments. She is very diligent and hard working undergraduate.

I thank my friends: Dr. Vasumathi Kode, Dr. Mansi Parekh, Dr. Su Nayak, Dr. Lisa Dyer and Dr. Carolina Pardo for their help, advice and support. They are all wonderful people.

This entire journey would not have been complete without my family's support and encouragement. I thank my parents, older brother and my loving husband for their unconditional love and support. I specially thank my husband for putting up with me all through my Ph.D. program. He has always been my confidence booster and a great critic of my work.

TABLE OF CONTENTS

page

LIST OF TABLES

LIST OF FIGURES

LIST OF ABBREVIATIONS

Anoikis	Detachment-induced cell death
7-AAD	7-aminoactinomycin D
APAF-1	Apoptotic protease activating factor 1
ASK1	Apoptosis signal-regulating kinase
ATP	Adenosine trinucleotide phosphate
BCL2	B-cell lymphoma 2
BAD	Bcl2-associated death promoter protein
BAX	Bcl2-associated X protein
BID	BH3 interacting-domain death agonist
BMF	Bcl2-modifying factor
CA	Carbonic anhydrase
C/EBPβ	CCAAT/enhancer-binding protein β
DCA	Dichloroacetate
DCIS	Ductal carsinoma in situ
ECM	Extracellular matrix
EGFR	Epithelial growth factor receptor
EMT	Epithelial to mesenchymal transition
ER	Estrogen receptor
ERR	Estrogen-related receptors
ErbB2	Erythroblastosis oncogene B
ERK	Extracellular signal-regulated Kinase
ETC	Electron transport chain
EV	Empty vector
FADD	Fas-associated via death domain

$FADH_2$	Flavin adenosine dinucleotide
FAK	Focal adhesion kinase
FH	Fumarate hydratase
FLIP	FLICE (FADD-like IL-1β-converting enzyme)-inhibitory protein
FOXO3A	Forkhead family of transcription factor 3a
G6P	Glucose-6-phosphate
GPx	Glutathione peroxidase
GSH	L-Glutathione (reduced form)
HER2	Human epidermal growth factor receptor 2
H&E	Hematoxylin and Eosin
HK	Hexokinase
IDC	Invasive ductal carcinoma
IDH2	Isocitrate dehydrogenase 2
ILC	Invasive lobular carcinoma
ILK	Integrin-linked kinase
LA	Lipoic acid
LCIS	Lobular carcinoma in situ
LDH	Lactate dehydrogenase
MCL1	Myeloid cell leukemia 1 protein
MEK	Mitogen-activated protein kinase kinase
MnSOD	Manganese superoxide dismutase
NADH	Nicotinamide adenine dinucleotide
NADPH	Nicotinamide adenine dinucleotide phosphate
NFκB	Nuclear factor kappa-light-chain-enhancer of activated B cells
OCR	Oxygen consumption rate

PE	Phycoerythrin
Poly-Hema	Poly(2-hydroxyethyl methacrylate)
PPP	Pentose phosphate pathway
PTEN	Phosphatase and tensin homolog
PI3K	Phosphoinositide 3-Kinase
PDH/C	Pyruvate dehydrogenase complex
PDK	Pyruvate dehydrogenase kinase
PFK 1	Phosphofructokinase 1
PGC 1α	Peroxisome proliferator-activated receptor γ coactivator-1 alpha
PKM2	Phospho fructokinase isoform M2
PPARα	Peroxisome proliferator-activated receptor-α
PR	Progesterone receptor
p53	Tumor protein 53
ROS	Reactive oxygen species
SDH	Succinate dehydrogenase (SDH)
shRNA	short-hairpin RNA
SOD	Superoxide dismutase
TCA	Tricarboxylic acid cycle
TNFα	Tumor necrosis factor α
VEGF	Vascular endothelial growth factor
VHL	von-Hippel Lindau
v-Src	Viral sarcoma
XIAP	X-linked inhibitor of apoptosis protein

Abstract of Dissertation Presented to the Graduate School
of the University of Florida in Partial Fulfillment of the
Requirements for the Degree of Doctor of Philosophy

ACQUISITION OF ANOIKIS RESISTANCE BY ATTENUATION OF MITOCHONDRIAL RESPIRATION AND REACTIVE OXYGEN SPECIES

By

Sushama Kamarajugadda

December 2011

Chair: Jianrong Lu
Major: Medical Sciences - Biochemistry and Molecular Biology

Cancer cells commonly exhibit aberrant glucose metabolism characterized by a preference for aerobic glycolysis rather than mitochondrial oxidation. However, the significance of this phenomenon, known as the Warburg effect, remains incompletely understood. To metastasize, cancer cells must overcome matrix detachment-induced apoptosis, or anoikis. It is unclear whether tumor metabolism contributes to anoikis resistance and metastasis. Here we show when detached from matrix, untransformed mammary epithelial cells (MCF10A) undergo metabolic reprogramming by markedly upregulating pyruvate dehydrogenase (PDH) kinase 4 (PDK4) through estrogen-related receptor gamma (ERRγ), thereby attenuating the flux of pyruvate into mitochondrial oxidation. Depletion of PDK4 or activation of PDH enhances mitochondrial respiration and oxidative stress in suspended MCF10A cells and sensitizes them to anoikis. Therefore, decreased glucose oxidation confers resistance to anoikis in untransformed mammary epithelial cells. Consistent with this finding, matrix-detached MCF10A cells also elevate the antioxidant manganese superoxide dismutase (MnSOD) to alleviate oxidative stress and prolong survival in suspension.

Cancer cells, due to reduced glucose oxidation, inherently possess survival advantage in suspension. Normalization of glucose metabolism by activating PDH restores anoikis in metastatic breast cancer cells MDA-MB-231. Depletion of PDK1 curtails MDA-MB-231 cells metastatic potential by reducing the lung tumor incidence *in vivo*. Taken together, our study suggests that intervention of tumor metabolism by developing therapy against PDK may open new avenues for anti-metastasis treatment.

CHAPTER 1
INTRODUCTION

Overview

Anoikis in Normal Cells

Definition and significance

Anoikis is a Greek term meaning “homelessness”. It is a kind of cell death triggered by loss of cell adhesion or inappropriate cell anchorage[1]. It prevents a detached cell from reattaching to an inadequate or inappropriate matrix[2]. The physiological relevance of anoikis is to maintain tissue homeostasis, and proper development[3]. Binding of integrin proteins to the extracellular matrix (ECM) provides survival signals, which helps in establishing appropriate cell-matrix interactions. Any association of detached cells with inappropriate matrix would lead to incorrect integrin engagement followed by activation of proapoptotic genes, and consequently anoikis[4].

Mechanisms underlying anoikis

Under normal physiological conditions, cells are protected from anoikis in three different scenarios: (i) During reattachment of the cell to an appropriate matrix, (ii) detachment of a cell to move towards a chemo attractant, and (iii) through cell-cell contacts[2]. It is well established that the integrins associated with the ECM are critical for cell survival[4]. They are activated by various signaling molecules such as focal adhesion kinase (FAK), integrin linked kinase (ILK), phosphoinositide 3 kinase (PI3K)/Akt or protein kinase B (PKB), and extracellular signal-related kinase (ERK)[5,6].

Upon detachment of cells from ECM, anoikis is activated either by an extrinsic /death receptor pathway[7,8] or an intrinsic/mitochondrial pathway[9] (Figure 1-1). In the intrinsic pathway, cells undergo apoptosis due to activation of pro-apoptotic B-cell

lymphoma 2 (BCL2) family proteins. This is followed by release of cytochrome C from mitochondria and activation of downstream caspase events. Several reports have shown that pro-apoptotic BH3 only proteins of BCL2 family like Bim[5], Bcl2-modifying factor (BMF)[9-11], and Bcl2-associated death promoter protein (BAD)[12] are activated during cell detachment and trigger anoikis. These pro-apoptotic genes are activated by different signaling pathways such as fork head family of transcription factor 3a (FOXO3a) signaling[13]. Matrix detachment inactivates survival signaling pathways such as epidermal growth factor receptor-mitogen-activated protein kinase kinase-extracellular signal-regulated kinase (ERK1/2) [14] and epithelial growth factor receptor (EGFR) involving PI3K pathways[5], which may result in activation of certain pro-apoptotic genes. Therefore, oncogenes such as erythroblastosis oncogene B2 (ErbB2) and viral sarcoma (v-Src) suppress anoikis through ERK-mitogen-protein kinase pathway in cultured mammary epithelial acini[15]. It has been shown that hypoxia suppresses Bim and BMF expression via ERK signaling and inhibits luminal clearing during morphogenesis in an *in vitro* three-dimensional mammary epithelial culture[16]. On the other hand, the extrinsic pathway involving death receptors like Fas and tumor necrosis factor α (TNFα) may trigger apoptosis in certain cells upon detachment[17]. This pathway activates caspase 8, which may trigger apoptosis with or without the involvement of intrinsic pathway. The pro-apoptotic BH3 interacting-domain death agonist (BID) protein is cleaved by caspase 8 and the truncated BID activates the intrinsic pathway during anoikis[18]. To date, the involvement of the death receptor pathway in anoikis is ambiguous. However, the involvement of intrinsic pathway is well established.

Another mechanism driving anoikis during detachment is protein 53 (p53). p53 is a crucial molecule that regulates cell cycle, maintains genomic stability, inhibits angiogenesis and is hence known as a tumor suppressor protein. It has been shown that inhibition of p53 increases anoikis resistance in fibroblasts[19] and thyroid epithelial cells[20]. Furthermore, inhibition of $\alpha_v\beta_3$ integrin activates p53 leading to anoikis in endothelial cells[21]. The tumor suppressor gene phosphatase and tensin homolog (PTEN), which is transactivated by p53, restores anoikis in breast cancer cells[22]. These studies confirm the role of p53 in inducing anoikis upon detachment from ECM in different cell lines.

Anoikis Resistance in Tumor Cells

Signficance of anoikis resistance

Unlike normal cells, tumor cells are resistant to anoikis. Anoikis resistance is a hallmark of malignant tumors for an anchorage independent growth and survival[23]. The underlying purpose of evading anoikis by a tumor cell is to survive in an environment outside its own niche. Anoikis resistance has been implicated in tumor invasion and metastasis.

Mechanisms underlying anoikis resistance

Tumor cells adopt different mechanisms to evade anoikis. One of them is the constitutive activation of survival signals like PI3K, mitogen-activated protein kinase kinase (MEK)/ERK etc, for proliferation, survival, and migration[24]. Another common strategy is the activation of epithelial to mesenchymal transition (EMT) by activating transcription factors such as snail, twist, slug, etc., EMT changes the tumor cell morphology by suppressing epithelial markers like E-Cadherin and up regulating mesenchymal markers like vimentin and fibronectin[25], allowing the tumor cells to

migrate and invade the distant organs even in the absence of matrix. In addition, a change in the expression pattern of integrin proteins plays a critical role in anoikis resistance. It has been shown that MCF10A cells overexpressing ErbB2 upregulate integrin α5 protein, which in turn enhances anoikis resistance by activating ErbB2 tyrosine phosphorylation[26]. Another plausible protection from anoikis implicates reactive oxygen species (ROS) in tumor cells. A recent report suggested that detachment from extracellular matrix leads to accumulation of ROS in prostrate cancer cells, which results in the activation of survival signals such as EGFR via src kinase[27]. However, the implication of ROS in anoikis is still controversial. Tumor cells upregulate apoptosis inhibiting proteins such as FLICE (FADD-like IL-1β-converting enzyme)-inhibitory protein (FLIP), an inhibitor of caspase 8, and X-linked inhibitor of apoptosis protein (XIAP), an inhibitor of caspase 3/7, upon loss of anchorage to evade apoptosis[23] (Figure 1-1). Over-expression of oncogenes such as ras has been reported in some tumor cells, which would activate survival-signaling pathways[28]. The hypoxic environment prevailing within a tumor also helps in promoting anoikis resistance by upregulating different survival and proliferation genes[29]. Hypoxia-regulated genes will be discussed in detail in tumor metabolism section.

Apart from the signaling pathways and the inhibitors of pro apoptotic genes, the role of metabolism in regulating anoikis resistance is quite intriguing. A genome wide micro-array study performed by Schmelzle T *et al.,* showed an upregulation of pyruvate dehydrogenase kinase isozyme 4 (PDK4), an important enzyme that regulates glucose metabolism, in MCF10A suspension culture[10]. The microarray data indicate a plausible

involvement of glucose metabolism in regulating anoikis. A detailed description of glucose metabolism is in the following section.

Glucose Metabolism

Importance and significance

Glucose metabolism is one of the major fuels for energy production. Glucose is transported across the plasma membrane via glucose receptors (Glut). The first rate-determing step in glucose metabolism is conversion of glucose to glucose-6-phosphate (G6P), which is carried out by Hexokinase (HK) enzyme. G6P enters the glycolytic pathway to generate Nicotinamide adenine dinucleotide (NADH), Adenosine triphosphate (ATP), and pyruvate and/or the pentose phosphate pathway (PPP) to generate Nicotinamide adenine dinucleotide phosphate (NADPH) and pentose sugars for nucleotide biosynthesis. In the presence of oxygen, pyruvate will enter mitochondria and be processed in the Krebs cycle or tricarboxylic acid (TCA) cycle to produce energy in the form of ATP required to drive various cellular processes. However, in the absence of oxygen (anaerobic condition), pyruvate is converted into lactate.

Lactate dehydrogenase (LDH)

LDH is an enzyme that catalyzes the interconversion of pyruvate to lactate under low oxygen conditions. LDH has five isoenzymes produced from two polypeptide chains M and H in different combinations[30]. The two genes LDHA and LDHB encode the polypeptide chains M and H respectively. The five isoenzymes are; LDH1-B4, LDH2-B3A1, LDH3-B2A2, LDH4-BA3, LDH5-A4[31]. Of all the isoforms, LDH5 is considered to be efficient in catalyzing pyruvate to lactate conversion. LDH1 is efficient in pyruvate formation, which is fed into the Krebs cycle[32].

Pyruvate dehydrogenase complex (PDC)

Function and Importance: PDC is a multienzyme complex present in mitochondria. PDC carries out the irreversible conversion of pyruvate to acetyl CoA and releases CO_2 and NADH. Thus, PDC activates the Krebs cycle and produces adenosine trinucleotide phosphate (ATP) *via* electron transport chain (ETC). When carbohydrate content is high in the body, PDC exists in an active dephosphorylated form to oxidize glucose and produce energy[33]. Under low carbohydrate content, PDC exists in an inactive phosphorylated form to limit the glucose consumption by non-neuronal tissue[33]. The key players to regulate phosphorylated and dephosporylated PDC forms in a tissues-specific manner are pyruvate dehyrogenase kinase (PDK)[34] and pyruvate dehydrogenase phosphatase (PDP)[35], respectively.

Structure and mechanism of PDC: The enzymatic reactions of PDC are catalyzed by E1-pyruvate dehydrogenase, E2-dihydrolipoyl transacetylase, and E3-dihydrolipoamide dehydrogenase (E3) components in a sequential manner (Figure 1-2)[36]. The core structure of PDC consists of a multidomain E2 and E3-binding protein (E3BP). The two N terminal lipoyl domains of E2 and one lipoyl domain of E3BP are designated as L1, L2, and L3, respectively[37]. The complex consists of 60 subunits of E2, which carries out the transacetylation reaction. E2 and E3BP provide E1-binding and E3-binding domain via a 20-30 amino acid linker region[38]. There are five sequential steps involved in the conversion of pyruvate to acetyl CoA by the PDC enzyme complex[37];

E1 catalyzes decarboxylation of pyruvate in the presence of the cofactor thiamine diphosphate.

E1 catalyzes reductive acetylation of lipoyl-lysine prosthetic groups present on the lipoyl domains of E2 and E3BP. It is considered to be the rate-limiting step.

E2 catalyzes the transfer of the acetyl group from dihydrolipoyl prosthetic groups to CoA (Cofactor).

E3 accepts the reducing equivalents and regenerates lipoyl prosthetic groups and meanwhile, reduces the thiol-FAD system.

E3 further transfers the reducing equivalents from FAD to NAD^+, thus producing $NADH+H^+$.

Regulation of PDC enzyme complex

As mentioned above, the PDC complex is highly regulated by PDK and PDP enzymes to maintain the glucose metabolic homeostasis within the tissues depending on carbohydrate availability (Figure 1-3)[34]. Below they are discussed in detail;

(i) Pyruvate dehydrogenase kinase (PDK): PDK is a serine kinase family enzyme, which regulates glucose metabolism by its inhibitory effects on PDC enzyme. PDK inactivates PDC enzyme by phosphorylating the E1α subunit. It exists as four different isoenzymes designated as PDK1, PDK2, PDK3, and PDK4[35]. The expression pattern for four isoenzymes is tissue-specific, which helps in regulating PDC activity depending on their metabolic requirements[39]. Of all, PDK2 is widely distributed with high expression in liver, heart and kidney. PDK4 is expressed in liver, heart, kidney, and oxidative skeletal muscle whereas expression of PDK1 is limited to heart, and PDK3 is abundantly expressed in testis[39].

PDK is a dimer consisting of a C-terminal catalytic domain (cat) and a regulatory N terminal (R domain)[38]. The ATP/ADP binding site is located on the cat domain and binding of regulatory ligands occurs at the R domain. PDK binds to the PDC complex

via the lipoyl domain of E2 and thus obtains access to the E1 substrate[38]. The binding affinity of the four isoforms for the lipoyl domain of E2 subunit is different, which in turn regulates their enzymatic activity. Greatest binding affinity is observed for PDK3 followed by PDK1=PDK2 and PDK4, respectively[36]. PDC complex is phosphorylated at E1α subunit by PDK enzyme. PDK enzyme phosphorylates E1α subunit at three different serine residues; ser-293 (phosphorylation site 1), ser-300 (phosphorylation site 2) and, ser-232 (phosphorylaiton site 3)[40]. The activity of PDK is enhanced by PDH products i.e., acetyl CoA and $NADH+H^+$. On the other hand, ADP and increased pyruvate levels inhibit PDK activity to reactivate PDC[39]. Of all four isoenzymes, PDK2 is very sensitive to its regulatory effectors like NADH and acetyl CoA (positive regulators) and, ADP and pyruvate (negative regulators). On the other hand, PDK3 is insensitive to the inhibitory effects of pyruvate and ADP when compared with PDK1, 2, and 4[36,39].

PDK1[41,42] and PDK3[43,44] genes are activated by hypoxia inducible transcription factor (HIF1α) under hypoxic condition to reduce mitochondrial respiration and promote tumor growth. PDK2 and PDK4 genes are elevated during starvation[45] and diabetes[46] in various tissues to reduce the oxidation of pyruvate to acetyl CoA . The different activators of PDK2 and PDK4 are: peroxisome proliferator-activated receptor γ coactivator-1 alpha (PGC-1α)[47], estrogen-related receptors (ERRalpha and ERRgamma)[48], peroxisome proliferator-activated receptor-α (PPARα)[42,49] , thyroid hormone (T(3))[50], and CCAAT/enhancer-binding protein β (C/EBPβ)[51].

Inhibition of PDK to activate PDC is an important therapeutic strategy in the treatment of diabetes[52], heart ischemia, and in cancer[53]. PDK4 activity is inhibited in diabetic obese zuker mice by AZ7545 inhibitor[52]. AZ7545 binds to lipoyl domain of E2

component and prevents binding of PDK. Dichloroacetate (DCA) is another inhibitor of PDK, which is widely used to treat lactic acidosis in children deficient of PDC[54], and in cancer cells where activation of PDC leads to tumor regression[53]. DCA prevents PDK activity by binding to L2 binding pocket at N-terminal region of PDK[55].

(ii) Pyruvate dehyrogenase phosphatase (PDP): PDP belongs to 2c class of protein phosphatases. It activates PDH enzyme by dephosphorylating the E1α subunit. PDP has two isoforms, PDP1 and PDP2 consisting of ~56kda catalytic subunit (PDPc) and a large ~95.6kDa regulatory subunit (PDPr)[35]. Both isoforms require Mg^{+2} for their activation and their activity is highly regulated by this metal. Insulin upregulates PDP activity and activates the PDC complex to metabolize the high glucose content present within the tissue[37].

Reactive oxygen species (ROS)

Reactive oxygen species (ROS) are the free radicals derived from the molecular oxygen. They are highly unstable, reactive and cause damage to the DNA, protein, and lipids. The major source of ROS production is the mitochondrial electron transport chain (ETC)[56]. The TCA cycle not only oxidizes acetyl CoA to CO_2 but also produces reducing equivalents such as $NADH^+$ and flavin adenine dinucleotide ($FADH_2$). These reducing equivalents' are the source for electrons, which reduce the oxygen molecule to generate water molecule via ETC. During this process, some electrons are leaked out of the respiratory complexes and react with oxygen molecule to form reactive oxygen species[57]. The first ROS species produced is the highly unstable superoxide anion ($O_2^{\bullet -}$), which is readily dismutated by superoxide dismutases to generate hydroperoxyl ($HO_2^{\bullet}$). The two molecules of $HO_2^{\bullet}$ with each other react to form hydrogen peroxide (H_2O_2) and water (H_2O). Unlike superoxide anion, H_2O_2 is not a strong oxidant. In the

presence of transition metal ions such as Fe^{2+}, H_2O_2 is converted into a powerful oxidizing agent that damages the DNA and leads to lipid oxidation[58]. Another initial ROS species generated is nitric oxide ($NO^{\bullet}$). The sources of $NO^{\bullet}$ are vascular endothelium, nerve terminals and mitochondrial NO synthase (NOS)[59]. The interaction between $NO^{\bullet}$ and $O_2^{\bullet -}$ produces $ONOO^-$, which is quickly converted into a very cytotoxic peroxynitrous acid (ONOOH) radical.

Lower levels of ROS helps in cellular proliferation and gene transcription by activating signaling pathways[60]. Higher levels of ROS damage the cellular DNA, lipid or proteins. Therefore, maintaining redox balance within the cell is crucial for cell survival and maintenance. Increased ROS levels are eliminated by upregulation of ROS scavengers such as superoxide dismutase (SOD1, 2, and 3), glutathione peroxidase, peroxiredoxins, glutaredoxin, thioredoxin and catalase. A more detailed description about endogenous antioxidants is provided in Chapter five.

Apart from mitochondria, ROS are generated during detoxification of cytochrome P450[61] and b_5 families of enxymes[62], peroxisomes[63], and plasma membrane bound oxidases such as phagocytic NADPH oxidase[64] etc.

The role of reactive oxygen species in regulating anoikis is controversial. Several reports suggest that the impact of ROS on anoikis is both positive[65] and negative[66]. Although, the growing body of evidence indicates accumulation of ROS upon detachment from ECM leads to cell death in endothelial cells[67], mammary epithelial cells[68], keratinocytes[69] etc.

Glucose metabolism is one of the major fuels to produce ATP and in the process generates ROS in normal cells. However, cancer cells have altered glucose

metabolism, which helps them survive and proliferate in varying microenvironments. A detailed description is in the following section.

Tumor Metabolism

Warburg effect and its significance

Aberrant energy metabolism is one of the hallmarks of cancer cells[70]. Tumor cells have an altered glucose metabolism when compared with normal cells. Unlike normal cells, tumor cells utilize glycolysis (conversion of pyruvate to lactate) for their energy production even in the presence of oxygen termed as “aerobic glycolysis”[71.] Otto Warburg first observed this phenomenon in 1920 and it is therefore known as the “Warburg effect”. It is now well accepted that enhanced glycolysis facilitates cell proliferation[72], which requires not only ATP but also synthesis of nucleotides, lipids, and proteins.

Advantages of Warburg effect

Mitochondrial respiration yields higher energy (38 ATP) when compared with glycolysis (2ATP). Despite this advantage, most tumor cells favor glycolysis over mitochondrial respiration. Initially, Otto Warburg assumed that cancer cells favor aerobic glycolysis due to damaged mitochondria[71]. However, subsequent reports disproved this assumption by showing functional and intact mitochondria in different tumor cells[72-74], making it difficult to understand the significance of less energy efficient aerobic glycolysis over mitochondrial respiration in cancer cells.

In general, cancer cells consume much more glucose through increased glucose uptake and glycolysis. There are several theories to explain the advantages of the Warburg effect or the altered glucose metabolism in cancer cells. The first and the most popular theory attributed to hypoxic environment in tumors. Hypoxia stabilizes and

induces the hypoxia inducible transcription factor 1 alpha (HIF1α), which upregulates several glycolytic genes such as Glut1 receptors, Hexokinase II, LDHA[75], PDK1[41,42], and PDK3[43] etc., So, mitochondrial respiration may be very efficient in producing 18 times the ATP per mole of glucose but the rate of anaerobic glycolysis is 100 times higher in tumor cells[76]. In addition, increased glycolysis within the tumor cells result in increased release of H^+ ions into the surrounding environment leading to acidosis[75]. The acidified environment of tumor cells increases the expression of H^+ transporters and Na^{+2}-H^+ exchangers to attenuate the surrounding cellular toxicity.

The second theory to explain the selective advantage of Warburg effect in tumor cells is due to the stimulation of pentose phosphate pathway (PPP). The PPP pathway has both oxidative and non-oxidative branches. The oxidative branch utilizes glucose to yield ribose, which is used for the production of building blocks such as RNA and DNA. It has been shown that tumor cells upregulate transketolase, an important enzyme of PPP pathway, for their proliferation[77]. The oxidative branch also generates NADPH. NADPH is an important cofactor of glutathione reductase, which is an endogenous antioxidant. Thus, the production of NADPH induces antioxidant defense mechanism within the cells to prevent oxidative damage[78]. Moreover, the highly proliferating cancer cells require increasing amounts of biomass (amino acids, lipids and DNA) for their growth and survival. To meet these demands, the intermediate metabolites produced during glycolysis may be shunted as anabolic precursors for the synthesis of amino acids and nucleosides[72].

The third theory to explain the preferential use of aerobic glycolysis in tumor cells is to escape ROS from mitochondria. Since mitochondria are the major source of ROS

production, the actively dividing tumor cells may evade mitochondrial respiration to prevent excessive release of ROS. There have been some reports that support this theory: (1) forced expression of PDK1 in HIF1α mutant cells increased ATP levels, reduced ROS production, rescued the cells from apoptotic induction[42], and reduced the tumor size in mice xenograft models[79], (2) pharmacological inhibition of PDK2 with DCA induced apoptosis in Hela cells by decreasing mitochondrial membrane potential, and increasing H_2O_2 production and Kv channels[53], and (3) Depletion of LDHA has reduced tumor growth and maintenance due to increased ROS levels[73].

Therefore, the Warburg effect in cancer cells not only provides macromolecular biosynthetic elements required for its growth and survival, but also maintains cellular redox homeostasis. However, it is unclear how glucose metabolism regulates tumor cells during metastasis.

Oncogenes inducing the Warburg effect

While the Warburg effect is favored by most of the cancer cells, it is still unclear whether it is the cause or the effect of malignant phenotype. Cancer is a genetic disease resulting from mutations in cellular pathways that trigger abnormal cell growth and proliferation. Several oncogenes and tumor suppressors are closely connected to metabolic pathways and any alteration in their activity can promote aerobic glycolysis[80].

The activated Ras or Src oncogenes have been shown to increase glucose uptake and activate a number of glycolytic enzymes[81]. Another oncogenic transcription factor Myc has been shown to directly upregulate LDHA at RNA level[82] and several other glycolytic genes as well[83]. Further, Myc induces phosphofructose kinase isoform M2 (PKM2), which converts phosphoenolpyruvate to pyruvate[84]. Thus, establishing the critical role of Myc in inducing aerobic glycolysis similar to HIF 1. The oncogene AKT,

which is activated by PI3K signaling, enhances aerobic glycolysis by activating hexokinase 2, phosphofructokinase 1 (PFK 1), and several other glycolytic genes[85].

Apart from oncogenes, the loss of tumor suppressor gene functions such as PTEN[86], and p53[87] favor aerobic glycolysis in some tumor cells.

Mutations in mitochondrial enzymes that favor the Warburg effect

The mutations in mitochondrial metabolic enzymes have reinforced the role of metabolism in tumorigenesis. The three key enzymes of TCA cycle with mutations are: Fumarate hydratase (FH), succinate dehydrogenase (SDH), and isocitrate dehydrogenase 2 (IDH2). The mutations in FH and SDH lead to accumulation of fumarate and succinate intermediates, which inhibits prolyl hydroxylases that are responsible for the degradation of HIF 1α [88]. As a result, even in the presence of normal oxygen levels, these mutations stabilize HIF 1α transcription factor and enhances aerobic glycolysis to trigger tumorigenesis in some tumors[89]. IDH2 mutations have been found in low-grade gliomas[90,91]. Similar to FH and SDH mutations, IDH2 mutation stabilizes HIF 1α gene.

The altered glucose metabolism and its role in tumor growth and survival have been well studied. Another important feature of cancer cells is to metastasize and invade distant organs. Resistance to anoikis is a critical step for the tumor cells to undergo metastasis. Therefore, it is very important to explore the key regulators that promote anoikis resistance. Since the Warburg effect has been implicated in solid tumor growth, it is quite intriguing to understand its role in anoikis resistance and tumor metastasis *in vivo*. To elucidate the functional role of glucose metabolism in anoikis resistance and tumor metastasis, we have chosen human breast cancer as our model system.

Human Breast Cancer

Breast cancer is the cancer that begins in different areas of breast; the ducts, and the lobules. It is the second-most common cancer in the United States for women and its incidence rate is 122.8 per 100,000 women each year[92]. Recent advances of early detection and diagnosis of breast cancer has reduced the risk of death. But, if tumor metastasizes to distant organs, the mortality rate is still high. Breast cancer can invade different organs such as lung, liver, brain and bones via the lymphatic system. Breast cancer is highly heterogeneous in nature.

Types of Breast cancer

The different types of breast cancers include non-invasive, invasive, recurrent and metastatic types. These classifications are based on their invasiveness, point of origin, and hormone receptor status.

Ductal Carcinoma in situ (DCIS) - It is non-invasive type of breast cancer occurring inside the milk ducts and has not spread beyond its point of origin. This cancer has the best prognosis because they express hormone-receptor positive cells (ACS). It is not life threatening but the recurrence rate is under 30%

Invasive Ductal Carcinoma (IDC) - It is sometimes referred to as infiltrating ductal carcinoma and is the most common type of breast cancer. It is invasive type of ductal carcinoma, which invades the fatty tissues of breast and the lymph nodes (ACS). It can affect women of any age but most common in older women (ACS). About 80% of all invasive breast cancers are IDS.

Lobular Carcinoma In Situ (LCIS) - It is the non-invasive type of breast cancer occurring in the milk-producing lobules. Like DCIS, they are responsive to hormone therapy as they contain hormone receptor cells.

Invasive Lobular Carcinoma (ILC) - it is the second most common type of breast cancer after IDS. About 10% of all invasive breast cancers are ILC. The cancer begins in the milk-producing lobules of the breast. Over the time, ILC can spread to lymph nodes and the other areas of the body.

In our entire study, we use untransformed immortalized mammary epithelial cell lines MCF10A, primary immortalized human mammary epithelial cell lines (HMEC), Ras-transformed mammary epithelial cell line (10ACA1.1), and triple negative (Estrogen receptor-negative (ER^-), progesterone receptor-negative (PR^-), and human epidermal growth factor receptor 2 ($HER2^-$) negative), breast cancer cell line (MBDA-MB-231) to study the role of glucose metabolism in promoting anoikis resistance and tumor metastasis. MCF10A cells are derived from fibrotic tissue and they are ER negative, EGF receptor-negative, HER2 negative but E-Cadherin positive. They are immortalized but do not form tumors *in vivo*. HMEC cells are derived from normal human reduction mammoplasty tissue, immortalized and ER positive cells. They do not form tumors *in vivo*. Therefore, these two cell lines are used as control or normal cells. MDA-MB-231 is a triple negative and derived from an adenocarcinoma tissue. It is a highly aggressive and metastatic tumor cell line.

The goal of our study is to elucidate the role of glucose metabolism in regulating anoikis in both normal and metastatic breast cell lines. We discovered that upon detachment from matrix, the normal mammary epithelial cells and metastatic breast cancer cells upregulate PDK to reduce mitochondrial oxidation to evade ROS and resist anoikis. Further, we demonstrated that either forced activation of PDH or depletion of PDK4 sensitized these cells to anoikis in suspension culture condition. We further

demonstrated that metastatic breast tumor cells take advantage of the Warburg effect upon detachment from matrix to resist anoikis and metastasize to distant organs. Our study implicates PDKs as potential therapeutic targets for the breast tumor metastasis.

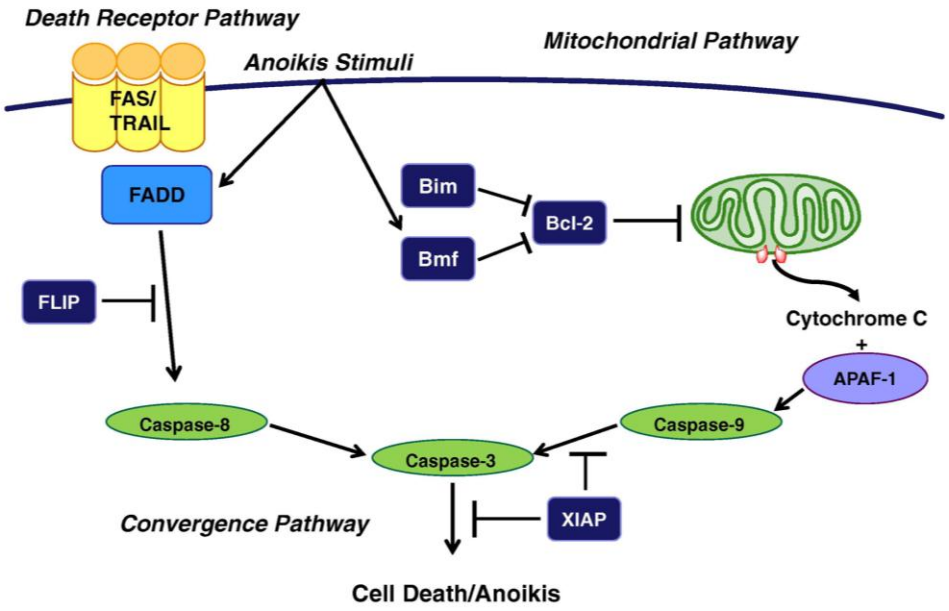

Figure 1-1. Mechanisms regulating anoikis and anoikis resistance. Upon matrix detachment, the intrinsic and extrinsic apoptotic signaling pathways are activated causing cell death/anoikis. Cancer cells activate FLIP or XIAP to inhibit these pathways and resist anoikis. See text for detail description. FLIP= FLICE (FADD-like IL-1β-converting enzyme)-inhibitory protein, XIAP= X-linked inhibitor of apoptosis protein, FADD= Fas-associated via death domain, Bcl2= B-cell lymphoma 2, Bmf= Bcl2-modifying factor, APAF-1= Apoptotic protease activating factor 1.

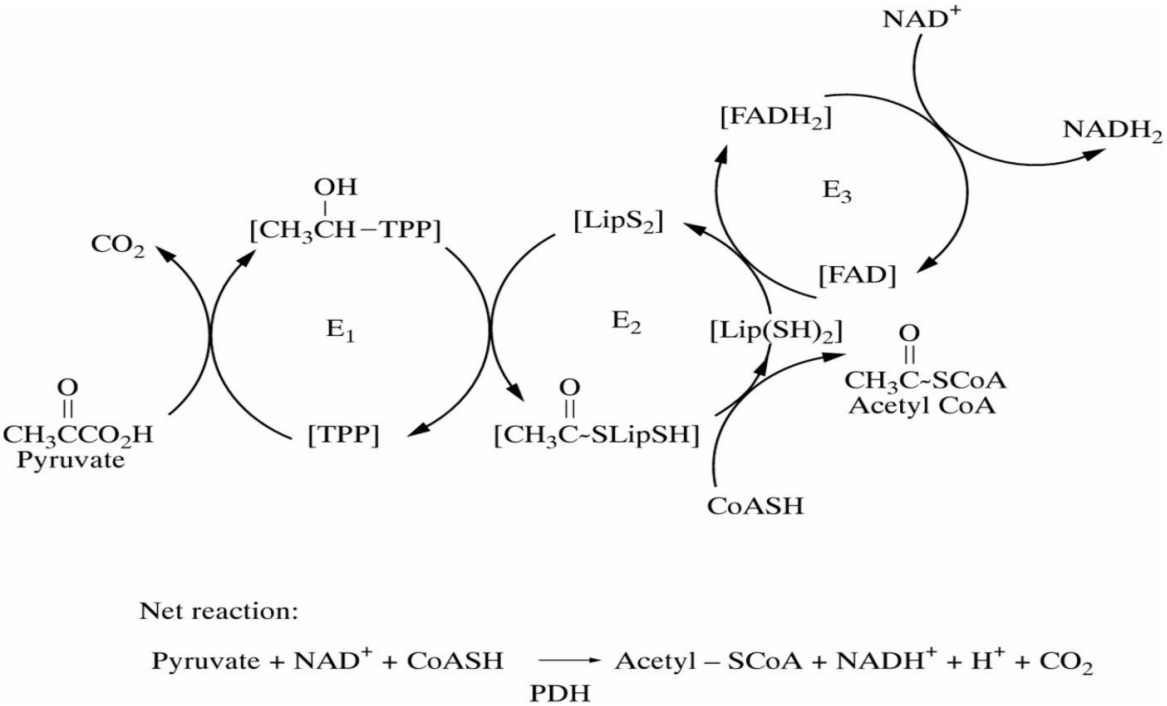

Figure 1-2. Pyruvate dehydrogenase complex (PDH) and its reaction. Schematic representation of PDH structure showing its subunits E1, E2, and E3. The chemical equation of the reaction carried out by PDH enzyme is represented below. For more detailed description of this complex, see the text. E1-pyruvate dehydrogenase, E2-dihydrolipoyl transacetylase, and E3-dihydrolipoamide dehydrogenase.

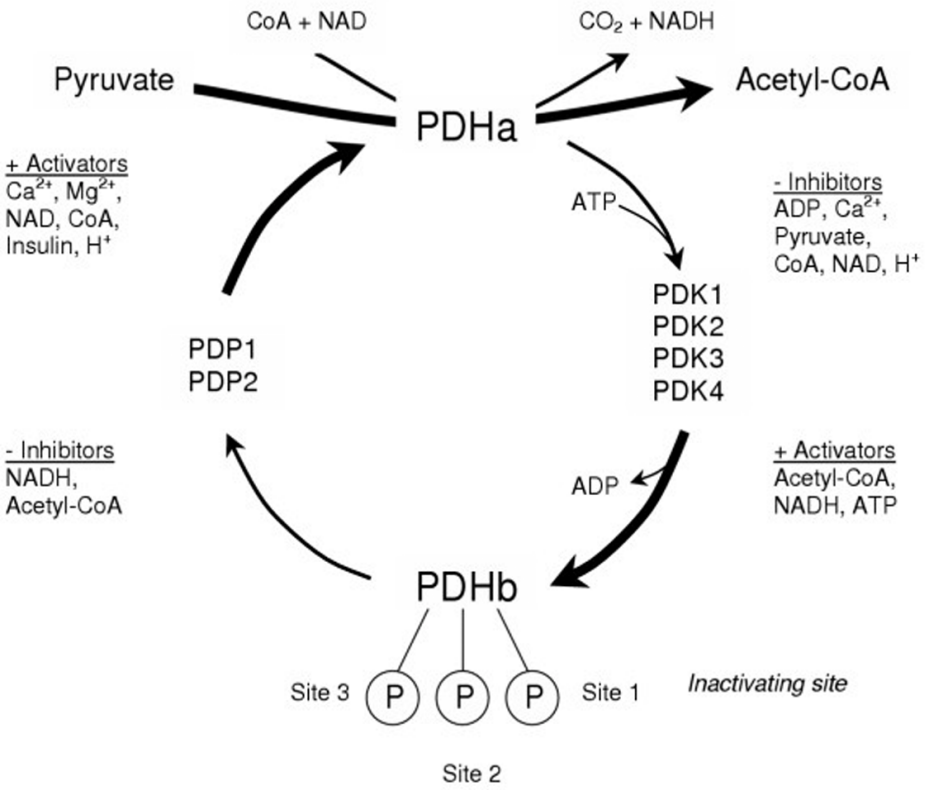

Figure 1-3. Regulation of PDH complex. The diagram represents the negative and positive regulators of PDH complex. A detailed description is provided in the text. PDH= Pyurvate dehydrogenase complex, PDK= Pyruvate dehydrogenase kinase, PDP= Pyruvate dehydrogenase phosphatase.

CHAPTER 2
MATERIALS AND METHODS

Cell Culture

The immortalized human breast epithelial cell line MCF10A and primary human mammary epithelial cells HMEC were purchased from ATCC. The Ras-transformed MCF10CA1.1 cells were obtained from Barbara Ann Karmanos Cancer Institute. All these three cell lines were cultured in Dulbecco' Modified Eagle Medium/Ham's F12 50/50 mix (DMEM/F12) medium (Cellgro, #10-090-CV) supplemented with 5% horse serum (GIBCO #16050122), 20 ng/mL epidermal growth factor (EGF, Sigma #E-9644), 10 µg/mL insulin (Sigma #I-1882), 0.5 µg/mL hydrocortisone (Sigma #H-0135), 100 µg/mL streptomycin and 100 units/mL penicillin (Cell gro #30-002-CI).

The transformed Human embryonic kidney (HEK) 293 cells Pheonix A and HEK293-FT cells were purchased from ATCC. The metastatic breast cancer cell line MDA-MB-231 was a kind gift from Dr. Kevin Brown (University of Florida). All these cell lines were cultured in Dulbecco' Modified Eagle Medium (DMEM) (#40-101-CV) supplemented with 10% bovine calf serum (BCS, HyClone #SH30072.03), 100 µg/mL streptomycin and 100 units/mL penicillin.

All assays in MCF10A and HMEC were performed 24 hours after incubation and in MCF10ACA1.1 and MDA-MB-231 were performed 48 hours after incubation under attached and suspended conditions unless otherwise noted.

Reagents

Poly(2-hydroxyethyl methacrylate) (Poly-Hema) was obtained from Sigma,Cat #P3932. The pharmacological ROS scavengers or antioxidants the reduced form of L-

glutathione (GSH) (Cat no #G4251) and α-Lipoic acid (Cat no #T5625) were purchased from Sigma-Aldrich.

Plasmids

Full length human cDNAs of PDH E1α (Cat no. #MHS1011-58712), PDK1 (Cat no. #MHS1010-7429799), 2 (Cat no. #MHS1011-61425), 3 (Cat no. #MHS1010-73978), and 4 (Cat no. #MHS1010-7429396) were obtained from OpenBiosystems.

Poly-Hema Coated Plates for Suspension Culture Cells

The adherent cells were cultured under suspension culture conditions by coating the plates with poly-hema chemical solution following manufacturer's protocol. 10 mg/mL of Poly-Hema (10x Stock) was made by dissolving in 95% ethanol and rotating overnight at 65°C incubator for complete solubility. The plates were coated with 1:10 dilution of 10X stock (final conc of 12 mg/mL) dissolved in 95% ethanol and air-dried. For 35 mm plates, 0.5 mL of 12 mg/mL poly-hema respectively was used to completely coat the plates. Once the plates were completely dry, the cells were added and grown with specific culture media for a specific time period depending on the assay performed.

RNA Isolation, and Northern blotting

RNA was extracted from both attached and suspended MCF10A cells following Invitrogen's protocol. The MCF10A cells were grown under normal adherent and poly-hema coated suspended culture conditions in 35 mm plates for 24 hours incubation. For the adherent cells, the media was aspirated and 1 mL Trizol reagent (Invitrogen, #15596-026) was added to homogenize the cells. The suspended cells were collected by centrifugation at 900 rpm for 3 minutes, followed by homogenization of cells with 1 mL Trizol reagent. To separate RNA from DNA and protein contents, 0.1 mL of chloroform was added to each homogenized samples. Followed by, centrifugation at

12,000 x g for 15 minutes at 4°C to separate aqueous and phenol-chloroform phases. Approximately 500 µL of aqueous solution was extracted from each sample to a new tube. The RNA was precipitated with 75% isopropanol (v/v) and centrifuged at 12,000 g for 10 minutes at 4°C. Later, the RNA pellets were washed with 1 mL of 75% ethanol. After washing, the RNA pellets were air-dried for 5 minutes before dissolving in sterile-filtered TE (10mM Tris pH 8.0, 1mM EDTA) and stored at -80°C until used. The concentration of extracted RNA was measured at 260/280 nm wavelength using UV spectrophotometer.

Approximately 10 µg of RNA from attached and suspension samples were loaded onto 0.8% agarose gel to separate the RNA using gel electrophoresis. After separation, the RNA from the agarose gel was transferred to nylon membrane in 10X SSC buffer (made from 20X SSC: 3 M NaCl, 0.3 M Na_3Citrate.H_2O, adjust the pH to 7.0 with 1N HCl) overnight at room temperature. After transfer, the membrane was hybridized with a specific probe radioactively labeled with ^{32}P in a hybridization buffer (Millipore, #S4031) at 42°C overnight in a rotating incubator. The probes were ~2.3 kb, ~1.5 kb, ~0.8 kb, and ~0.4 kb targeted to PDK1, PDK2, PDK3, and PDK4 respectively. They were generated by excising a part of cDNA from each gene with a suitable restriction enzyme digestion. After 24 hours of incubation with radiolabeled probe, the membrane was washed with 100 mL of 0.2X SSC with 0.1% SDS at 55°C for 5 -15 minutes until the background noise was reduced. Later, the membrane was dried, wrapped in a saran wrap to perform autoradiography.

Reverse Transcription, and Real-Time PCR

RNA was extracted from the target cells following the same procedure as described above. Approximately 1 µg of total RNA from attached and suspended cells was added

to a reaction mixture containing DEPC-treated ddH_2O, 2.5 μM dNTP, and 5 nM random primers to a total volume of 16 □L. The entire mixture was incubated at 70°C for 5 minutes, and quenched quickly on ice. Later, 2 μL of 10X M-MuLV RT buffer (NEB), 1 μL RNase inhibitor (Promega), and 1 μL M-MuLV Reverse Transcriptase (NEB) were added to the reaction to make up a final volume of 20 μL. Then, the samples were incubated at 42°C for 1 hour. Followed by heat-inactivation at 65°C for 20 minutes, dilution of the sample with ddH_2O to 200 μL.

Each real-time PCR reaction mixture consisted of; 1 μL of cDNA generated from reverse transcription, 1 μL of 5 μM primer mix working solution, 8 μL ddH_2O, and 10 μL of 2X SYBR Green PCR Master Mix (Applied Biosystems). The primers used for four PDKs were from the published report [93]. All the samples were run in triplicates for each reaction and results were expressed after normalization with endogenous beta-actin expression as relative quantities. Reactions with no template were also included on real-time PCR plate for each set of primers as negative control. More than two-fold difference in gene expression was considered as significant. The thermal cycling parameters were: 95°C for 10 minutes, 40 cycles of 95°C for 15 seconds for denaturing step and 60°C for 60 seconds for product extension. At the end of each run, melting curve analysis was performed. StepOne (48-well), or StepOnePlus (96-well) real-time PCR machines (Applied Biosystems) were used for data collection. Primers used were listed in Table 2-1.

Short-hairpin RNA (shRNA) Vector Construction

Oligos for shRNA construction were designed using shRNA psm2 designer at RNAi Central (http://cancan.cshl.edu/RNAi_central/RNAi.cgi?type=shRNA). The accession numbers for human PDK1, PDK4, MnSOD, and ERRγ were entered to

design specific shRNAs. The target sequences for all the genes were listed in Table 2-2. To generate a high-fidelity oligo, it was broken into two fragments when ordering from Invitrogen (Table 2-2). The breaks in the two fragments were designed with overlapping, complimentary loop regions so they anneal and extend during PCR into the full-length oligo. The desiccated oligos were dissolved in TE buffer and combined to a final working solution of 1 μM. 5 μM mir30 PCR primers were used for amplification using Phusion High-Fidelity DNA Polymerase (Finnzymes). Mir30 primer sequences were as follows: Forward 5'-AAGCCCTTTGTACACCCTAAGCCT-3' and reverse 5'-ACCTGGTGAAACTCACCCAGGGATT-3'.

The PCR was performed by mixing 1 μL of 1 μM mixed oligos, 1 μL of 5 μM mir30 PCR primers, 1 μL of Phusion polymerase, 2 μL of 10 mM dNTP mix, and distilled water to a final volume of 20 μL. The reaction was first denatured at 98˚C for 30 seconds, followed by 35 cycles of 1) denaturation at 98˚C for 10 seconds, 2) annealing at 60˚C for 30 seconds, and 3) extension at 72˚C for 30 seconds. The reaction included a final round of extension at 72˚C for 5 minutes. After PCR, the fragment was gel purified using QIAquick Gel Extraction Kit (Qiagen). The purified fragment was digested with XhoI and EcoRI restriction enzymes for at least 2 hours at 37˚C. The retrovirus vector pLMP was also digested in parallel. The pLMP vector sequence and information can be found in Figure 2-1 (Openbiosystems). The enzymes were heat inactivated at 65˚C for 30 minutes. The digested fragment and vector were mixed at a 7:1 ratio, respectively and ligated with 1 μL of T4 DNA ligase and 1X ligase buffer (NEB) in 10 μL final volume for 1 hour - overnight. The ligated DNA was transformed into DH5α competent E. Coli cells by heat-shock at 37˚C for 45 seconds. The cells were allowed to recover in LB,

incubated at 37˚C for 30 minutes with agitation. The cells were plated onto 50 µg per mL ampicillin LB agar plates and incubated overnight at 37˚C for selection of positive clones. Clones were manually picked and amplified in 5 mL LB culture with 50 µg per mL ampicillin selection overnight at 37˚C with agitation.

Plasmid DNA MiniPrep

1 mL of the overnight culture was transferred to a microcentrifuge tube. The bacterial cells were centrifuged at 8000 rpm for 1 minute. The cell pellets were resuspended with 200 µL P1 Buffer (50 mM Tris-Cl pH 8.0, 10 mM EDTA) each. The cells were then lysed by adding 200 µL P2 Lysis Buffer (200mM NaOH, 1% SDS w/v) to each tube and mixed by inversion. Next, 200 µL P3 Neutralization Buffer (3 M potassium acetate) were added to each tube and mixed by inversion. The samples were centrifuged at 14000 rpm for 5 minutes to pellet precipitated proteins. 0.5 mL of the supernatant was transferred to a new tube and reserved. The protein pellet was discarded. 1 mL of 100% ethanol was added to the reserved supernatant and mixed to precipitate DNA. The precipitated DNA was pelleted by centrifugation at 14000 rpm for 10 minutes. The supernatant was discarded. The DNA pellets were washed once in 1 mL 70% ethanol and the supernatants were removed. The DNA pellets were air dried for 5 to10 minutes. The DNA was dissolved in 30 to 50 µL TE (1 M Tris-Cl, 0.5 M EDTA pH 8) containing 20 µg/mL RNase A.

Retroviral Short Hairpin RNA Production and Transduction of Target Cells

Purified DNA was sequenced to confirm shRNA oligo insertion prior to retrovirus production. To generate retroviral particles, 1.5 µg of shRNA vector (Figure 2-1) containing the specific knockdown sequence was transiently transfected into

transformed HEK293 cells called Phoenix. The Phoenix cells were co-transfected with retroviral helper plasmids; 1 μg each of Gag-Pol and Env to facilitate packaging of shRNA into retroviral particles and increase their production. Cells were seeded at ~60% confluency 24 hours prior to transfection. They were transfected using Turbofect Transfection Reagent (Fermentos, #R0531) by 2 μL of the transfection reagent in 200 μL PBS. The two diluted reagents were incubated at room temperature for 20 minutes to form a cationic lipid-mediated transfection complex. The complex was added directly to cells dropwise. The cells were then incubated from 12 hours to overnight before switching to fresh media. The cells were incubated for an additional 48 hours. The virus-containing media was collected and passed through a 45 μm filter to exclude cell debris. The viral media was aliquoted and used immediately to infect target cells. Excess aliquots were stored at -80˚C, or disposed after bleaching.

Target cells were trypsinized and plated 24 hours prior to retroviral infection. Adherent cells were infected by replacing culture media with the infection cocktail, which 46 consisted of 1:1 viral media: culture media and 4 μg/mL polybrene. The cells were incubated for 24 hours, and then the infection cocktail was replaced with fresh media. The cells were incubated for an additional 24 hours.

After the 24 hours of recovery in fresh media, the cells were treated with 2 μg/mL puromycin dihydrochloride (Cellgro) to begin selection of transformed cell. Uninfected target cells were treated in parallel to estimate selection completion, which is typically complete 48 hours after addition of puromycin. The selection media was replaced with fresh culture media after selection and transformed cells were allowed to expand to desired density. The cells were then trypsinized and dissociated into a uniform

suspension and aliquoted. The transformed cell stocks were stored in freezing media (bovine serum albumin containing 10% v/v DMSO) at -80˚C, maintained as polyclonal culture, or further selected for monoclonal culture.

Protein Isolation and Immunoblotting

Cells grown under attached and suspended culture conditions were first washed in cold PBS for two times. Then, the cells were lysed with 50-200 µL of lysis buffer (50 mM Tris pH7.5, 1 mM EDTA, 1% (v/v) SDS, 1% 2-β mercaptoethanol, 20 mM dithiothreitol). The samples were boiled for 10 minutes to completely lyse the cells. Later, 6X sample lading buffer (4X Tris-SDS pH 6.8, 30% glycerol. 10% SDS, 0.6M dithiothreitol, 0.012% bromophenol blue) was added to all the samples. The samples were either stored at -20°C until use or loaed onto the SDS-PAGE gel for analysis.

The samples were resolved by first adding the appropriate amount of 6X sample buffer and boiled for 5 minutes. The samples were loaded onto 10% Tris-HCl polyacrylamide separating gels /4% stacking gel at 1mm thickness for electroporation in 1X running buffer (25 mM Tris, 190 mM glycine, 0.2% SDS). The gel was then electrotransferred onto polyvinylidene fluoride (PVDF) membrane using Trans-Blot Semi-Dry Electrophoretic Transfer Cell (BioRad) in 1X transfer buffer (20 mM Tris, 192 mM glycine, 10% methanol). Membranes were stained with Fast Green (0.1% Fast Green FCF, 50% methanol, 10% acetic acid) for 5 minutes at room temperature to ensure transfer and equal loading. Stained membranes were washed 2-3 times in TBST (30 mM Tris pH 7.5, 200 mM NaCl, 0.1% (v/v) Tween-20), and incubated in 3% (w/v) non-fat dry milk in TBST blocking solution for one hour at room temperature on a shaker. Blocked membranes were rinsed in TBST, followed by, probing with diluted primary antibody in TBST for one hour at room temperature, or overnight at 4˚C. The

membranes were then washed 3 times at room temperature in TBST for 5 minutes each. Next, they were incubated in diluted peroxidase-conjugated secondary antibodies in TBST for 30 minutes at room temperature. The membranes were then washed 3 times at room temperature in TBST for 5 minutes each. The membrane was probed with Pierce ECL substrate solution (Thermo Scientific) to detect the bound antibodies. Followed by, autoradiography to expose the membrane to X-ray film. Specific primary antibodies, secondary antibodies and their respective dilutions listed in Table 2-3.

Site-Directed Mutagenesis

The constitutively active PDH E1α was generated by PCR using full length PDH E1α cDNA as template. The three serine sites of PDH E1α cDNA; S232, S293, and S300 were mutated to alanine by site-directed mutagenesis using PCR with the following set of PCR primers: S232A: Forward- 5'TGGAATGGGAACAGCTGTTGAGAG AGCGGCAGCC 3' and reverse- 5' CTCTCTCAACAGCTGTTCCCATTCCATAGCGATT 3'; S293, 300A: Forward-5'TACCACGGACACGCCATGAGTGACCCGGGAGTCGCTT ACCGTACACGAGAAGAAATT 3' and RP-5'CGTGTACGGTAAGCGACTCCCGGGTC ACTCATGGCGTGTCCGTGGTAACGGTA 3'. DNA sequence coding for the mutation sites is underlined. Also, the FLAG tag sequence is underlined. Also, 5' NheI and 3' FLAG-tag with XhoI restriction sites were introduced to mutated PDH E1α by PCR using following set of primers: Forward-5' GAGAGCTAGCCGCTGCCGCCACTGCCT3' and reverse-5'GGAACTCGAGTTATTTATC**GTCATCGTCTTTGTAGTC**ACTGACTGACTTA AACTTGATCC 3' The restriction site (NheI and XhoI) sequences and the FLAG tag DNA sequence are underlined and highlighted in bold and underlined respectively. The PCR reaction was set up for a total of 25 µL reaction volume using: 1 µL (0.1ng) of full length PDH E1α cDNA, 5 µL of 5x Phusion reaction buffer, 1 µL of 5 µM primers, 4 µL

of 2.5 mM dNTPs, 0.5 µL of Phusion DNA polymerase enzyme, and 13.5 µL of ddH_20. The PCR cycling conditions were: denaturing step at 98˚C for 30 seconds, followed by 35 cycles of 1) denaturing at 98˚C for 10 seconds, 2) annealing at 60˚C for 30 seconds, and 3) extension at 72˚C for 30 seconds. Followed by, final extension step at 72˚C for 5 minutes. The amplicon was cloned into a lentiviral expression vector pCSCGW2 using restriction enzyme digestion of NheI and XhoI.

Lentiviral Over Expression of Constitutively Active FLAG-tagged PDH E1α

To produce lentiviral particles, 1.5 µg each of the pCSCGW2 plasmid containing constitutively active PDH E1α and pCSCGW2 alone as empty vector (EV) were transiently transfected into the HEK293FT a transformed HEK293 cell line using 2 µL of TurboFect as transfection reagent. Along with the above-mentioned plasmids, 1 µg each of two lentiviral helper plasmids; MD2G (envelope plasmid) and PAX (packing plasmid) were co-transfected to facilitate virus production and packaging. After 48 hours post-transfection, the media carrying viral particles was collected and filtered through a 45 µm filter to eliminate cell debris. The viral media was harvested to either infect the target cells, or stored at -80◦C.

To over express constitutively active PDH E1α, MCF10A and MDA-MB-231 cells were plated 24 hours prior to lentiviral infection in a 60 mm petriplates. After 24 hours, the media from the cultured cells (MCF10A and MDA-MB-231) was replaced with viral cocktail containing 1 part of viral media carrying either EV or FPDH E1α and 1 part of culture media. 4 µg/mL of polybrene was added to the viral cocktail to increase viral transduction efficiency. After 24 hours of incubation, the viral media was replaced with fresh media for the recovery of the cells. After 48 hours post-infection, the cells are transferred from 60 mm to 100 mm plates for amplication. Later, the cells were sorted

for GFP-positive cells using FACSORT instrument at ICBR Flow Cytometry Core facility, University of Florida. After sorting, one million GFP positive cells were collected from each group; EV and FPDH E1α carrying MCF10A and MDA231 cells respectively. After recovery of GFP sorted cells, immunoblotting (IB) was performed using anti-FLAG antibody to confirm the expression of FLAG-tagged PDH E1α expression in both MCF10A and MDA-MB-231 cells.

Measurement of PDH Activity

PDH activity was measured using Dipstick assay kit from MitoSciences (# MSP30) following their protocol. Cells were grown under attached and suspended culture conditions in 35 mm plates. Then the cells were trypsinized, washed twice in cold PBS and collected by centrifugation at 900 rpm for 3 minutes. After washing, the cells were lysed by adding 5 volumes of 10X sample buffer and 1/10 volume of detergent provided by the kit. The samples were incubated for 10 minutes on ice followed by centrifugation at 3000 rpm for 10 minutes. During this step, the mitochondrial extract was isolated as supernatant from the cell debris. The extract was immediately used for protein concentration using BCA kit.

One mg of extract from each sample was loaded onto 96-well plate. The equal volume of blocking solution provided by the kit was added to the wells with the sample. The dipsticks provided by the kit were gently added to the sample mix in the microplate well. The samples were allowed to wick up onto the dipsticks towards wicking pads within an hour. Later, 40 µL of sample buffer was added to each microwell plate with dipstick to wash. After 5-15 minutes, 300 µL of activity buffer (330 µL of sample buffer, 16.6 µL of 20X reaction mix, 13.3 µL of diaphorase, and 0.7 µL of NBT reagent provided by kit per one dipstick) was added to an empty microwell for each dipstick. Now, the

wicking pad was removed from each dipstick and placed in a well with activity buffer. The signal appeared 5-7mm from the bottom of the dipstick within 20 minutes. After one hour, the signal was completely developed. So, the dipsticks were transferred to another microwell plate containing 300 µL of deionized water to wash the stick. The dipsticks were dried and the signal was measured by using Canon flatbed scanner. The PDH activity was represented in arbitrary units and the experiment was repeated at three different times.

Trypan Blue Exclusion Assay

Cells were grown under attached and suspended culture conditions in 35 mm plates. The suspended cells were collected by centrifugation at 900 rpm for 3 minutes. Then both the attached and suspended cells were trypsinized, washed in PBS once, and resuspended in 1 mL PBS. To 50 µL of sample, equal volume of 0.4% Trypan blue dye was added. 10 µL of the sample mixture was added to the hemocytometer slide and the number of live (unstained) vs dead (stained blue) cells were counted. The percentage of cell viability was determined by dividing total number of unstained cells to total number of stained+unstained cells X 100. The experiment was repeated at least for three different times in duplicates.

Caspase 3/7 Activity Assay

Caspase 3/7 assay was performed using caspase 3/7 glo assay kit (# G8090) from Promega. Cells were grown under attached and suspended culture conditions in 35 mm plates. The suspended cells were collected by centrifugation at 900 rpm for 3 minutes. Then both the attached and suspended cells were trypsinized, washed in PBS twice and resuspended in 3 volumes of hypertonic buffer (HTB). Cells were lysed in hypertonic buffer (HTB: 10 mM HEPES, pH7.9 at 4°C, 1.5 mM $MgCl_2$, 10 mM KCl, add

0.2 mM PMSF, 0.5 M DTT freshly added before use). The protein concentration of samples was measured using the BCA kit. 75-100 μg of protein samples were loaded in each of the 96-well microplates. The volume of each sample was adjusted to 20 μL using HTB. Equal volume of caspase 3/7 substrate provided by the kit was added to all the samples in the wells. The samples were incubated for 30 minutes at room temperature on a shaker. Later, caspase 3/7 activity was measured in relative luminiscence unit (RLU) per second using luminometer following the manufacturer's instruction. The samples were assayed in duplicates at three independent experiments.

Annexin V/7-AAD Analysis

Cells were grown under attached and suspended culture conditions in 35 mm plates. The suspended cells were collected by centrifugation at 900 rpm for 3 minutes. The attached were trypsinized. Both attached and suspended cells were washed twice with PBS, followed by, $1x10^5$ cells staining with 5 μL each of PE Annexin V (Phycoerythrin) and 7-AAD (aminoactinomycin D) from BD Pharmingen for 15 minutes at room temperature. Cells were analyzed within an hour using Becton Dickson's Facsort. Cellquest software was used to analyze the data as in [FL2H, FL3H] log scale two-dimensional diagram. The results were from three independent samples.

Measurement of Oxygen Consumption Rate

Oxygen consumption was measured using 96-well Oxygen biosensor plates from BD Biosciences. Cells were grown under attached and suspended culture conditions in 35 mm plates. Adherent cells were trypsinized and counted. One million cells from attached and suspension cultures were loaded to 96-well BD biosensor plate to measure oxygen consumption rate for two hours at 10 minutes interval. Fluorescence

was measured using excitation/emission (Ex/Em) 590/630. The assay was performed in duplicates from three independent samples.

Measurement of Intracellular ROS

Intracellular ROS was measured using the Amplex red hydrogen peroxide / peroxidase kit from Invitrogen. Cells were grown under attached and suspension conditions in 35 mm plates. Cells were trypsinized, washed twice in PBS, followed by, lysis using hypertonic buffer (HTB: 10 mM HEPES, pH7.9 at 4°C, 1.5 mM $MgCl_2$, 10 mM KCl, add 0.2 mM PMSF fresh before use). Equal amount of protein was loaded in 96 well plate and ROS levels were measured by adding equal volume of amplex red hydrogen peroxide/ peroxidase substrate as per manufacturer's protocol. Fluorescence measured using Ex/EM of 590/630. The assay was performed in duplicates from three independent samples.

Measurement of Intracellular Lactate

Intracellular lactate was measured using the lactate assay kit from Biovision (# K607-100). Cells were grown under attached and suspended culture conditions in 35 mm plates. The suspended cells were collected by centrifugation at 900 rpm for 3 minutes. Then both the attached and suspended cells were trypsinized, washed in PBS twice and resuspended in 1 mL PBS. One million cells were added to 96-well microplate. The volume was adjusted to 50 µL using lactate assay buffer provided by the kit. Equal volume of reaction mix (46 µL lactate assay buffer, 2 µL probe, and 2 µL enzyme mix provided by kit) was added to each well with sample. The samples were incubated for 30 minutes at room temperature. Later, measured lactate levels for fluorescence at Ex/Em of 590/630. The assay was performed in duplicates from three independent samples.

Experimental Metastasis Assay in Mice

Four to five weeks old female SCID/Beige mice were purchased from Harlan. Empty vector and PDK1 depleted MDA-MB-231 cells were cultured under adherent conditions. After trypsinization, two million cells were resuspended in 200 µL PBS, and injected via intravenous route in a total number of six mice for each group. Forty days post injection; lungs were harvested from the mice after euthanasia. After harvesting, the lungs were washed twice in 5 mL PBS. 10 mL Bouin's solution was added to each lung and incubated overnight on a shaker for fixation. The tumor nodules turned white after bouin's fixation and the number of lung tumor nodules was counted manually from the surface of each lung. The University of Florida IACUC approved all procedures.

Tissue Sectioning and H&E Staining

Tissue sectioning, processing, and Hematoxylin and Eosin (H&E) staining were performed by the Cell and Tissue Analysis Core (CTAC) facility at University of Florida. Lung tissues were paraffin-embedded and sectioned at 5 µm. For H&E staining, the sections were deparaffinized and rehydrated. For deparafinization, the following steps were followed; the slides with lung sections were dipped for 2 minutes in xylene. This step was repeated three additional times followed by, two times wash in absolute ethanol for 1 minute each. Then, washed the slide twice in 95% ethanol for 30 seconds, 70% ethanol for 45 seconds and finally in water for 1 min). After deparaffinization, the sections were stained with Hematoxylin, a basic dye that stains the nuclei. The sections were washed with water and citric acid, known as clarifier. It removes the excess hemotoxylin dye from the sections. Then, the slides were treated with potassium hydroxide followed by a quick rinse in water. The sections were equilibrated in 95% ethanol. Then, the sections were stained with Eosin for 15-30 seconds. Eosin is an acid

dye used most commonly to counterstain hematoxylin. After Eosin staining, the slides were washed three times in 100% ethanol followed by xylene wash. After staining, the sections were mounted and pictures were taken using upright light microscopy at 5X magnification.

Statistics

Data were represented as the mean ± S.D. Student's two-tailed t-test was used to calculate p-values and $p<0.05$ regarded as statistically significant.

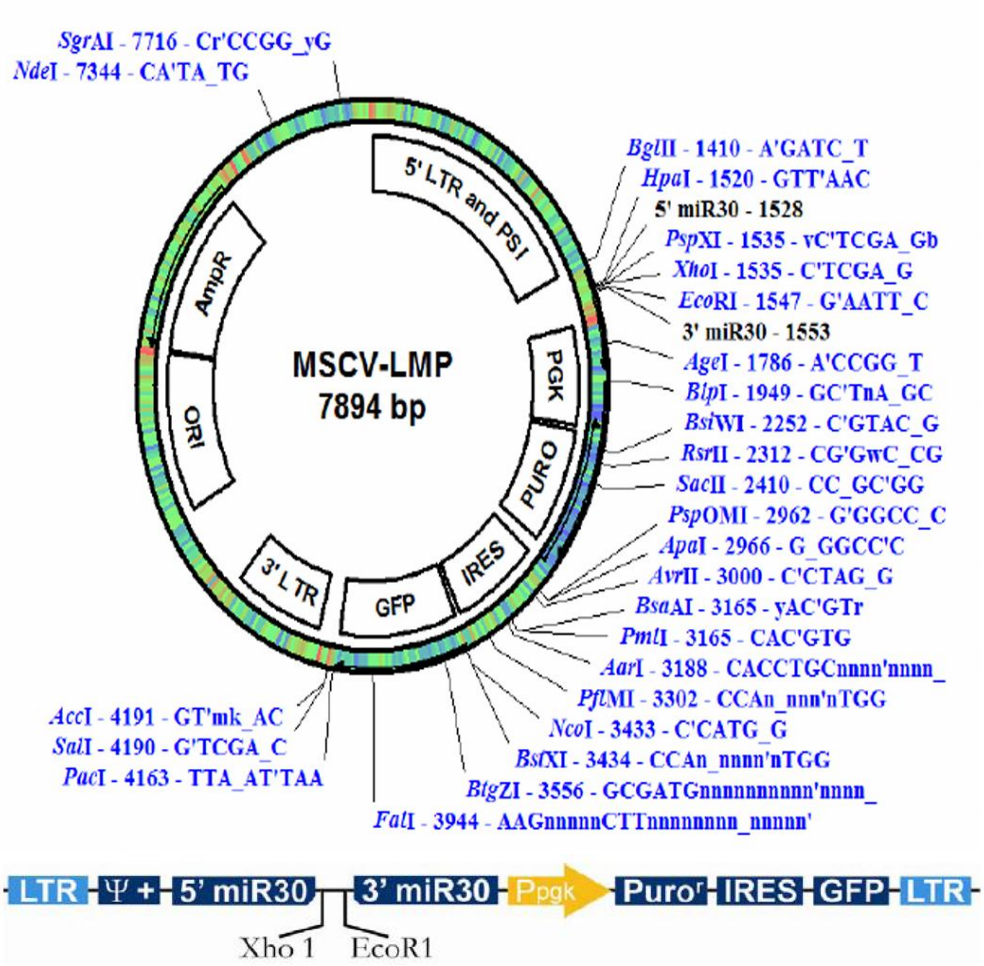

Figure 2-1. Cloning vector information for microRNA-adapted retroviral vector. Cloning vector information for microRNA-adapted retroviral vector. A) Vector map and unique restriction sites of MSCV-LMP cloning vector. B) Xho1-EcoR1 cloning site for shRNAmir expression using retroviral 5‟ LTR and PSI (Ψ) promoter. PGK promoter (Ppgk) drives expression of selection cassettes. Puror cassette allows for selection of stable integrates. IRES-GFP served as marker for stable integration. Abbreviations: LTR is long terminal repeats. MiR is microRNA. Ppgk is phosphoglycerate kinase promoter. Puro is puromycin. IRES is internal ribosome entry site. GFP is green fluorescence protein.

Table 2-1. Primers used for real-time RT-PCR

Name	Forward	Reverse	Tm
PDK1	CTATGAAAATGCTAGGCGTCTGT	AACCACTTGTATTGGCTGTCC	60°C
PDK2	AGGACACCTACGGCGATGA	TGCCGATGTGTTTGGGATGG	60°C
PDK3	GCCAAAGCGCCAGACAAAC	CAACTGTCGCTCTCATTGAGT	60°C
PDK4	TTATACATACTCCACTGCACCA	ATAGACTCAGAAGACAAAGCCT	60°C
MnSOD	TACGTGAACAACCTGAAC	TATCTGGGCTGTAACATCT	60°C
ERRγ	TCTTGCTAATTCAGACTCCAT	GCAGTGTCATCAGCATCTTG	60°C
β-Actin	AGAAAATCTGGCACCACACC	AGAGGCGTACAGGGATAGCA	60°C

Table 2-2. shRNA Oligos designed for retrovirus-mediated knockdown

Oligo Name	Gene targeted	Sequence
shPDK1	PDK1	TTCTACATGAGTCGCATTTCAA
shPDK4-1	PDK4	ACCAACGCCTGTGATGGATAAT
shPDK4-2	PDK4	TATTTATCATCTCCAGAATTAA
shMnSOD	MnSOD	AAGGAACAACAGGCCTTATTCC
shERRγ	ERRγ	CAGTGGGAGCTACAGTTCA

Table 2-3. Antibodies used for Immunoblotting (IB)

Antibody	Species	Isotype	Company	Catolog number	Dilution
FLAG	N/A	Mouse-IgG	Sigma	F-1804	1:3000
PDK1	Human	Rabbit-IgG	Cell Signaling	3820s	1:1000
PDK2	Human	Rabbit-IgG	Epitomics	2282-1	1:2000
PDK4	Human	Rabbit-IgG	Abgent	AP7041b	1:500
MnSOD	Human	Rabbit-IgG	Santa Cruz	30080	1:1000
LDHA	Human	Rabbit-IgG	Cell Signaling	2012s	1:1000
ERRα	Human	Rabbit-IgG	Gene Tex	108166s	1:2000
α-Tubulin	Human	Mouse-IgG	Sigma	T-6199	1:5000
HRP-Donkey anti-Mouse	Mouse	Donkey-IgG	Jackson Immunoresearch	715-035150	1:5000
HRP-Donkey anti-Rabbit	Rabbit	Donkey-IgG	Jackson Immunoresearch	715-035152	1:8000

CHAPTER 3
INFLUENCE OF GLUCOSE METABOLISM ON ANCHORAGE-INDEPENDENT SURIVIVAL IN MAMMARY EPITHELIAL CELLS

Background

Apart from providing energy and biofuels for the maintenance of life, glucose metabolism also regulates cell death processes such as necrosis, autophagy and apoptosis[94]. Of these processes, the effect of glucose metabolism on apoptosis is very well studied. Several groups demonstrated that glucose deprivation leads to attenuation of anti-apoptotic genes such as myeloid cell leukemia 1 protein (MCL-1), activation of BH3-only proteins such as Noxa and Bim[95], and activation of proapoptotic genes such as Bcl2-associated X protein (BAX)[96,97]. Furthermore, it has been reported that NADPH, which is primarily generated from the pentose phosphate pathway (PPP), protects cells from apoptosis by reducing ROS levels under various conditions[98].

The impact of glucose metabolism on anoikis (detachment induced cell death) is still being studied. Schafer *et al*., demonstrated when detached from ECM, the untransformed mammary epithelial cells reduce glucose uptake leading to ATP deficiency known as “metabolic defect”[68]. Furthermore, the attenuation of glucose uptake due to matrix detachment reduces the pentose phosphate pathway (PPP), hence, reduces antioxidant capacity, and consequently increases ROS production[68]. The above study focused on antioxidant rescue from anchorage-independent cell death, but it is not clear how the metabolic impairment is connected to anoikis/detachment-induced cell death.

The main focus of our study is to understand how glucose metabolism influences anchorage-independent survival in human mammary epithelial cells. Our study provides evidence that decreased glucose oxidation promotes anchorage-independent survival

by attenuating ROS production. Furthermore, we show for the first time the functional role of PDKs in cell survival. PDKs inhibit the entry of pyruvate into TCA cycle and hence reduce glucose oxidation, promoting anoikis resistance in untransformed mammary epithelial cells.

Results

Induction of PDK upon Detachment from ECM

Pyruvate, derived from glycolytic activity, is primarily converted to acetyl-CoA in the mitochondria by the pyruvate dehydrogenase (PDH) complex in normal cells. In most cancer cells, pyruvate is mostly converted into lactate by the lactate dehydrogenase (LDH). Thus, the fate of pyruvate represents a pivotal point between normal and tumor cell metabolism. Furthermore, glucose metabolism plays a critical role in regulating cell viability under variety of stressful conditions[98]. As normal cells show increased sensitivity to anoikis when detached from matrix, we decided to investigate the influence of glucose metabolism on anoikis in normal mammary epithelial cells by examining the regulation of PDH and LDH upon cell detachment from ECM.

As described in introduction, PDH is a multi-subunit enzymatic complex and its activity is inhibited by phosphorylation on the E1α subunit by pyruvate dehydrogenase kinases (PDKs) 1-4[99]. We examined the expression of all four PDK isoenzymes at RNA level by quantitative RT-PCR in two different mammary epithelial cell models; primary human mammary epithelial cell line (HMEC) and untransformed human mammry epithelial cell line (MCF10A) under attached and suspended conditions. PDK4 transcript in suspended HMEC cells (Figure 3-1A), and PDK2 and PDK4 isoenzymes in suspended MCF10A cells (Figure 3-1B) were significantly upregulated, whereas PDK1

and PDK3 showed only marginal changes (Figure 3-1). Thus, the results demonstrate that upon matrix detachment PDK4 is induced in HMEC and MCF10A cells.

The rest of the study is focused on MCF10A (untransformed, immortalized mammary epithelial cell line). To validate if PDK4 is the major PDK isoenzyme in suspended MCF10A cells, we measured the absolute quantity of all four PDK RNAs. PDK1 and PDK4 transcripts were found to be the most abundant PDKs in suspended MCF10A cells, whereas PDK2 was negligible (Figure 3-2A). Consistent with RNA expression, PDK4 isoenzyme was abundant at the protein level in suspended MCF10A cells and not detected under adherent conditions (Figure 3-2B). Although PDK1 was upregulated at the RNA level in suspended MCF10A cells (Figure 3-1B), no significant change at the protein level was observed under attached and suspended conditions (Figure 3-2B). PDK2 was not detectable at the protein level regardless of the cell matrix contact status (Figure 3-2B).

Another important enzyme that regulates the fate of pyruvate is LDH enzyme. It interconverts pyruvate to lactate in the cytoplasm. Therefore, we decided to examine its role in matrix detachment. As mentioned in introduction, LDH5 is the most efficient isoenzyme encoded by the LDHA gene. Hence, we investigated the expression of LDHA in MCF10A under attached and suspended conditions. Western blotting showed no significant change in protein levels of LDHA when cells lost adhesion to ECM (Figure 3-3). Thus, the results confirm the induction of PDK4 when detached from matrix but no significant change in the LDH enzyme.

Upregulation of PDK4 Antagonizes Anoikis

To define the effect of matrix detachment-induced PDK4 on anoikis, we depleted PDK4 in MCF10A cells using two independent retroviral short hairpin RNAs (shRNAs).

In parallel, we transduced MCF10A cells with retrovirus carrying empty vector (EV) to serve as a control. The efficient knockdown of PDK4 was verified by both Northern blotting analysis (Figure 3-4A) and quantitative RT-PCR (Figure 3-4B) in attached and suspended MCF10A cells. Thus, the two independent shRNAs targeted against PDK4 significantly diminished 80% of PDK4 expression.

We further investigated if the depletion of PDK4 caused increased anoikis in MCF10A cells. Normally, MCF10A cells undergo anoikis or detachment-induced cell death upon detachment from matrix[15,16]. Depletion of PDK4 showed a further increase of cell death in MCF10A suspension cells (based on Trypan blue exclusion assay) (Figure 3-5A). Since PDK4 was not expressed in adherent MCF10A cells, knockdown of PDK4 did not induce any significant cell death (Figure 3-5A). To validate that the increase in cell death was due to increased apoptosis, we first measured the caspase 3/7 activity using Promega's caspase 3/7 glo assay. When cells were attached to matrix, no significant induction of caspase activity was observed in either EV or PDK4-depleted MCF10A cells (Figure 3-5B). Upon detachment, PDK4-depleted MCF10A cells displayed higher caspase activity than the suspended EV cells (Figure 3-5B). To further validate that depletion of PDK4 enhanced apoptosis in MCF10A suspension cells, we performed another apoptosis assay i.e., PE annexin V/7-AAD analysis. Similar to caspase activity, no significant difference in PE annexinV/7-AAD staining was detected between the EV and PDK4-depleted MCF10A attached cells (Figure 3-5C and 3-5D). However, detachment from matrix showed an increased PE annexinV/7-AAD staining in both cell groups (Figure 3-5C). Compared to EV cells, PDK4-depleted cells exhibited elevated early stage (29% vs. 14%) and late stage (11% vs. 5%) apoptosis when

detached from matrix (Figure 3-5D). Thus, the results suggest that upon detachment from matrix, mammary epithelial cells upregulate PDK4 to resist anoikis and prolong their survival in suspension.

Activation of PDH Sensitizes Cells to Anoikis

PDKs phosphorylate PDH enzyme and inactivate its activity. Since MCF10A cells showed a significant upregulation of PDK4 in suspension cells, we measured the PDH activity using Mitosciences DipStick assay kit under attached and suspended culture conditions. The PDH activity was significantly downregulated in matrix-detached cells compared with attached cells (Figure 3-6). The results suggest the mammary epithelial cells potently activate PDK enzyme when detached from matrix to reduce glucose oxidation by decreasing PDH activity.

To investigate the functional significance of reduced PDH activity in matrix detached cells, we decided to study the effect of PDH activation on anoikis. PDKs inactivate PDH by phosphorylating the E1α subunit at three serine residues 232, 293,and 300[99]. We constructed a constitutively active form of PDH E1α by substituting these serines with alanines, inserted a FLAG peptide at the C-terminal end, and introduced it into MCF10A cells by lentiviral infection. Forced expression of PDH E1α was confirmed by Western blotting using anti-FLAG antibody (Figure 3-7A). To confirm if the forced overexpression of constitutively active PDH E1α in MCF10A is functional, we measured PDH activity. As expected, the MCF10A transduced with active PDH E1α displayed increased PDH activity under both attached and suspended conditions (Figure 3-7B).

We investigated the effect of increased PDH activation on anoikis. When MCF10A cells were transduced with constitutively active PDH E1α, they showed an enhanced

cell death under suspended conditions (Figure 3-8A). No detectable cell death by PDH E1α was observed under attached conditions (Figure 3-8A). To determine if the increased cell death is due to increased apoptosis, we measured caspase 3/7 activity. As expected, the MCF10A cells transduced with active PDH E1α showed increased caspase activity in suspension cells (Figure 3-8B). These findings suggest that increased PDH activity sensitizes MCF10A cells to anoikis. Because activation of PDH essentially phenocopied depletion of PDK4, we conclude that PDK4 modulates anoikis through PDH.

Depletion of PDK4 Increases Mitochondrial Oxidation

Pyruvate is converted irreversibly into acetyl CoA by the PDH enzyme to turn on the TCA cycle. As described in the introduction, PDH is tightly regulated by PDK and PDPs. PDKs inhibit PDH activity and attenuate the TCA cycle. Therefore, we expect that depletion of PDK4 in MCF10A would lead to increased PDH activity. An increased PDH activity would increase the TCA cycle to produce ATP or energy for other biosynthetic process. During the process of ATP production by oxidative phosphorylation, the reactive oxygen species (ROS) would be generated as a byproduct. Infact, mitochondrion is the main source for the production of ROS. Therefore, we hypothesize that depletion of PDK4 increases ROS levels in MCF10A suspension cells.

To test this model, we measured PDH activity in PDK4-depleted MCF10A cells grown under attached and suspended conditions. As expected, the knockdown of PDK4 increased PDH in suspended cells (Figure 3-9A). Since PDK4 was not expressed in adherent cells, depletion of PDK4 did not alter the PDH activity in MCF10A attached cells (Figure 3-9A). Increased PDH activity should increase mitochondrial oxidation of

glucose and this in turn increases oxygen consumption rate. To test this, we measured the oxygen consumption rate (OCR) in PDK4-depleted cells using BD oxygen biosensor plates. There was no significant difference in OCR between EV and PDK4-depleted MCF10A cells under adherent condition (Figure 3-9B). Upon detachment, MCF10A carrying EV cells significantly reduced the oxygen consumption rate (Figure 3-9B), which was consistent with increased PDK4 expression (Figure 3-1B) and reduced PDH activity (Figure 3-6) during the process. The suspended PDK4-depleted MCF10A cells showed significantly higher OCR than the suspended control cells (Figure 3-9B).

As the depletion of PDK increased mitochondrial respiration in MCF10A suspended cells, we investigated if the depletion of PDK4 had any impact on the ROS production. We measured the intracellular ROS levels using Invitrogen's Amplex red hydrogen peroxide/peroxidase assay kit. Although the MCF10A cells undergo anoikis, but no significant increase in ROS levels was observed in suspended cells compared to adherent ones (Figure 3-9C). Consistent with increased mitochondrial activity, PDK4-depleted MCF10A cells accumulated higher ROS levels compared to the control cells under suspension culture (Figure 3-9C). Thus, our results suggest that depletion of PDK4 augments mitochondrial oxidation and ROS levels specifically in matrix detached MCF10A cells.

Treatment with Antioxidant Rescues PDK4-Depleted Cells from Anoikis

Based on our results; we infer that depletion of PDK4 or increased PDH activity sensitizes cells to anoikis. Furthermore, depletion of PDK4 increased ROS levels in suspended MCF10A cells. ROS are known to cause damage to all cellular components due to their oxidative nature. Since Mitochondria are the major sources for ROS production and plays a critical role in the regulation of cell death especially intrinsic

apoptotic pathway (as described in the introduction), we decided to investigate the impact of ROS on anoikis in PDK4-depleted MCF10A cells.

To test if ROS contributed to anoikis, we treated cells with two different antioxidants: reduced form of glutathione (GSH) and α-lipoic acid (LA), to scavenge the intracellular ROS. GSH is one of the most prevalent intracellular reducing agents to maintain redox homeostasis. GSH reacts with ROS to form a relatively less stable GSSG (oxidized form), which is quickly converted back to the reduced form (GSH) by endogenous glutathione reductase. Thus, the reduced form of glutathione removes ROS. α-lipoic acid (LA) is another antioxidant that is readily converted into the reduced form by intracellular antioxidant enzymes such as glutathione reductase. The reduced form has potent antioxidant effects, which scavenges ROS. The treatment with antioxidants had little or no effect on apoptosis of adherent cells, but significantly suppressed detachment-induced apoptosis in both EV and PDK4-depleted MCF10A cells, as measured by caspase 3/7 activity (Figure 3-10). Although MCF10A-EV cells did not show any increase in ROS levels upon detachment, the antioxidant treatment rescued these cells from anoikis. The plausible explanation could be upon detachment from matrix, the epithelial cells may become sensitive to ROS.

Taken together, our results suggest that when detached from matrix, mammary epithelial cells upregulate PDK4 to attenuate PDH activity and hence the mitochondrial oxidation of pyruvate. This metabolic reprogramming reduces oxidative stress, and promotes resistance to anoikis.

Estrogen-Related Receptor Activates PDK4 in Response to Cell Detachment

Our study indicates that PDK4 plays a critical role in matrix detachment-induced metabolic shift and promotes anoikis resistance. Therefore, it is important to determine

the key activator of PDK4 following matrix detachment. It was well established that PDK4 was a direct target of the estrogen-related receptors (ERRs)[100-103]. ERRs are orphan nuclear receptors and play a key role in regulating mitochondrial biogenesis and fatty acid oxidation[104]. ERR have three members: ERRα, ERRγ, and ERRβ. The first two members are expressed in metabolically active tissues, whereas ERRβ is largely restricted to embryonic cells[104].

We first examined the expression of ERRα and ERRγ in MCF10A cells under attached and suspended culture conditions. The western blotting of ERRα did not display any significant change at protein level upon detachment (Figure 3-11A). By contrast, ERRγ was significantly induced at RNA level by cell detachment (Figure 3-11B). Since ERRγ was dramatically upregulated in suspended cells, we investigated its role in the induction of PDK4. To test that, we efficiently depleted ERRγ with a lentiviral shRNA, as shown by qRT-PCR (Figure 3-12A). Upon depletion of ERRγ, the induction of PDK4 was substantially reduced at RNA level in MCF10A suspended cells (Figure 3-12B). Next, we tested if the depletion of ERRγ had a similar effect on anoikis as PDK4 depletion in MCF10A. Consistent with PDK4 depleted MCF10A cells, depletion of ERRγ significantly induced cell death in suspended cells as shown by trypan blue exclusion assay (Figure 3-13A). Furthermore, this increased cell death was due to increased apoptosis (as shown by caspase 3/7 assay) in ERRγ-depleted MCF10A suspended cells (Figure 3-13B). No significant cell death (Figure 3-13A) or apoptosis (Figure 3-13B) was observed in ERRγ-depleted adherent cells. Thus, our results confirm that the induction of PDK4 in MCF10A suspension culture cells is by ERRγ and depletion of ERRγ sensitizes cells to anoikis, which is consistent with PDK4 depletion.

Summary

Glucose metabolism not only produces energy in the form of ATP but also regulates cell death processes. Anoikis is a form of cell death that occurs when an epithelial cell detaches from ECM. We focused on understanding how glucose metabolism was affected by matrix detachment and how it impacted anoikis or detachment-induced apoptosis. Based on our results, we conclude that upon detachment from matrix, untransformed mammary epithelial cells potently upregulate ERRγ expression, which in turn activates the transcription of PDK4 and, consequently results in decreased glucose oxidation and prolonged cell survival in suspension (Figure 3-14).

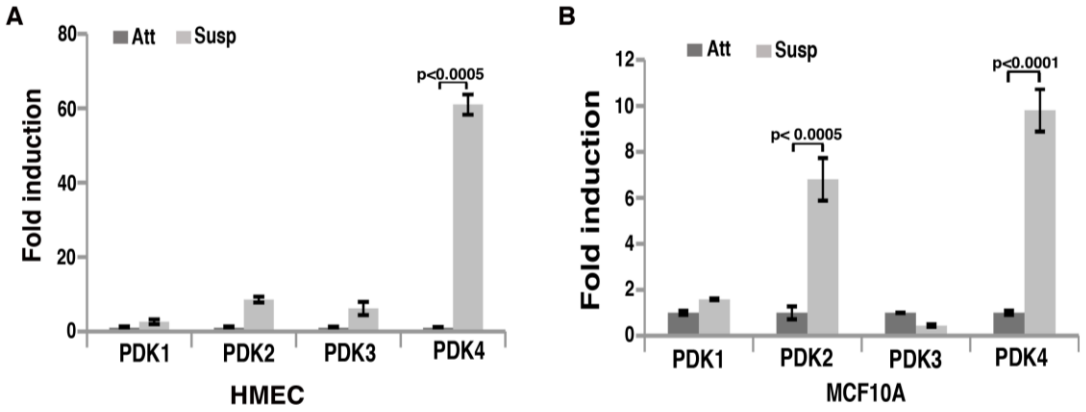

Figure 3-1. Matrix detachment induces PDK4 expression in mammary epithelial cells. HMEC and MCF10A cells were grown in a 35 mm plates under attached and poly-hema coated suspended culture conditions for 24 hrs. After 24 hrs of incubation, the cells were collected to extract RNA using Trizol reagent. 2 µg of RNA was used from each sample to synthesize cDNA by Moloney Murine Leukemia Virus (M-MulV) reverse transcriptase. 1 µL of cDNA was used to run realtime quantitative PCR reaction with SYBR® green PCR mix. The relative RNA levels of PDK1, PDK2, PDK3, and PDK4 were normalized to endogenous β-Actin in (A) HMEC and (B) MCF10A. These data represent triplicate experiments. Error bars were expressed as standard error of the mean (S.E.M.). Statistical analysis was performed using paired Student's t-test. Att = Attached, Susp = Suspended, and PDK = Pyruvate dehydrogenase kinase isozyme 1, 2, 3, and 4.

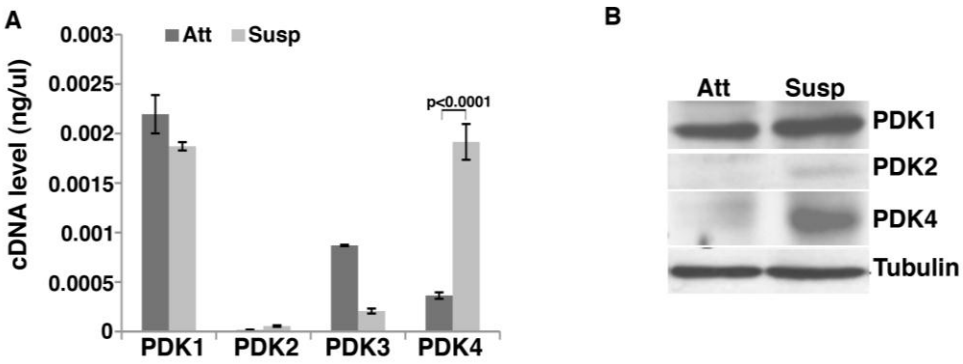

Figure 3-2. Induction of PDK4 at RNA and protein level in MCF10A suspension cells. MCF10A cells were grown in a 35 mm plates under attached and poly-hema coated suspended culture conditions for 24 hrs. (A) Realtime qRT-PCR. After 24 hrs of incubation, the cells were collected to extract RNA using Trizol reagent. 2 µg of RNA was used from each sample to synthesize cDNA by Moloney Murine Leukemia Virus (M-MulV) reverse transcriptase. 1 µL of cDNA was used to run realtime quantitative PCR reaction with SYBR® green PCR mix. 100 ng of pure cDNAs of PDK1, 2, 3, and 4 respectively were diluted to 1, 10, 100, and1000 times and realtime quantitative PCR was run simultaneously to generate standard curve for each PDK isozyme. The absolute expression of PDK1, 2,3 and 4 under attached and suspended culture conditions in MCF10A cells were obtained by comparing the ct values with the respective PDK standard curve. The data represent three independent experiments. Error bars were expressed as standard error of the mean (S.E.M.). Statistical analysis was performed using paired Student's t-test. (B) Immunoblotting. After 24 hrs of incubation, the cells under attached and suspended culture conditions were collected and lysed in denature lysis buffer with 0.1 % β-Mercaptoethanol. The samples were analyzed by 10% SDS-PAGE, followed by Immunoblotting using antibodies against PDK1, 2, 4, and α-Tubulin as loading control. Att =Attached, Susp = Suspended, and PDK = Pyruvate dehydrogenase kinase isozyme 1, 2, 3, and 4.

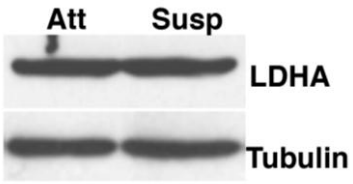

Figure 3-3. Expression of LDHA in attached and suspended MCF10A cells. MCF10A cells were grown in a 35 mm plates under attached and poly-hema coated suspended culture conditions for 24 hrs. After 24 hrs of incubation, the cells under attached and suspended culture conditions were collected and lysed in denature lysis buffer with 0.1 % β-Mercaptoethanol. The samples were analyzed by 12% SDS-PAGE, followed by Immunoblotting using polyclonal anti-LDHA antibody and mouse anti-tubulin antibody as loading control. Att = Attached, Susp = Suspended, and LDHA = Lactate dehyrogenase isoform A.

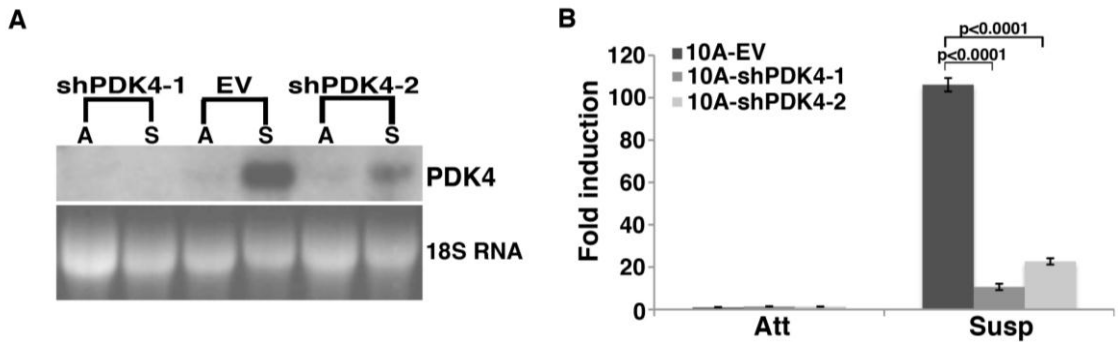

Figure 3-4. Depletion of PDK4 using retroviral short hairpin RNA in MCF10A cells. MCF10A-EV and PDK4 depleted MCF10A cells were grown in a 35 mm plates under attached and poly-hema coated suspended culture conditions for 24 hrs. After 24 hrs of incubation, the cells were collected to extract RNA using Trizol reagent. (A) Northern blotting. 10 µg of RNA from each sample was loaded onto 0.8% agarose gel, followed by 32P-labeled northern blotting was performed to analyze knockdown efficiency of PDK4 using PDK4 specific probe. 18s RNA was used for loading. (B) Realtime qRT-PCR. 2 µg of RNA was used from each sample to synthesize cDNA by Moloney Murine Leukemia Virus (M-MulV) reverse transcriptase. 1 µL of cDNA was used to run realtime quantitative PCR reaction with SYBR® green PCR mix. The relative RNA levels of PDK4 were normalized to endogenous β-Actin. These data represent triplicate experiments. Error bars were expressed as standard error of the mean (S.E.M.). Statistical analysis was performed using paired Student's t-test. A or Att = Attached, S or Susp = Suspended, EV = Empty vector, sh = shorthairpin RNA 1 and 2, and PDK4 = Pyruvate dehydrogenase kinase isozyme 4.

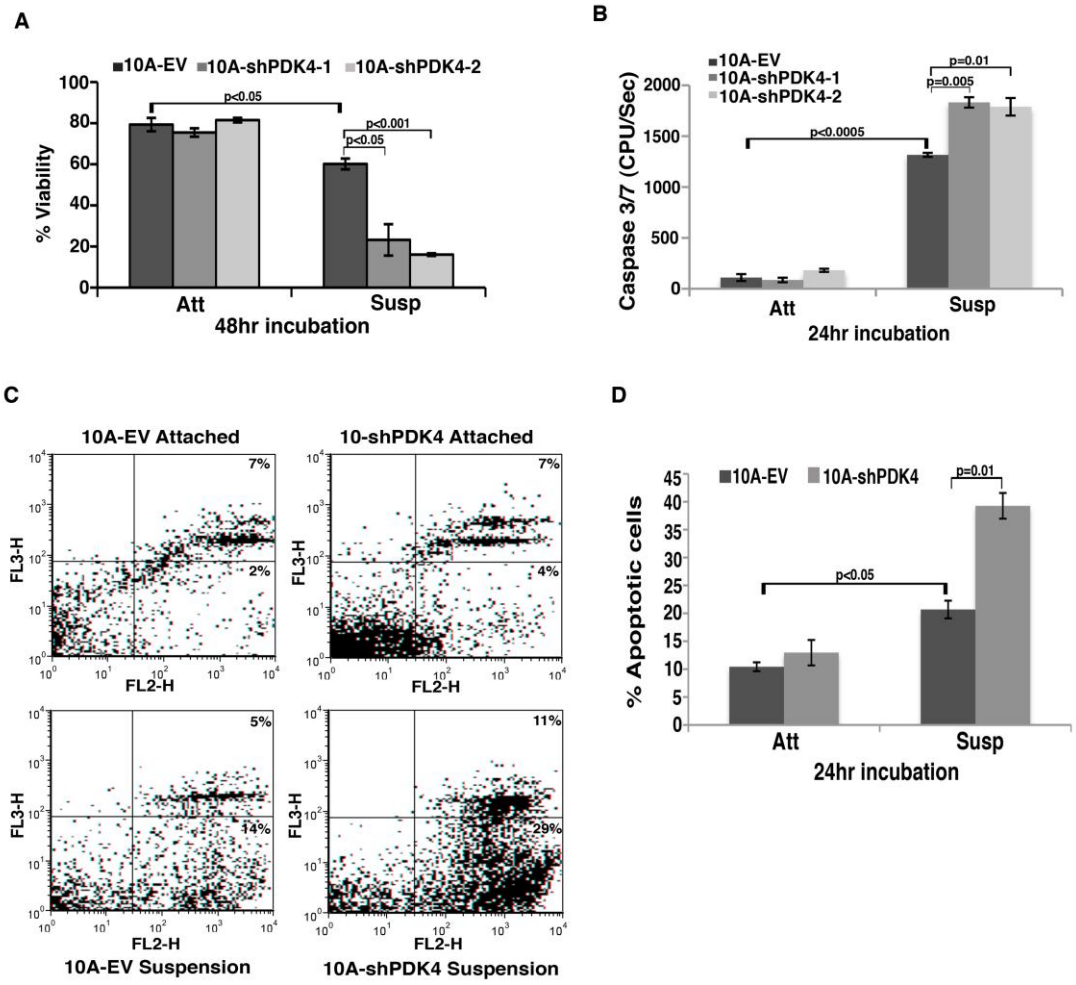

Figure 3-5. Knockdown of PDK4 sensitizes MCF10A cells to anoikis. MCF10A-EV and PDK4 depleted MCF10A cells were grown in a 35 mm plates under attached and poly-hema coated suspended culture conditions. (A) Trypan Blue (TB) exclusion assay After 48 hrs of incubation, the cells were collected from all the samples, trypzined, washed, and resuspended in 1 mL PBS. 1:1 ratio of 0.4% trypan blue dye was added to 50 µL of sample. The percentage of viable cells was counted by excluding dead cells stained blue using hemocytometer. (B) Caspase 3/7 glo assay. After 24 hrs of incubation, the cells were collected, washed and lyed in hypertonic buffer (HTB) to extract cytoplasmic protein. 100 µg of protein lysate adjusted to 20 µL volume by HTB for each sample was loaded onto 96-well microplate. Equal volume of caspase 3/7 glo substrate was added to measure caspase 3/7 activity using Luminometer. (C, D) PE-Annexin V/ 7-AAD analysis. After 24hr of incubation, the cells were collected washed twice in PBS and $1*10^5$ cells were resuspended in 100 µL of PBS. 5 µL each of PE-Annexin V and 7-AAD were added to the cells and incubated for 15 minutes at room temperature. Later, the cells were immediately analyzed by FACScan machine. A total number of 10,000 cells were analyzed for each sample (C) The dot plot representing the percentage of total number of cells that were unstained or live (Lower left

quadrant), stained positive for PE-Annexin V only (Lower right quadrant), stained positive for PE-Annexin V and 7-AAD (Upper right quadrant) and stained positive for 7-AAD alone (Upper left quadrant). FL2-H x-axis represents PE-Annexin V positive and FL3-H y-axis represent 7-AAD positive cells. (D) Statistical representation of total percentage of apoptotic cells (percentage of PE-AnnexinV only + percentage of PE-AnnexinV and 7-AAD cells). All error bars represent standard deviation (n=3). Statistical analysis was performed using paired Student's t-test. Att = Attached, Susp = Suspended, EV = Empty vector, sh = shorthairpin RNA 1 and 2, PDk4 = Pyruvate dehydrogenase kinase isozyme, PE = Phycoerythrin, 7-AAD = 7-Aminoactinomycin D, and FL2H or FL3H = fluorescence emission at its highest peak represented in logarithmic scale.

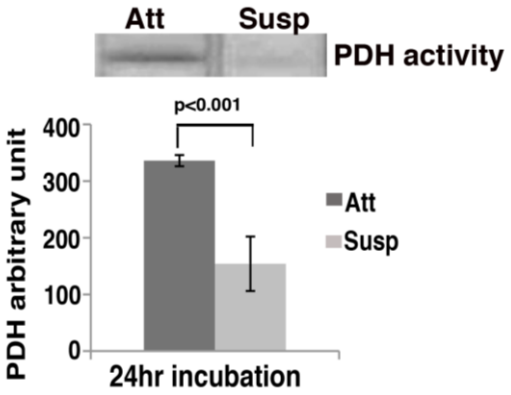

Figure 3-6. Detachment from matrix attenuates PDH activity in MCF10A cells. PDH activity was measured using Mitosciences PDH Dipstick assay kit. MCF10A cells were grown in a 35 mm plates under attached and poly-hema coated suspended culture conditions for 24 hrs. After 24 hrs of incubation, the cells were collected, washed in PBS, and lysed by adding 5 volumes of 10X sample buffer + 1/10 volume of detergent provided by the PDH activity measured using Mitoscience dipstick assay kit. After measuring protein concentration using BCA kit, 1 mg of protein was loaded onto 96-well microplate to analyze PDH activity by the kit. The signal produced by PDH activity was quantitatively represented as arbitrary units using densitometry. The data represent n=3. Att = Attached, Susp = Suspended, and PDH = Pyruvate dehydrogenase complex.

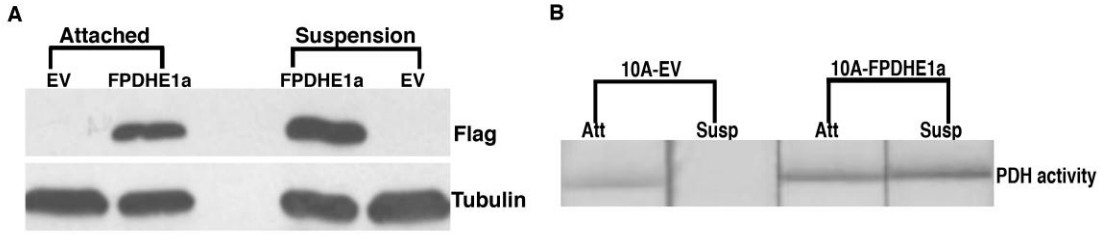

Figure 3-7. Forced expression of constitutively active PDH E1α in MCF10A cells. MCF10A cells were transduced with lentivirus carrying empty vector and FLAG-tagged PDH E1α. MCF10A-EV and 10A-FPDH E1α cells were grown in a 35 mm plates under attached and poly-hema coated suspended culture conditions for 24 hrs. (A) Immunoblotting. After 24 hrs of incubation, the cells under attached and suspended culture conditions were collected and lysed in denature lysis buffer with 0.1 % β-Mercaptoethanol. The samples were analyzed by 10% SDS-PAGE, followed by Immunoblotting using mouse polyclonal anti-FLAG antibody (1:2000) and mouse anti-tubulin antibody (1:5000) as loading control. (B**)** PDH activity assay. After 24 hrs of incubation, the cells were collected, washed in PBS, and lysed by adding 5 volumes of 10X sample buffer + 1/10 volume of detergent provided by the PDH activity measured using Mitoscience dipstick assay kit. After measuring protein concentration using BCA kit, 1 mg of protein was loaded onto 96-well microplate to analyze PDH activity by the kit. Att = Attached, Susp = Suspended, EV = Empty vector, and FPDH E1α = FLAG tagged E1α subunit of pyruvate dehydrogenase complex.

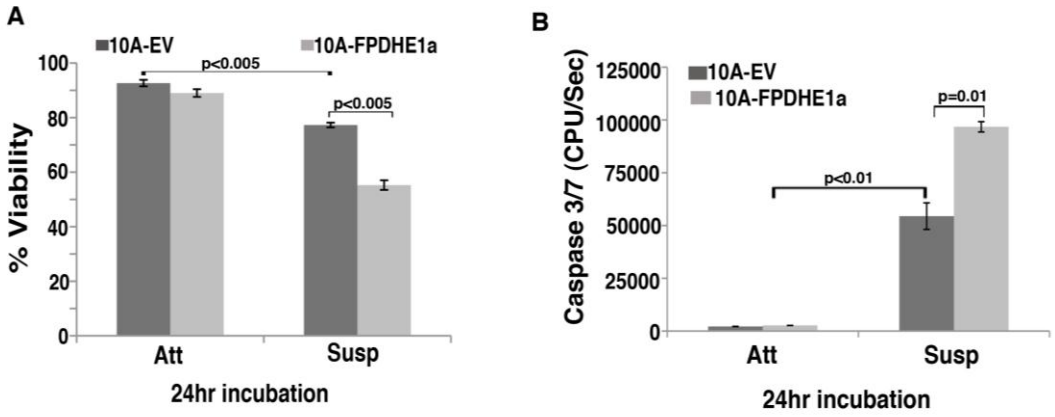

Figure 3-8. Activation of PDH sensitizes MCF10A cells to anoikis. MCF10A-EV and 10A-FPDH E1α cells were grown in a 35 mm plates under attached and poly-hema coated suspended culture conditions for 24 hrs. A) Trypan Blue (TB) exclusion assay After 24 hrs of incubation, the cells were collected from all the samples, trypzined, washed, and resuspended in 1 mL PBS. 1:1 ratio of 0.4% trypan blue dye was added to 50 µL of sample. The percentage of viable cells was counted by excluding dead cells stained blue using hemocytometer. (B) Caspase 3/7 glo assay. After 24 hrs of incubation, the cells were collected, washed and lyed in hypertonic buffer (HTB) to extract cytoplasmic protein. 100 µg of protein lysate adjusted to 20 µL volume by HTB for each sample was loaded onto 96-well microplate. Equal volume of caspase 3/7 glo substrate was added to measure caspase 3/7 activity using Luminometer. All error bars represent standard deviation (n=3). Att = Attached, Susp = Suspended, EV = Empty vector, and FPDH E1α = FLAG tagged E1α subunit of pyruvate dehydrogenase complex.

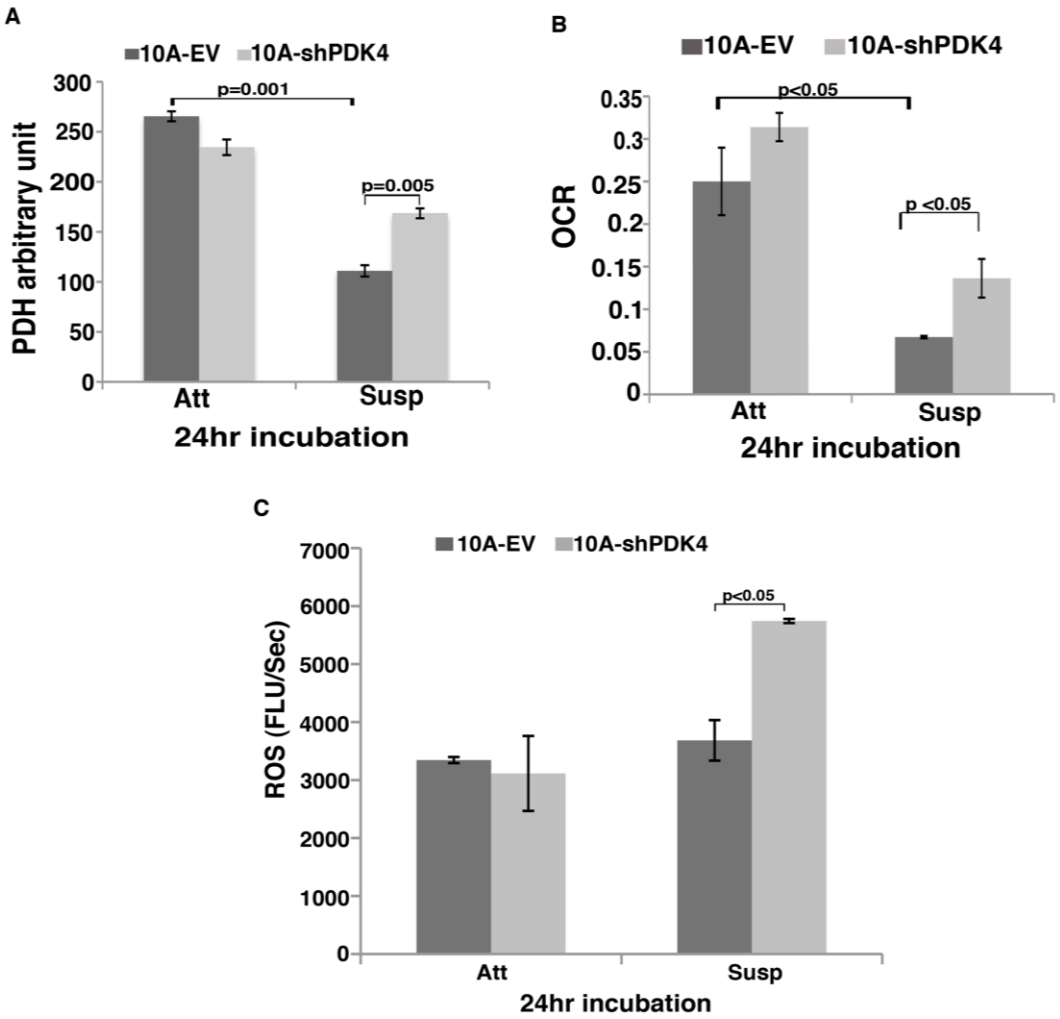

Figure 3-9. Depletion of PDK4 increases mitochondrial oxidation in MCF10A suspended cells. MCF10A-EV and PDK4 depleted MCF10A cells were grown in a 35 mm plates under attached and poly-hema coated suspended culture conditions for 24 hrs. (A) PDH activity assay. After 24hr of incubation, the cells were collected, washed in PBS, and lysed by adding 5 volumes of 10X sample buffer + 1/10 volume of detergent provided by the PDH activity measured using Mitoscience dipstick assay kit. After measuring protein concentration using BCA kit, 1 mg of protein was loaded onto 96-well microplate to analyze PDH activity by the kit. The signal produced by PDH activity was quantitatively represented as arbitrary units using densitometry. (B) Measurement of oxygen consumption rate (OCR). After 24 hrs of incubation, one million cells were loaded onto the 96-well BD Oxygen biosensor plates to measure oxygen consumption for 2hrs at 10 min interval. (C) Measurement of ROS by Amplex red hydrogen peroxide/peroxidase assay. After 24 hrs incubation, the cells were collected, washed in PBS, and lysed the cells with hypertonic buffer. Equal amount of protein was loaded onto 96-well microplate and Amplex red hydrogen peroxide/peroxidase substrate was added to analyze the ROS levels at fluorescence wavelength of 590/630 nm

(excitation/emission). All error bars represent standard deviation (n=3). Att = Attached, Susp = Suspended, EV = Empty vector, sh = short hairpin RNA, PDK4 = Pyruvate dehydrogenase kinase isozyme, PDH= Pyruvate dehydrogenase complex, OCR= Oxygen consumption rate, ROS = Reactive oxygen species, and FLU= Fluoroscence units.

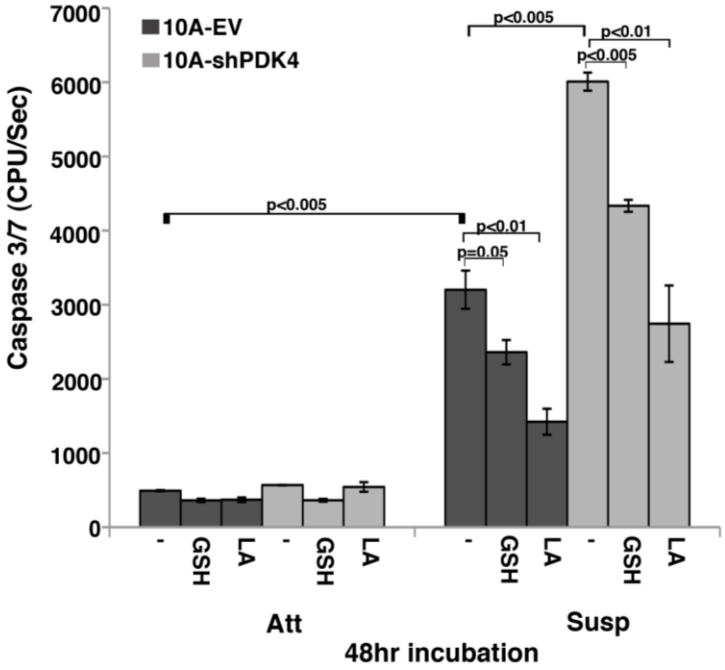

Figure 3-10. Antioxidant treatment rescues PDK4 depleted MCF10A cells from anoikis. Caspase 3/7 glo assay. MCF10A-EV and PDK4 depleted MCF10A cells were grown in a 35 mm plates under attached and poly-hema coated suspended culture conditions for 48 hrs. The cells were treated with (i) untreated represented as -, (ii) 2.5 mM L-glutathione represented as GSH, and (iii) 100 μM α-Lipoic acid represented as LA for 48 hrs. After 48 hrs of incubation, the cells were collected, washed and lyed in hypertonic buffer (HTB) to extract cytoplasmic protein. 100 μg of protein lysate adjusted to 20 μL volume by HTB for each sample was loaded onto 96-well microplate. Equal volume of caspase 3/7 glo substrate was added to measure caspase 3/7 activity using Luminometer. All error bars represent standard deviation (n=3). Att = Attached, Susp = Suspended, EV = Empty, sh = short hairpin RNA, PDK4 = Pyruvate dehydrogenase kinase isozyme 4, (-) = untreated, GSH = L-glutathione, and LA= α-Lipoic acid.

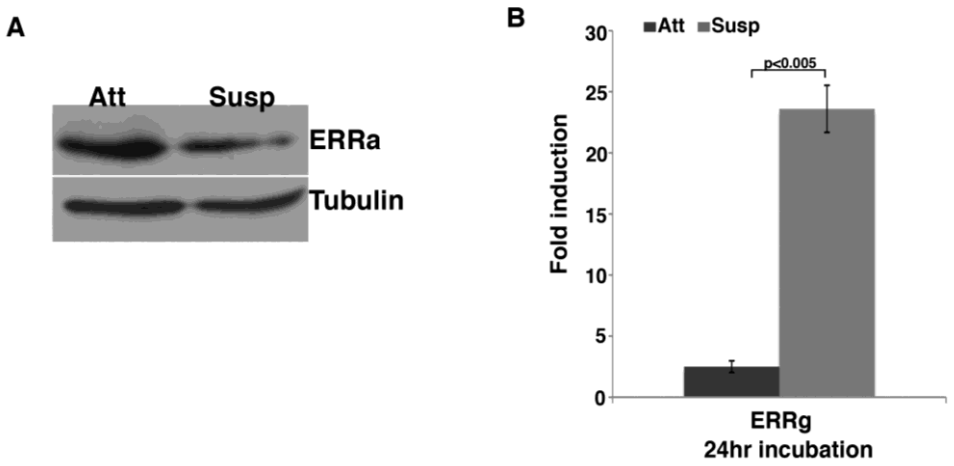

Figure 3-11. Induction of ERRγ in MCF10A suspended culture conditions. MCF10A cells were grown in a 35 mm plates under attached and poly-hema coated suspended culture conditions for 24 hrs. (A) Immunoblotting. After 24 hrs of incubation, the cells under attached and suspended culture conditions were collected and lysed in denature lysis buffer with 0.1 % β-Mercaptoethanol. The samples were analyzed by 10% SDS-PAGE, followed by Immunoblotting using polyclonal anti-ERRα antibody and mouse anti-tubulin antibody as loading control. (B) Realtime qRT-PCR. After 24 hrs of incubation, the cells were collected to extract RNA using Trizol reagent. 2 µg of RNA was used from each sample to synthesize cDNA by Moloney Murine Leukemia Virus (M-MulV) reverse transcriptase. 1 µL of cDNA was used to run realtime quantitative PCR reaction with SYBR® green PCR mix. The relative RNA levels of ERRγ were normalized to endogenous β-Actin. All error bars represent standard deviation (n=3) Att = Attached, Susp = Suspended, ERRa = Estrogen related receptor isoform alpha, and ERRg = Estrogen related receptor isoform gamma.

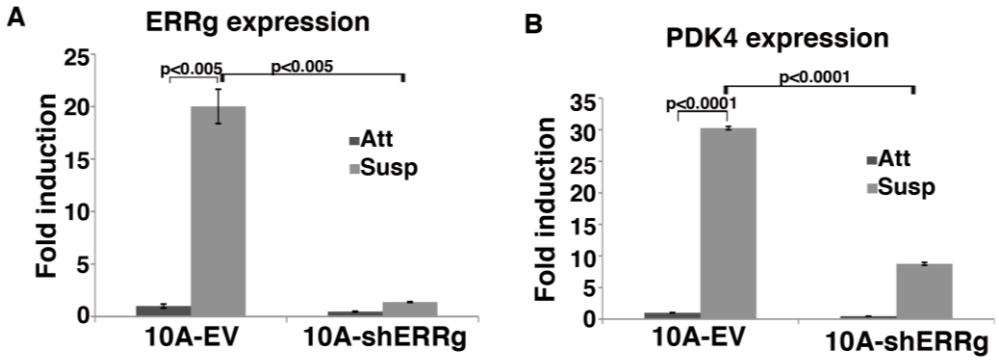

Figure 3-12. Depletion of ERRγ represses PDK4 induction in MCF10A suspended cells. MCF10A cells were transduced with a retroviral empty vector ("EV") or shRNA targeting ERRγ ("shERRg"). Cells were grown in a 35 mm plates under attached and poly-hema coated suspended culture conditions for 24 hrs and total RNA was extracted and analyzed by quantitative RT-PCR. (A) Depletion of ERRγ in MCF10A. (B) Attenuation of PDK4 induction following cell detachment in ERRγ depleted MCF10A. All error bars represent standard deviation (n=3). Att = Attached, Susp = Suspended, ERRg = Estrogen related receptor isoform gamma, and PDK4 = Pyruvate dehydrogenase kinase, sh = shorthairpin RNA.

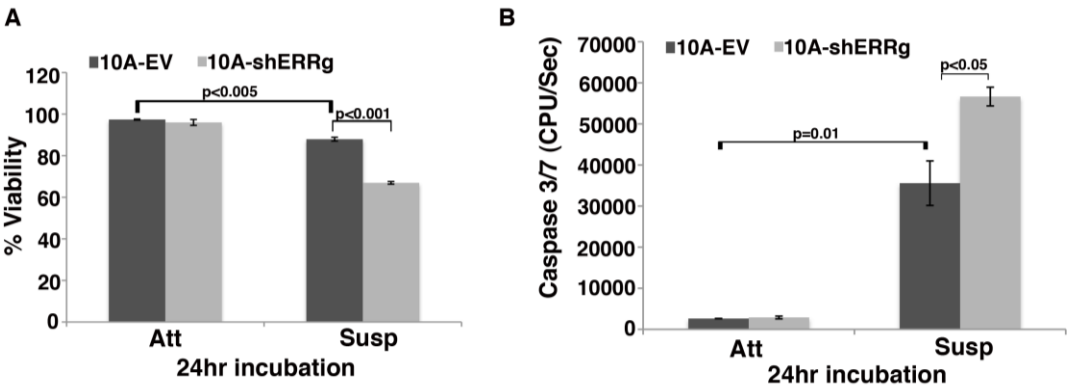

Figure 3-13. Depletion of ERRγ increases anoikis in MCF10A suspended cells. MCF10A cells were transduced with a retroviral empty vector ("EV") or shRNA targeting ERRγ ("shERRg"). Cells were grown in a 35 mm plates under attached and poly-hema coated suspended culture conditions for 24 hrs. (A) Trypan Blue (TB) exclusion assay. After 24hr of incubation, the cells were collected from all the samples, trypzined, washed, and resuspended in 1 mL PBS. 1:1 ratio of 0.4% trypan blue dye was added to 50 µL of sample. The percentage of viable cells was counted by excluding dead cells stained blue using hemocytometer. (B) Caspase 3/7 glo assay. After 24hr of incubation, the cells were collected, washed and lyed in hypertonic buffer (HTB) to extract cytoplasmic protein. 100 µg of protein lysate adjusted to 20 µL volume by HTB for each sample was loaded onto 96-well microplate. Equal volume of caspase 3/7 glo substrate was added to measure caspase 3/7 activity using Luminometer. All error bars represent standard deviation (n=3). Att = Attached, Susp = Suspended, ERRg = Estrogen related receptor isoform gamma, and sh = shorthairpin RNA.

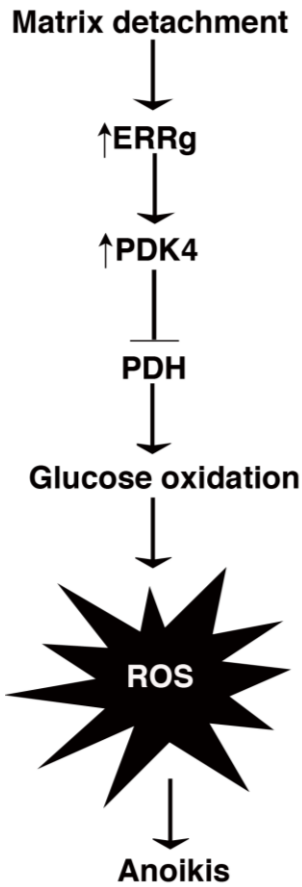

Figure 3-14. Summary model. Upon detachment from ECM, the MCF10A cells upregulate ERRγ to induce PDK4 to attenuate mitochondrial oxidation in order to prevent ROS production and thereby resist anoikis.

CHAPTER 4
PDK PROMOTES ANOIKIS RESISTANCE AND TUMOR METASTASIS IN BREAST CANCER CELLS

Background

Tumor cells are formed due to genetic alterations in signaling pathways leading to abnormal cell growth and survival. The two major signaling pathways that are often found mutated in different tumors are Ras-extracellular signal-regulated kinase (ERK) and the Phosphatidyllinositol-3-OH kinase (PI(3)K)-AKT pathways[29]. These aberrant mutations cause inappropriate cell growth and survival. The rapidly dividing and proliferating tumor cells eventually outgrow their vascular supply, resulting in a hypoxic environment (low oxygen levels). The major consequence of hypoxia is to activate different hypoxia-inducible genes, which include glycolysis related genes such as Hexokinase II, Glut1 receptors, LDHA, PDK1, PDK3, pH regulated genes such as Carbonic anhydrase 9 and CA12, and angiogenic genes such as vascular endothelial growth factor (VEGF) and angiopoietin 2[105]. All these genes help tumor growth and invasion. Furthermore, the hypoxic environment favors tumor metastasis by activating epithelial to mesenchymal transition (EMT), regulating integrin interactions to facilitate tissue rupture and invasion, and upregulating vascular endothelial growth factor (VEGF) for angiogenesis and vascular formation[106].

Cancer cells possess both altered energy metabolism and resistance to anoikis, but the connection between them is yet to be elucidated. Schafer et al., were the first to demonstrate the potential link between glucose metabolism and anoikis in untransformed mammary epithelial cells[68]. Their report showed that detachment from ECM led to metabolic defect in MCF10A cells. Forced overexpression of oncoprotein ErbB2/HER2 rescued these cells from oxidative stress, restored ATP generation, and

supported anchorage-independent cell survival. However, it is less clear how ATP deficiency is linked to cell death.

In the current study, we show that breast tumor cells have attenuated oxidative metabolism of glucose compared to the normal cells. Furthermore, detachment from ECM in cancer cells exhibits a dramatic shift from mitochondrial respiration towards glycolysis by upregulating PDKs. In other words, the tumor cells show a further increase in aerobic glycolysis to survive and metastasize to distant organs. Activation of mitochondrial oxidation either by depletion of PDK or forced over-expression of PDH E1α sensitizes cancer cells to anoikis and abrogates their metastatic potential. These observations indicate that the Warburg effect in tumor cells promotes anoikis resistance and contributes to the malignant phenotypes.

Results

Induction of PDK4 Promotes Anoikis Resistance in RAS-Transformed Mammary Epithelial Cells

Induction of PDK4 in Ras-transformed MCF10A cells (10ACA1.1)

Our study has demonstrated that matrix detachment induced PDK4 via ERRγ in untransformed mammary epithelial cells (Chapter 3). Next, we investigated if a similar survival mechanism existed in Ras- transformed MCF10A derivative cell line (MCF10A CA1.1). These cells not only harbor the activated oncogene Ras but also certain unindentified spontaneous mutations which led to generation of a highly tumorogenic cell line[107]. Similar to MCF10A, MCF10CA1.1 cells upregulated PDK4 at RNA level under the detached condition as shown by northern blotting (Figure 4-1). No detectable expression of PDK4 was observed under attached culture condition (Figure 4-1).

PDK4 resists anoikis in Ras-transformed MCF10A cells (MCF10ACA1.1)

To test the functional significance of PDK4 in MCF10ACA1.1, PDK4 was depleted in MCF10CA1.1 cells with two independent retroviral shRNAs and their knockdown efficiency was confirmed by northern blotting. The depletion of PDK4 in MCF10ACA1.1 was approximately 80% by shPDK4-1 and ~90% by shPDK4-2 when compared to the empty vector (EV) under detached condition (Figure 4-1). Unlike untransformed MCF10A cells, MCF10CA1.1 transduced with EV did not exhibit significant cell death when placed in suspension; however, depletion of PDK4 sensitized them to cell death (Figure 4-2A). The significant decrease in cell viability in PDK4 depleted MCF10ACA1.1 detached cells was due to increased anoikis as shown by caspase 3/7activity (Figure 4-2B).

Collectively, our results indicate that matrix detachment leads to induction of PDK4 to promote anoikis resistance in both untransformed and malignant mammary epithelial cells.

Warburg Effect Promotes Anoikis Resistance and Metastasis in Breast Tumor Cells

Matrix detachment favors Warburg effect in MDA-MB-231 cells

The hallmark of cancer cells is anoikis resistance. Since most cancer cells prefer aerobic glycolysis to mitochondrial respiration, we hypothesized that reduced mitochondrial oxidation provides survival advantage to malignant tumor cells when detached from matrix. To test our hypothesis, we investigated the impact of Warburg effect on anoikis resistance in an aggressive, metastatic, and highly glycolytic triple-negative breast cancer cell line MDA-MB-231[108]. First, we compared the PDH activity in MDA-MB-231 cells cultured under attached and suspended conditions. As expected,

the MDA-MB-231 cells displayed lower PDH activity under attached conditions (Figure 4-3) compared to MCF10A (Figure 1-7); however, the suspended MDA-MB-231 cells demonstrated a significant decrease in PDH activity compared to attached cells (Figure 4-3). Thus, our data suggest that upon detachment from matrix, breast tumor cells demonstrate a further reduction in mitochondrial activity.

Forced activation of mitochondrial oxidation induces anoikis in MDA-MB-231

We investigated the significance of reduced mitochondrial activity in MDA-MB-231 under suspension culture conditions. As performed in MCF10A, we ectopically expressed the constitutively active form of PDH E1α with c-terminal FLAG tag in MDA-MB-231 using lentiviral transduction method. Meanwhile, we infected MDA-MB-231 with lentivirus carrying empty vector (EV) as control. Overexpression of PDH E1α was confirmed by western blotting (Figure 4-4A). To test if the ectopically expressed PDH E1α was enzymatically active, we measured PDH activity in these cells. The MDA-MB-231 cells expressing constitutively active form of PDH E1α showed significantly increased PDH activity compared to MDA-MB-231 cells expressing EV (Figure 4-4B).

Next, we investigated the impact of increased mitochondrial activity on anoikis in MDA-MB-231 cells. Since cancer cells are resistant to detachment-induced cell death, MDA-MB-231 cells transduced with EV did not display significant cell death under detached culture conditions (Figure 4-5A); however, forced increase of PDH activity sensitized MDA-MB-231 cells to cell death only under detached culture conditions (Figures 4-5A). The increased anoikis was attributed to increased apoptosis in MDA-MB-231 cells expressing constitutively active form of PDH E1α (Figure 4-5B). These results suggest that breast tumor cells significantly attenuate mitochondrial oxidation to survive longer after detachment from matrix.

PDK1 enhances Warburg effect in matrix detached MDA-MB-231 cells

To this point, our results suggest that breast tumor cells display a significant decrease of mitochondrial oxidation upon matrix detachment to survive longer. To test if the PDK isozymes regulate the mitochondrial activity under detached condition as observed in MCF10A and RAS-transformed MCF10A cells, we examined the expression of all four PDKs under attached and suspended culture conditions. PDK4 RNA was significantly upregulated in MDA-MB-231 cells upon matrix detachment (Figure 4-6A), but its overall abundance was trivial when compared with other PDKs (Figure 4-6B). PDK1 was the predominant PDK isoenzyme in MDA-MB-231 cells both under attached and detached culture conditions as identified by quantitative RT-PCR (Figure 4-6B). Although the RNA level of PDK1 in MDA-MB-231 cells did not change upon detachment from matrix, its protein level was significantly increased compared to attached cells (Figure 4-6C).

These data indicate that MDA-MB-231 cells upregulate PDK1 to downregulate mitochondrial oxidation in suspension. Therefore, to activate mitochondrial oxidation in MDA-MB-231 cells, we depleted the predominant PDK isoenzyme i.e., PDK1 using two independent retroviral short hairpin RNAs. The knockdown efficiency of PDK1 was confirmed by western blotting (Figure 4-7A). The depletion of PDK1 led to increased PDH activity in MDA-MB-231 cells both under attached and detached culture conditions (Figure 4-7B), indicating a glucose metabolic shift toward mitochondrial oxidation from glycolysis. To test that, we measured intracellular lactate levels in PDK1 depleted MDA-MB-231 cells. As expected, MDA-MB-231 cells carrying EV produced increased lactate levels in suspended cells compared to attached ones (Figure 4-7C); however, depletion of PDK1 significantly decreased lactate production both under attached and detached

culture conditions (Figure 4-7C). Since we observed a significant decrease in lactate levels and increase in PDH activity, we measured the oxygen consumption rate (OCR) in PDK1 depleted MDA-MB-231 cells to confirm an increase in mitochondrial respiration. Consistent with our observations, MDA-MB-231 cells displayed decreased OCR in detached cells compared to attached cells (Figure 4-7D), but knockdown of PDK1 increased O_2 consumption rate in these cells both under attached and suspended culture conditions (Figure 4-7D). These results suggest that matrix detachment further enhances the glycolytic phenotype in MDA-MB-231 cells and depletion of PDK1 in these cells reverses the Warburg effect, shifting glucose metabolism from glycolysis towards mitochondrial oxidation.

Depletion of PDK1 activates mitochondrial oxidation and abrogates anoikis resistance in MDA-MB-231 cells

Depletion of PDK1 significantly reversed the Warburg effect in MDA-MB-231 cells both under attached and detached culture conditions; therefore, we investigated the potential effect of this metabolic shift on anoikis. Not surprisingly, MDA-MB-231 cells expressing EV did not show any significant cell death (Figure 4-8A) or apoptosis (Figure 4-8B) when grown in suspension. Although depletion of PDK1 increased PDH activity and reversed the Warburg effect in MDA-MB-231 cells under attached culture condition, it did not induce cell death (Figure 4-8A) or apoptosis (Figure 4-8B). Only when MDA-MB-231 cells were detached from matrix did depletion of PDK1 induce cell death (Figure 4-8A) and apoptosis (Figure 4-8B).

Together, these results suggest that normalization of glucose metabolism by depletion of PDK or activation of PDH is capable of restoring anoikis in breast cancer cells.

PDK1 enhances breast tumor metastasis *in vivo*

Resistance to anoikis is one of the critical steps for tumor metastasis. Depletion of PDK1 sensitized the highly malignant MDA-MB-231 cells to anoikis by reversing the Warburg effect *in vitro*, therefore, we examined the physiological relevance of this metabolic manipulation on cancer metastasis. A common experimental model to analyze tumor metastasis *in vivo* is tail vein injection experimental metastasis assay. It measures the ability of cancer cells to survive in the blood circulation, extravasate, and form metastatic colonies at distant secondary sites.

MDA-MB-231 cells carrying EV and PDK1-depleted MDA-MB-231 cells were cultured under adherent conditions, then trypsinized, and equal number of cells ($1*10^6$ cells/200 µL) from each group were intravenously injected into immunodeficient mice (Six mice in each group). After 40 days post-injection, control MDA-MB-231 cells gave rise to about 100 tumor nodules per lung in all 6 mice analyzed (Figure 4-9A). Consistent with our *in vitro* observations, the mice injected with PDK1-depleted MDA-MB-231 cells produced significantly less number of lung tumor nodules (Figure 4-9A). The immunohistochemical staining of Hemotoxylin and Eosin (H&E) did not show any significant morphological differences between control and PDK1-depleted lung tumor tissues (Figure 4-9A). There was a five-fold decrease in the lung tumor nodule formation in mice injected with PDK1-depleted MDA-MB-231 cells compared to control mice (Figure 4-9B). Therefore, reversal of the Warburg effect by depletion of PDK1 not only sensitized metastatic cancer cells to anoikis *in vitro*, but also profoundly decreased their metastatic potential *in vivo*.

Summary

Tumor cells exhibit aerobic glycolysis / Warburg effect and resistance to anoikis to survive and thrive the harsh environments. It has been well established that Warburg effect helps tumor growth and survival. However, its role in promoting anoikis resistance and tumor metastasis glucose is still not clear. Therefore, we focused our study understanding the role of altered glucose metabolism in regulating anoikis resistance to promote metastasis *in vivo*. Based on our results, we conclude that upon detachment from ECM, tumor cells take advantage of their altered glucose metabolism i.e., Warburg effect by upregulating the PDKs to survive and invade the distant organs. Furthermore, depletion of PDK or forced activation of PDH increases mitochondrial respiration and, thus sensitizes these tumor cells to anoikis and abrogates their metastatic potential *in vivo.* Therefore, our study implicates that the PDK enzymes are potential therapeutic drug targets to prevent both tumor growth and metastasis.

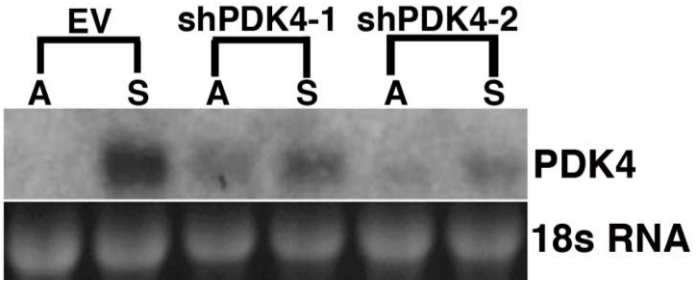

Figure 4-1. Detachment from matrix upregulates PDK4 in Ras-transformed MCF10A cells (MCF10ACA1.1). Northern blotting. 10ACA1.1-EV and PDK4 depleted 10ACA1.1 cells were grown in a 35 mm plates under attached and poly-hema coated suspended culture conditions for 48 hrs. After 48 hrs of incubation, the cells were collected to extract RNA using Trizol reagent. 10 µg of RNA from each sample was loaded onto 0.8% agarose gel, followed by ^{32}P-labeled northern blotting was performed to analyze knockdown efficiency of PDK4 using PDK4 specific probe. 18s RNA was used for loading. A = Attached, S = Suspended, EV= Empty vector, sh = Shorthairpin, and PDK4 = Pyruvate dehydrogenase kinase isozyme 4.

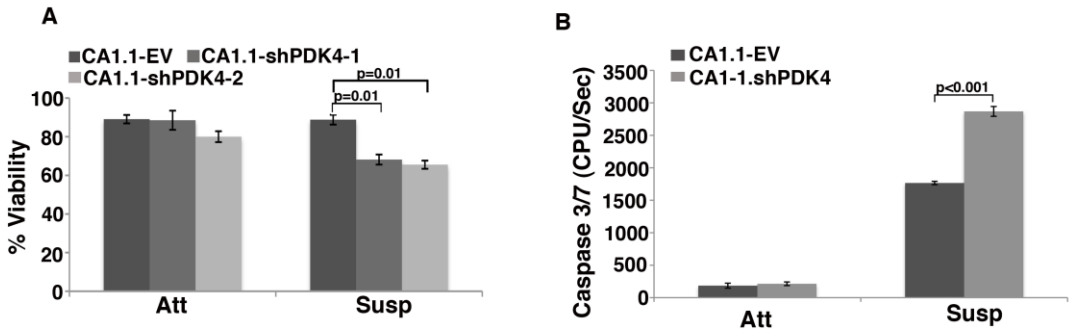

Figure 4-2. Depletion of PDK4 sensitizes MCF10ACA1.1 cells to anoikis. Activation of PDH sensitizes MCF10A cells to anoikis. 10ACA1.1-EV and PDK4 depleted 10ACA1.1 cells were grown in a 35 mm plates under attached and poly-hema coated suspended culture conditions for 48 hrs. (A) Trypan Blue (TB) exclusion assay After 48hr of incubation, the cells were collected from all the samples, trypzined, washed, and resuspended in 1 mL PBS. 1:1 ratio of 0.4% trypan blue dye was added to 50 µL of sample. The percentage of viable cells was counted by excluding dead cells stained blue using hemocytometer. (B) Caspase 3/7 glo assay. Only 10ACA1.1-shPDK4-2 was used for this assay. After 48 hrs of incubation, the cells were collected, washed and lyed in hypertonic buffer (HTB) to extract cytoplasmic protein. 100 µg of protein lysate adjusted to 20 µL volume by HTB for each sample was loaded onto 96-well microplate. Equal volume of caspase 3/7 glo substrate was added to measure caspase 3/7 activity using Luminometer. All error bars represent standard deviation (n=3). Att = Attached, Susp = Suspended, EV = Empty vector, sh =Shorthairpin, and PDK4=Pyruvate dehydrogenase kinase isozyme 4.

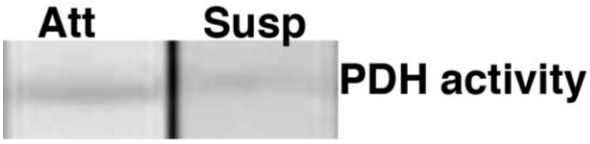

Figure 4-3. Matrix detachment attenuates PDH activity in MDA-MB-231cells. PDH activity assay. MDA-MB-231 cells were grown in a 35 mm plates under attached and poly-hema coated suspended culture condition for 48 hrs. After 48 hrs incubation, the cells were collected, washed in PBS, and lysed by adding 5 volumes of 10X sample buffer + 1/10 volume of detergent provided by the PDH activity measured using Mitoscience dipstick assay kit. After measuring protein concentration using BCA kit, 1 mg of protein was loaded onto 96-well microplate to analyze PDH activity by the kit. Att = Attached, Susp = Suspended, and PDH = Pyruvate dehydrogenase complex.

Figure 4-4. Forced expression of constitutively active PDHE1α in MDA-MB-231 cells. MDA-MB-231 cells were transduced with lentivirus carrying empty vector and FLAG-tagged PDH E1α. (A) Immunoblotting. MDA231-EV and MDA231-FPDH E1α cells were grown in a 35 mm plates under attached and poly-hema coated suspended culture conditions for 48 hrs. After 48 hrs of incubation, the cells under attached and suspended culture conditions were collected and lysed in denature lysis buffer with 0.1 % β-Mercaptoethanol. The samples were analyzed by 10% SDS-PAGE, followed by Immunoblotting using mouse polyclonal anti-FLAG antibody (1:2000) and mouse anti-tubulin antibody (1:5000) as loading control. (B**)** PDH activity assay. MDA231-EV and MDA231-FPDH E1α cells were grown in a 35 mm plates under attached culture condition for 48 hrs. After 48 hrs of incubation, the cells were collected, washed in PBS, and lysed by adding 5 volumes of 10X sample buffer + 1/10 volume of detergent provided by the PDH activity measured using Mitoscience dipstick assay kit. After measuring protein concentration using BCA kit, 1 mg of protein was loaded onto 96-well microplate to analyze PDH activity by the kit. Att = Attached, Susp = Suspended, EV = Empty vector, and FPDH E1α = FLAG tagged E1α subunit of pyruvate dehydrogenase complex.

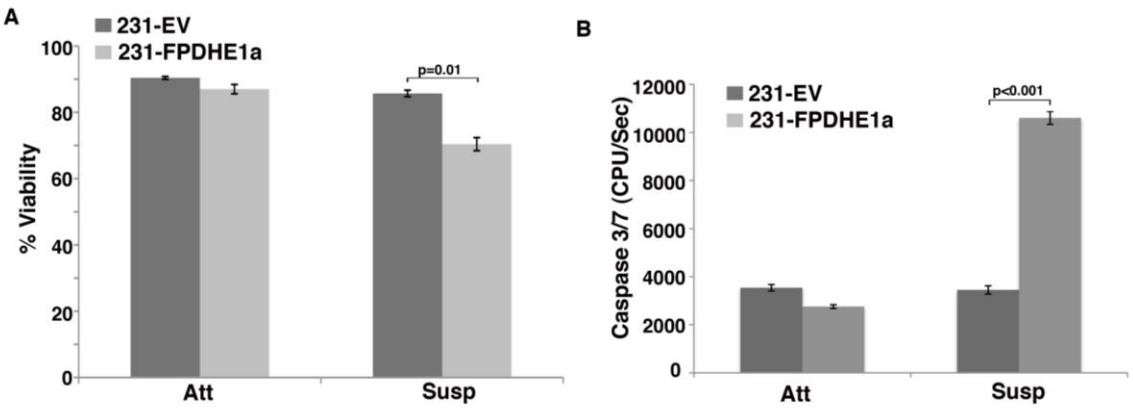

Figure 4-5. Forced activation of PDH induces anoikis in MDA-MB-231 cells. MDA231-EV and MDA231-FPDH E1α cells were grown in a 35 mm plates under attached and poly-hema coated suspended culture conditions for 48 hrs. (A) Trypan Blue (TB) exclusion assay After 48 hrs of incubation, the cells were collected from all the samples, trypzined, washed, and resuspended in 1 mL PBS. 1:1 ratio of 0.4% trypan blue dye was added to 50 µL of sample. The percentage of viable cells was counted by excluding dead cells stained blue using hemocytometer. (B) Caspase 3/7 glo assay. After 48 hrs of incubation, the cells were collected, washed and lyed in hypertonic buffer (HTB) to extract cytoplasmic protein. 100 µg of protein lysate adjusted to 20 µL volume by HTB for each sample was loaded onto 96-well microplate. Equal volume of caspase 3/7 glo substrate was added to measure caspase 3/7 activity using Luminometer. All error bars represent standard deviation (n=3). Att = Attached, Susp = Suspended, EV = Empty vector, and FPDH E1α= FLAG tagged E1α subunit of pyruvate dehydrogenase complex.

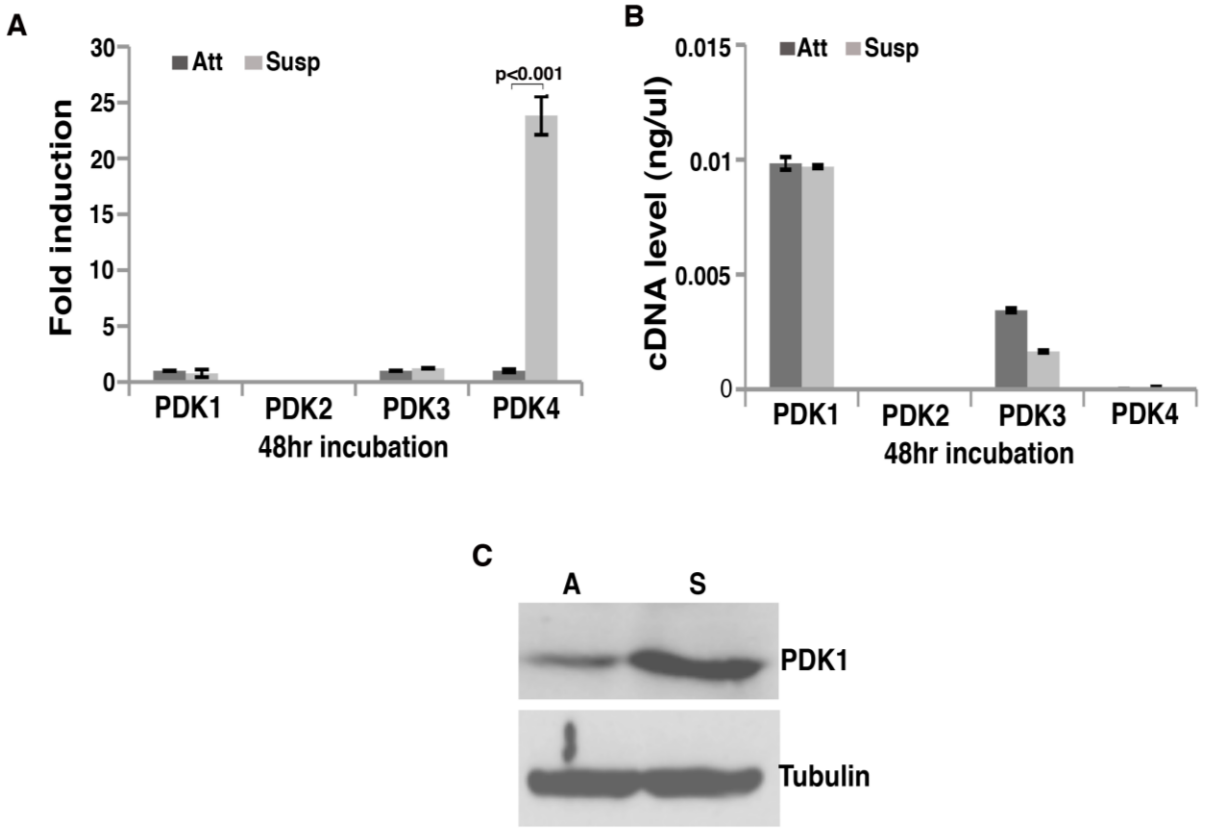

Figure 4-6. Induction of PDK1 at protein level in MDA-MB231 upon detachment from matrix. MDA-MB-231 cells were grown in a 35 mm plates under attached and poly-hema coated suspended culture conditions for 48 hrs. (A, B) After 48 hrs of incubation, the cells were collected to extract RNA using Trizol reagent. 2 µg of RNA was used from each sample to synthesize cDNA by Moloney Murine Leukemia Virus (M-MulV) reverse transcriptase. 1 µL of cDNA was used to run realtime quantitative PCR reaction with SYBR® green PCR mix. (A) Relative PDK expression. The relative RNA levels of PDK1, PDK2, PDK3, and PDK4 were normalized to endogenous β-Actin. (B) Absolute PDK expression. 100 ng of pure cDNAs of PDK1, 2, 3, and 4 respectively were diluted to 1, 10, 100, and1000 times and realtime quantitative PCR was run simultaneously to generate standard curve for each PDK isozyme. The absolute expression of PDK1, 2,3 and 4 under attached and suspended culture conditions in MDA-MB-231 cells were obtained by comparing the ct values with the respective PDK standard curve. (C) Immunoblotting. After 48 hrs of incubation, the cells under attached and suspended culture conditions were collected and lysed in denature lysis buffer with 0.1 % β-Mercaptoethanol. The samples were analyzed by 10% SDS-PAGE, followed by Immunoblotting using rabbit polyclonal anti-PDK1 (1:1000) and mouse anti-α-Tubulin antibody (1:5000) as loading control. The data represent three independent experiments. Error bars were expressed as standard error of the mean (S.E.M.). Statistical analysis was performed using paired Student's t-

test. Att = Attached, Susp = Suspended, and PDK = Pyruvate dehydrogenase kinase isozyme 1, 2, 3, and 4.

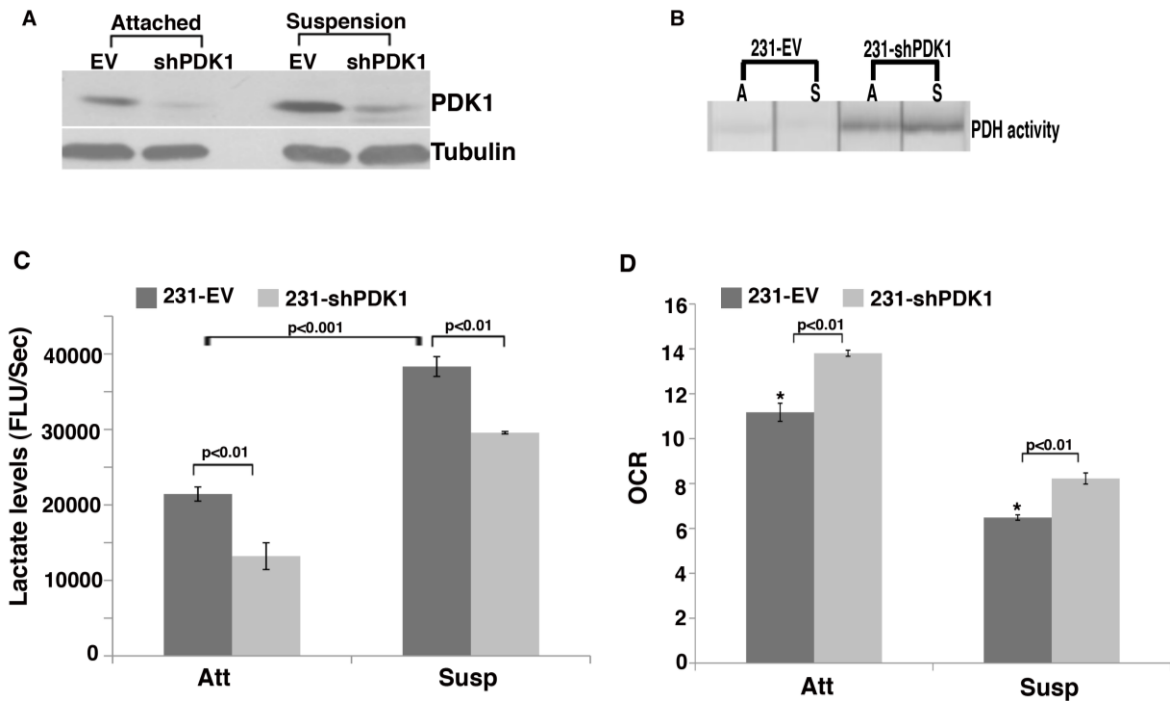

Figure 4-7. Depletion of PDK1 switches glucose metabolism towards mitochondrial oxidation in MDA-MB-231 cells. MDA231-EV and MDA231-shPDK1 cells were grown in 35 mm plates under attached and poly-hema coated suspended culture conditions for 48 hrs. (A) Immunoblotting. After 48 hrs of incubation, the cells under attached and suspended culture conditions were collected and lysed in denature lysis buffer with 0.1 % β-Mercaptoethanol. The samples were analyzed by 10% SDS-PAGE, followed by Immunoblotting using rabbit polyclonal anti-PDK1 (1:1000) and mouse anti-α-Tubulin antibody (1:5000) as loading control. (B) PDH activity assay. After 48 hrs of incubation, the cells were collected, washed in PBS, and lysed by adding 5 volumes of 10X sample buffer + 1/10 volume of detergent provided by the PDH activity measured using Mitoscience dipstick assay kit. After measuring protein concentration using BCA kit, 1 mg of protein was loaded onto 96-well microplate to analyze PDH activity by the kit. (C) Lactate assay. After 48 hrs of incubation, one million cells were added to 96-well microplate. Equal volume of reaction mix provided by kit was added to each sample to measure lactate levels at Ex/EM 0f 590/630 nm. (D) Measurement of oxygen consumption rate (OCR). After 48 hrs of incubation, one million cells were loaded onto the 96-well BD Oxygen biosensor plates to measure oxygen consumption for 2hrs at 10 minutes interval. The data represent three independent experiments. Error bars were expressed as standard error of the mean (S.E.M.). Statistical analysis was performed using paired Student's t-test. Att = Attached, Susp = Suspended, EV =Empty vector, PDK1 = Pyruvate dehydrogenase kinase 1.

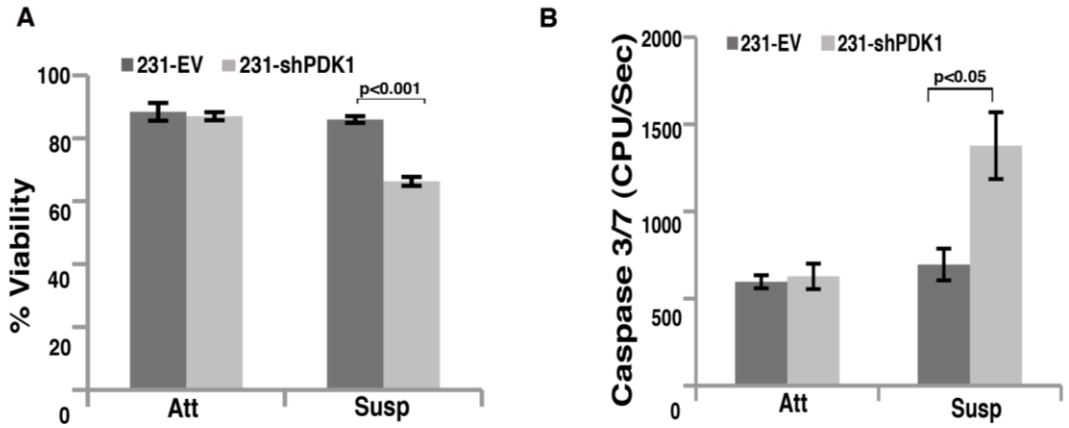

Figure 4-8. Depletion of PDK1 abolishes anoikis resistance in MDA-MB-231 cells. MDA231-EV and MDA231-shPDK1 cells were grown in 35 mm plates under attached and poly-hema coated suspended culture conditions for 48 hrs. (A) Trypan Blue (TB) exclusion assay After 48 hrs of incubation, the cells were collected from all the samples, trypzined, washed, and resuspended in 1 mL PBS. 1:1 ratio of 0.4% trypan blue dye was added to 50 µL of sample. The percentage of viable cells was counted by excluding dead cells stained blue using hemocytometer. (B) Caspase 3/7 glo assay. After 48 hrs of incubation, the cells were collected, washed and lyed in hypertonic buffer (HTB) to extract cytoplasmic protein. 100 µg of protein lysate adjusted to 20 µL volume by HTB for each sample was loaded onto 96-well microplate. Equal volume of caspase 3/7 glo substrate was added to measure caspase 3/7 activity using Luminometer. All error bars represent standard deviation (n=3). Att = Attached, Susp = Suspended, EV= Empty vector, and PDK = Pyruvate dehydrogenase kinase.

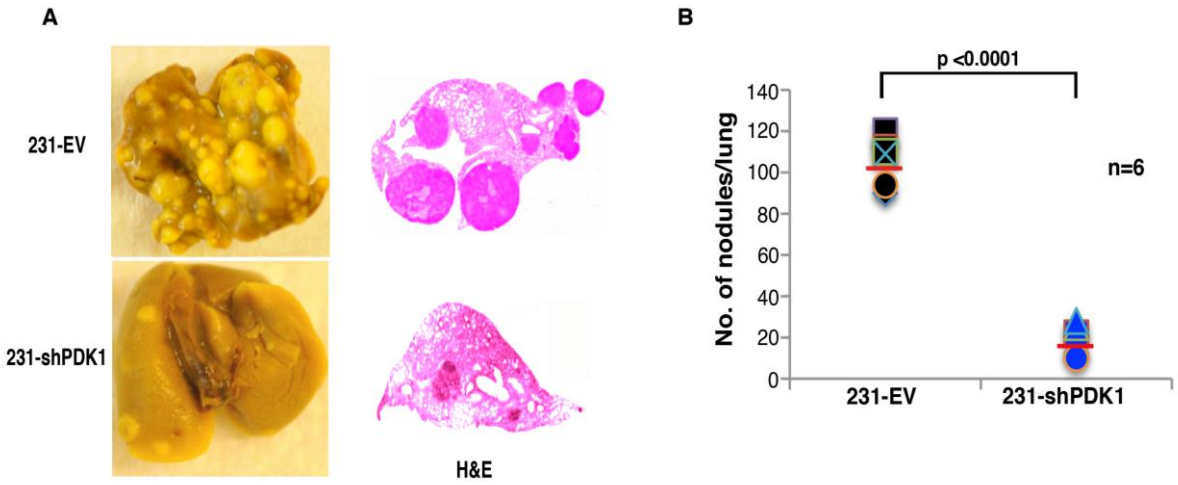

Figure 4-9. Depletion of PDK1 abrogates tumor metastasis *in vivo.* MDA231-EV and MDA231-shPDK1 cells were grown in 100 mm plates under attached condition. The cells were trypsinized and washed twice in PBS. Two million cells were resuspended in 200 µL of PBS and injected intravenously in six 4-5 weeks old nude mice for each group (231-EV and 231-shPDK1). Forty days post-injection, the lungs from the injected mice were harvested. (A) The entire lung picture with tumor nodules and H&E staning. For counting the nodules, the harvested lungs for fixed in Bouin's fixative. For H&E staining, the lung was fixed in 4% paraformaldehyde (PFA) solution for 24 hrs at room temperature. After 24 hrs, the lung is stored in 70% ethanol until tissue processing. The tissue processing, sectioning, paraffin embedding, and H&E staining procedure was performed by University of Florida Core tissue sectioning facility. Detailed description of H&E staining is in the text. Upper panel- lung from the mouse injected with MDA231-EV and lower panel-lung from the mouse injected with 231-shPDK1. (B) Statistical analysis. The lung tumor nodules for all six mice in each group are statistically represented. Statistical analysis was performed using paired Student's t-test. EV = Empty vector, sh =short hairpin, and PDK1 = Pyruvate dehydrogenase kinase 1.

CHAPTER 5
ANTIOXIDANT PROTECTION FROM DETACHMENT INDUCED OXIDATIVE STRESS IN MAMMARY EPITHELIAL CELLS

Background

Endogenous Antioxidants Defense System

The endogenous ROS levels are tightly regulated by both non-enzymatic and enzymatic antioxidant components. The non-enzymatic antioxidants include hydrophilic and lipophilic radical components such as α-tocopherol, ascorbic acid, reduced coenzyme Q10 and glutathione[109]. The enzymatic antioxidant defense system includes superoxide dismutases (SOD), which dismutase highly reactive superoxide anion to less reactive hydrogen peroxide. There are three different forms of SOD enzyme localized at different regions; SOD1 or copper superoxide dismutase (CuSOD) in cytosol[110], SOD2 or manganese superoxide dismutase (MnSOD) in mitochondrion[111], and SOD3 in extracellular matrix region[112]. Hydrogen peroxide is maintained at low levels by catalase and glutathione peroxidase (Gpx) enzymes, which convert H_2O_2 to H_2O and O_2[113]. The other enzymes that are involved in the reduction of oxidized forms of antioxidant molecules are; thioredoxin reductase, glutathione reductases and peroxiredoxin[113]. Therefore, the endogenous antioxidants balance the ROS levels to prevent damage from oxidative stress and maintain redox homeostasis.

Manganese Superoxide Dismutase (MnSOD)

MnSOD is one of the major antioxidants that scavenge the superoxide anion to generate hydrogen peroxide. It is a tetrameric enzyme localized to mitochondrion encoded by a nuclear gene located on chromosome 6q25. MnSOD is an antioxidant that resists apoptosis and protects cells from oxidative stress[114], inflammatory cytokines and ionizing radiation[115]. The mice lacking MnSOD enzyme die immediately after birth,

thus, illustrating its importance in maintenance of life[116,117]. The mice carrying heterozygous MnSOD gene display reduction in MnSOD activity, increase in mitochondrial oxidative damage, and higher incidence of tumor in older mice[118].

Several reports state that MnSOD acts as a tumor suppressor gene[119,120]. High levels of MnSOD have been reported to increase tumor metastasis and invasion[121,122]. MnSOD is highly expressed in estrogen receptor (ER) negative human breast cancer lines (MDA-MB-231, SKBR3) compared to ER-dependent human breast cancer cell lines (MCF7, T47D)[123]. The role of MnSOD in tumor growth, invasion and metastasis is controversial, but it is an important antioxidant that prevents oxidative stress and inhibits apoptosis.

Good ROS and Bad ROS

The physiological role of ROS is very dynamic and depends on its overall production. Mitochondrion generates ROS in a continuous process under aerobic conditions. Low or transient levels of ROS is beneficial for normal cells because it stimulates cellular proliferation and survival signaling pathways[124]. ROS oxidizes the cysteine residues of kinases and phosphotases and thus, activates the signaling molecules involved in proliferation, survival and growth. Some of those molecules may include apoptosis signal-regulating kinase (ASK1)[125], ERK[126], PI3K/AKT[127], and HIF1[128] etc.

Excessive production of ROS causes damage to all cellular components leading to cell death or senescence. The oxidative nature of ROS leads to alterations in mitochondrial membrane components such as lipid peroxidation, or protein thiol oxidation, which results in mitochondrial membrane permeabilization[129]. This is followed by release of apoptosis-inducing factors including cytochrome c from

mitochondria, and subsequent activation of the caspase cascade[130]. Furthermore, increased ROS production oxidizes cytochrome c leading to pro-apoptotic activity[130].

Under physiological conditions, oxidants and anti-oxidants are in harmony to maintain redox homeostasis. Any perturbation that causes imbalance between these two components leads to oxidative stress.

Matrix detachment causes an increase in the level of ROS in endothelial cells[67] and mammary epithelial cells[68]. Our data indicate that upon detachment, mammary epithelial cells modulate glucose metabolism by upregulating PDK4 to attenuate mitochondrial respiration to evade ROS production and resist anoikis (Figure 1-15). Furthermore, treatment with antioxidants not only rescued PDK4 depleted MCF10A cells but also the control MCF10A cells from apoptosis under detached culture conditions (Figure 1-11), suggesting matrix detachment renders mammary epithelial cells sensitive to ROS. To validate our observations, we examined the consequence of increased oxidative stress resulting from depletion of an endogenous antioxidant. Since our work mainly focuses on mitochondrial metabolism and ROS generated from it, we studied the impact of mitochondria antioxidant manganese superoxide dismutase (MnSOD or SOD2) on anoikis or detachment-induced apoptosis. Our work demonstrates for the first time that when detached from ECM, the mammary epithelial cells also modulate their endogenous antioxidant MnSOD levels to reduce oxidative stress and promote anoikis resistance.

Results

Induction of MnSOD in Matrix Detached Mammary Epithelial Cells

MnSOD catalyzes the dismutation of mitochondrial superoxide into hydrogen peroxide and oxygen, and hence is a key antioxidant. Also, our data suggest that matrix

detachment in mammary epithelial cells modulate glucose metabolism to evade ROS production from mitochondria. Therefore, we first examined the induction of MnSOD in HMEC and MCF10A at RNA level under attached and suspended culture conditions. We unexpectedly found that like PDK4, MnSOD RNA levels were significantly increased following detachment of HMEC (Figure 5-1A) and MCF10A cells (Figure 5-1B).

Consistent with RNA level, the protein level of MnSOD was also markedly elevated in MCF10A suspended culture cells (Figure 5-2). Thus, the data indicate upon detachment from extracellular matrix, mammary epithelial cells induce antioxidant MnSOD to combat oxidative stress to protect from anoikis.

Depletion of MnSOD Sensitizes Mammary Epithelial Cells to Anoikis

We further investigated the effect of MnSOD depletion on anoikis in MCF10A. MnSOD was depleted using retroviral shRNA and the knockdown efficiency was confirmed by western blotting (Figure 5-2).

Although MnSOD was expressed under attached culture conditions, depletion of MnSOD had little effect on cell death (Figure 5-3A). While in suspension culture conditions, knockdown of MnSOD significantly induced cell death in detached MCF10A cells (Figure 5-3A). To investigate if the increased cell death is due to increased apoptosis, we performed caspase 3/7 activity and PE annexin V/7-AAD staining in MnSOD depleted MCF10A cells in attached and suspended culture cells. As expected, knockdown of MnSOD displayed increased caspase 3/7 activity (Figure 5-3B) and PE annexin V/7-AAD staining (Figure 5-3C) when cells were in suspension. Compared to control cells, MnSOD-depleted cells exhibited elevated early stage (22% vs. 14%) and late stage (10% vs. 5%) apoptosis when detached from matrix (Figure 5-3D). Consistent with TB exclusion assay, no significant increase in apoptosis was observed in MnSOD

depleted MCF10A cells under adherent culture condition. These results support that increased oxidative stress enhances anoikis.

Epistatic Relationship Between PDK4 and MnSOD upon Matrix Detachment

Upon detachment, mammary epithelial cells upregulated both PDK4 and MnSOD. Our data provide evidence that depletion of either gene sensitized MCF10A to anoikis. Therefore, we decided to investigate if these two genes have an epistatic relationship. At RNA level, PDK4-depleted MCF10A cells expressed significantly higher MnSOD levels than control cells following cell detachment (Figure 5-4A). Conversely, MnSOD-depleted MCF10A cells induced more PDK4 than control cells in suspended culture condition (Figure 5-4B). However, the induction of MnSOD in PDK4-depleted MCF10A suspended cells was significantly higher than PDK4 induction in MnSOD-depleted MCF10A suspended culture cells. In addition, unlike PDK4, induction of MnSOD was not dependent on ERRγ (Figure 5-4C). But, like PDK4-depleted MCF10A cells, ERRγ-depleted MCF10A cells induced more MnSOD suspended cells (Figure 5-4C). These findings suggest that upon matrix detachment, PDK4 and MnSOD genes may compensate each other to evade ROS production and resist anoikis.

Summary

Taken together, we conclude that upon detachment, mammary epithelial cells simultaneously upregulate both ERRγ-PDK4 and MnSOD to reduce ROS levels (Figure 2-5). The loss of one gene may compensate for the other. Thus, it suggests an epistatic relationship exists between the two genes. These alterations in both metabolism and endogenous antioxidant system confer increased resistance to anoikis by eliminating oxidative stress and extend survival of cells in suspension (Figure 5-5).

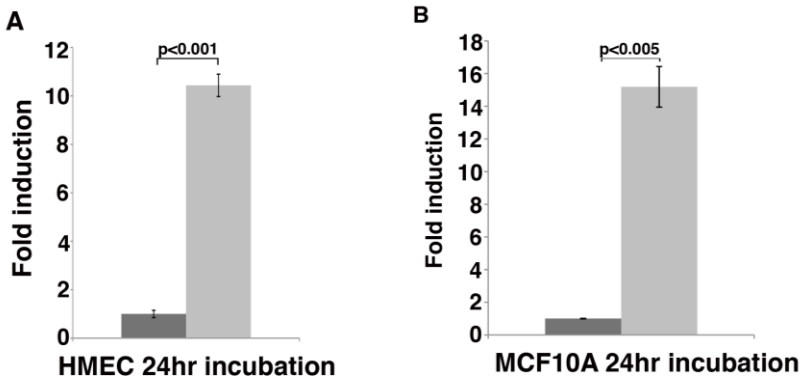

Figure 5-1. Induction of MnSOD in HMEC and MCF10A suspended cells. HMEC and MCF10A cells were grown in a 35 mm plates under attached and poly-hema coated suspended culture conditions for 24 hrs. After 24 hrs of incubation, the cells were collected to extract RNA using Trizol reagent. 2 µg of RNA was used from each sample to synthesize cDNA by Moloney Murine Leukemia Virus (M-MulV) reverse transcriptase. 1 µL of cDNA was used to run realtime quantitative PCR reaction with SYBR® green PCR mix. The relative RNA levels of MnSOD were normalized to endogenous β-Actin in (A) HMEC and (B) MCF10A. These data represent triplicate experiments. Error bars were expressed as standard error of the mean (S.E.M.). Statistical analysis was performed using paired Student's t-test. Att = Attached, Susp = Suspended, and MnSOD = Manganese superoxide dismutase.

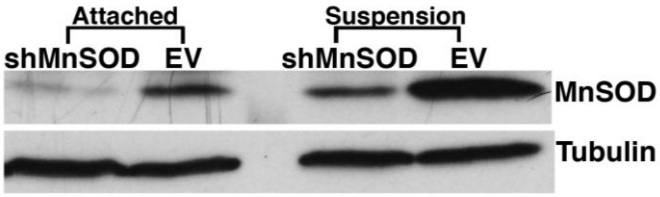

Figure 5-2. Knockdown of MnSOD in MCF10A cells. MCF10A cells were transduced with retrovirus carrying empty vector (10A-EV) and short hairpin RNA against MnSOD (10A-shMnSOD). The cells were grown under attached and poly-hema coated suspended cells for 24 hrs. After 24 hrs of incubation, the cells were collected and lysed in denature lysis buffer with 0.1 % β-Mercaptoethanol. The samples were analyzed by 12% SDS-PAGE, followed by Immunoblotting using rabbit polyclonal anti-MnSOD (1:1000) and mouse anti-α-tubulin antibody (1:5000) as loading control. Att = Attached, Susp = Suspended, and MnSOD = Manganese superoxide dismutase.

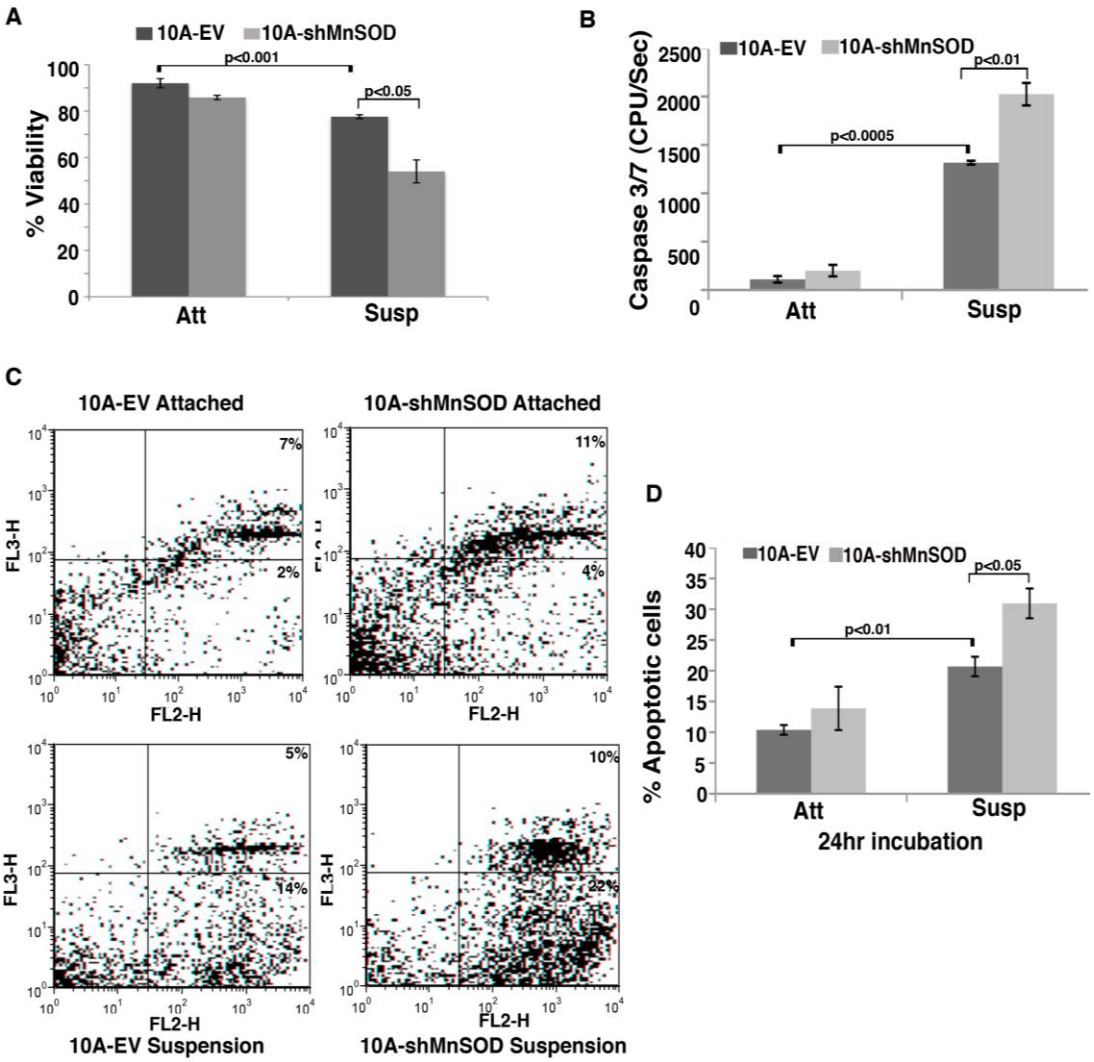

Figure 5-3. Depletion of MnSOD leads to increased anoikis in MCF10A. MCF10A-EV and MnSOD depleted MCF10A cells were grown in a 35 mm plates under attached and poly-hema coated suspended culture conditions for 24 hrs. (A) Trypan Blue (TB) exclusion assay After 24 hrs of incubation, the cells were collected from all the samples, trypzined, washed, and resuspended in 1 mL PBS. 1:1 ratio of 0.4% trypan blue dye was added to 50 µL of sample. The percentage of viable cells was counted by excluding dead cells stained blue using hemocytometer. (B) Caspase 3/7 glo assay. After 24 hrs of incubation, the cells were collected, washed and lyed in hypertonic buffer (HTB) to extract cytoplasmic protein. 100 µg of protein lysate adjusted to 20 µL volume by HTB for each sample was loaded onto 96-well microplate. Equal volume of caspase 3/7 glo substrate was added to measure caspase 3/7 activity using Luminometer. (C, D) PE-Annexin V/ 7-AAD analysis. After 24 hrs of incubation, the cells were collected washed twice in PBS and $1*10^5$ cells were resuspended in 100 µL of PBS. 5 µL each of PE-Annexin V and 7-AAD were added to the cells and incubated for 15 minutes at room temperature. Later, the cells were immediately analyzed by FACScan machine. A total number of

10,000 cells were analyzed for each sample (C) The dot plot representing the percentage of total number of cells that were unstained or live (Lower left quadrant), stained positive for PE-Annexin V only (Lower right quadrant), stained positive for PE-Annexin V and 7-AAD (Upper right quadrant) and stained positive for 7-AAD alone (Upper left quadrant). FL2-H x-axis represents PE-Annexin V positive and FL3-H y-axis represent 7-AAD positive cells. (D) Statistical representation of total percentage of apoptotic cells (percentage of PE-AnnexinV only + percentage of PE-AnnexinV and 7-AAD cells). All error bars represent standard deviation (n=3). Statistical analysis was performed using paired Student's t-test. Att = Attached, Susp = Suspended, EV = Empty vector, MnSOD = Manganese superoxide dismutase, PE = Phycoerythrin, 7-AAD = 7- Aminoactinomycin D, and FL2H or FL3H= fluorescence emission at its highest peak represented in logarithmic scale.

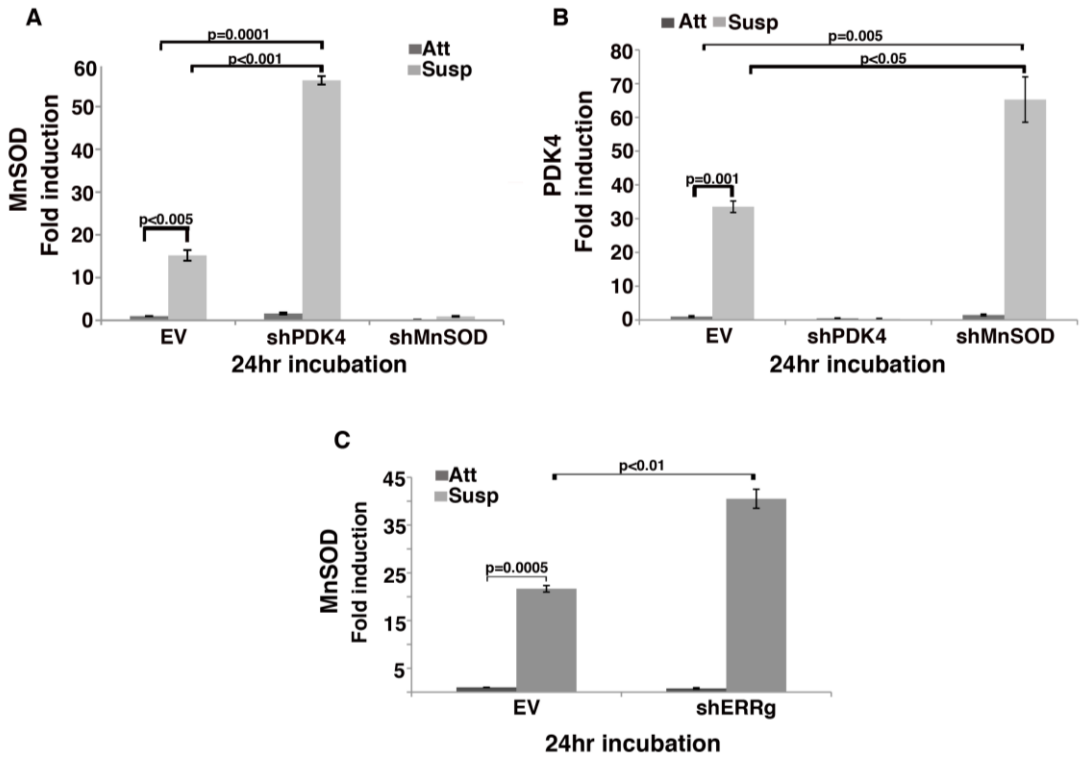

Figure 5-4. Epistatic relationship between PDK4 and MnSOD in MCF10A suspended culture cells. MCF10A-EV, 10A-shPDK4, and 10A-shERRγ cells were grown under attached and poly-hema coated suspended culture conditions for 24 hrs. After 24 hrs of incubation, the cells were collected to extract RNA using Trizol reagent. 2 µg of RNA was used from each sample to synthesize cDNA by Moloney Murine Leukemia Virus (M-MulV) reverse transcriptase. 1 µL of cDNA was used to run realtime quantitative PCR reaction with SYBR® green PCR mix. (A) qRT-PCR for MnSOD expression in EV, PDK4 depleted 10A and MnSOD depleted 10A cells (B) qRT-PCR for PDK4 in 10A-EV, PDK4 depleted MCF10A and MnSOD depleted MCF10A cells and (C) MnSOD in 10A-EV and 10A-shERRγ cells. These data represent triplicate experiments. Att = Attached, Susp = Suspended. EV = Empty vector, sh = Short hairpin RNA, PDK4 = Pyruvate dehydrogenase kinase isozyme 4, shPDK4 = PDK4 depleted MCF10A, shMnSOD = MnSOD depleted MCF10A, and shERRγ = ERRγ depleted MCF10A cells.

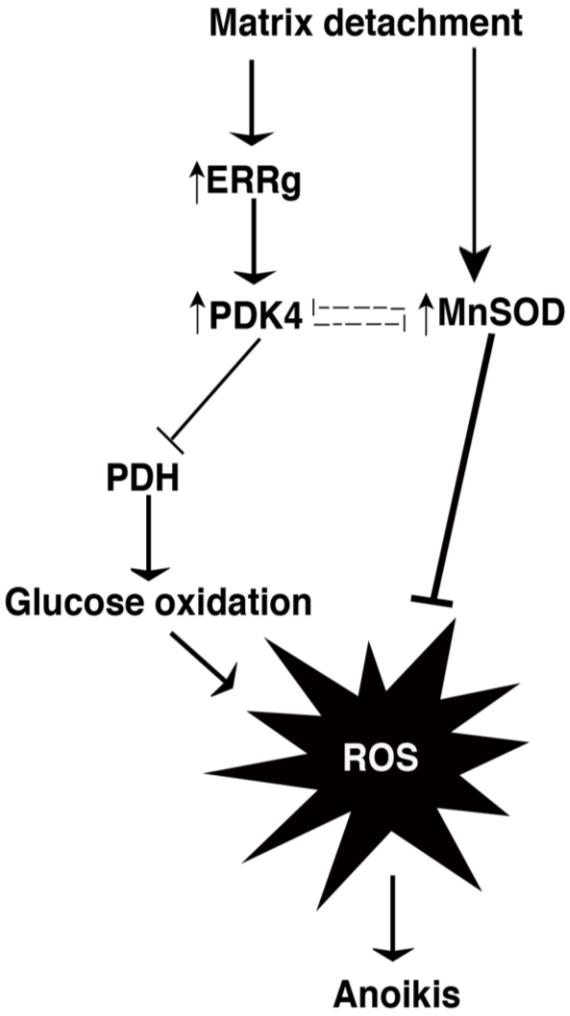

Figure 5-5. Summary model. Detachment from ECM induces MnSOD in MCF10A in parallel with ERRγ-PDK4 to prevent ROS production and resist anoikis. The loss of PDK4 is compromised by MnSOD and vice versa in order to evade oxidative stress during detachment and prolong cell survival.

CHAPTER 6
CONCLUSIONS AND FUTURE DIRECTIONS

Conclusions

The present study examines the role of glucose metabolism in the regulation of anoikis or detachment-induced cell death and its impact on breast cancer metastasis *in vivo*. Upon detachment from ECM, the normal epithelial cells undergo cell death known as anoikis to prevent irregular growth. Unlike normal cells, tumor cells resist anoikis to survive through blood circulation, invade and metastasize to distant organs. Compared to normal cells, tumor cells have altered glucose metabolism known as aerobic glycolysis or the Warburg effect. Since tumor metastasis is one of the leading causes of death among cancer patients, it is critical to understand the molecular mechanisms that contribute to this process. Although the Warburg effect contributes to tumor initiation, growth, and survival, its role in tumor metastasis is yet to be elucidated. To study the role of glucose metabolism in the development of anoikis resistance and tumor metastasis, we used untransformed mammary epithelial cells (MCF10A and HMEC), Ras-transformed mammary epithelial cells (MCF10ACA1.1) and highly metastatic breast cancer cells (MDA-MB-231) as our model systems.

The first part of this work examines the impact of glucose metabolism on cell survival during detachment in normal mammary epithelial cells. We have demonstrated that in response to cell detachment, HMEC and MCF10A cells markedly upregulate PDK4 to inhibit PDH, thereby attenuating the conversion of glycolysis-derived pyruvate to acetyl-CoA in the mitochondria and subsequent flux into the TCA cycle. This metabolic reprogramming diverts glucose-derived carbons away from mitochondrial oxidative metabolism, decreases oxygen consumption and mitochondrial ROS

production in MCF10A cells specifically under suspension culture conditions. These data indicate that matrix attachment has a profound effect on glucose oxidation in mammary epithelial cells. While Brugge *et al*., concomitantly reported the induction of PDK4 leading to attenuation of mitochondrial activity in MCF10A suspension cells[131], the impact of detachment-triggered metabolic shift on anoikis proves to be the novel aspect of this study.

In evaluating the functional significance of PDK4 induction in MCF10A cells specifically under suspension culture conditions, we have demonstrated that depletion of PDK4 accelerates anoikis by activating intrinsic apoptotic pathway. This increased cell death in MCF10A suspension cells by depletion of PDK4 is due to the activation of PDH, which in turn increases mitochondrial respiration and oxidative stress. In other words, MCF10A cells attenuate mitochondrial respiration by upregulating PDK4 to delay apoptosis upon matrix detachment. To prove that attenuation of mitochondrial oxidation prolongs cell survival under suspension culture conditions, we have constitutively activated PDH in MCF10A cells. Not surprisingly, activation of PDH sensitizes MCF10A cells to anoikis. These findings reveal how untransformed mammary epithelial cells manage to survive longer in the absence of matrix by reprogramming glucose metabolism. This study also provides direct evidence that decreased glucose oxidation promotes anoikis resistance in normal mammary epithelial cells.

Depletion of PDK4 induces significant cell death in MCF10A suspension cells but demonstrates a slight shift towards glucose oxidation. In other words, elimination of PDK4 may not have completely relieved PDH enzyme activity and hence we observe a partial increase in glucose oxidation. One possible explanation for this incomplete

activation of PDH enzyme is the presence of other PDK isozymes. Although PDK4 and PDK2 are induced upon matrix detachment in MCF10A cells, PDK1 and PDK4 are the most abundant of all the four isozymes. Also, the enzymatic inhibitory effect of PDK1 is higher than PDK4. Therefore, depletion of PDK4 in MCF10A cells partially activates the PDH enzyme due to the existence of PDK1. Similar to PDK4 depletion, it is possible that depletion of PDK1 in MCF10A cells may sensitize them to anoikis.

PDK4 depleted MCF10A cells markedly undergo anoikis in suspension due to increased oxidative stress through mitochondrial respiration. Pharmacological treatment with antioxidants rescued both the control and PDK4-depleted MCF10A cells from apoptosis under suspension culture conditions. Schafer *et al*., demonstrated that matrix detachment increases ROS production in MCF10A[68], but our data indicate no significant change in ROS levels. A plausible reason for antioxidants to protect control MCF10A cells from anoikis could be that matrix detachment may render cells sensitive to oxidative stress. This observation is further reinforced when MCF10A cells exhibited increased apoptosis due to forced activation of PDH specifically in suspension cells but not in attached ones. In other words, forced activation of PDH increases oxidative stress in MCF10A cells both under attached and suspended culture conditions but only suspension cells are sensitive to oxidative stress and therefore undergo anoikis.

It is intriguing that MCF10A cells activate the ERRγ-PDK4 axis following matrix detachment. Expression of PDK4 is usually stimulated by starvation, which consequently suppresses PDH and curtails glucose oxidation. This response conserves glucose reserves and allows the switch from the utilization of glucose to fatty acids as an energy source. On the other hand, ERRs are key regulators of fatty acid oxidation. It

was recently observed that matrix detachment led to reduced glucose uptake in MCF10A cells[68]. Therefore, cell detachment may mimic glucose starvation, and trigger the ERR-PDK4 program and metabolic shift in MCF10A cells.

Consistent with cell's metabolic shift to reduce glucose oxidation and oxidative stress response to detachment, MCF10A and HMEC suspended cells also stimulate expression of MnSOD, which mitigates the oxidative stress and extends the viability of cells in suspension. Coupling of a decrease in ROS generation and an increase in cellular antioxidant capacity to scavenge ROS represents an integrated strategy for cells to avoid oxidative damage and survive longer under the stress of matrix detachment. These observations reveal how cells manage to control oxidative stress to resist anoikis. Consistent with our observations, it has been reported that expression of MnSOD is elevated in aggressive breast cancer cells and contributes to tumor invasiveness and metastasis[123].

Our data provide the first direct evidence that attenuation of mitochondrial respiration promotes anoikis resistance in normal mammary epithelial cells. The second part of our work focuses on examining the influence of glucose metabolism on anoikis resistance and tumor metastasis in breast cancer cells. Since the untransformed mammary epithelial cells induce PDK4 to resist anoikis, we decided to examine the role of PDKs in Ras-transformed mammary epithelial cells (MCF10ACA1.1). As expected, MCF10ACA1.1 cells significantly upregulate PDK4 upon matrix detachment to protect cells from anoikis. Although MCF10ACA1.1 are highly metastatic in nature and induced PDK4 upon matrix detachment, they do not form significantly larger tumor nodules *in vivo* (data not shown). It is more clinically relevant to study the impact of glucose

metabolism on anoikis resistance in a breast cancer cell line derived from human patients. Therefore, we have focused our attention to a highly metastatic, aggressive, and triple negative breast cancer cell line MDA-MB-231.

MDA-MB-231 cells are highly glycolytic in nature. Because cancer cells exhibit a preference for aerobic glycolysis and a low rate of mitochondrial oxidation of glucose, we hypothesize that the Warburg effect intrinsically bestows a survival advantage upon cancer cells when they are detached from the matrix, and facilitates their metastatic spreading. Consistent with our hypothesis, MDA-MB-231 cells exhibit significantly lower PDH activity than the normal mammary epithelial cells under adherent culture conditions. Surprisingly, matrix detachment significantly attenuates PDH activity, increases lactate levels and decreases OCR in MDA-MB-231 cells. These observations prove that upon detachment from matrix, the highly aggressive breast cancer MDA-MB-231 cells further enhance the Warburg effect to promote anoikis resistance. Indeed, normalization of glucose metabolism in MDA-MB-231 cells by activation of PDH redirects pyruvate towards mitochondrial oxidation and restores their sensitivity to anoikis. Therefore, the attenuation of mitochondrial respiration protects breast cancer cells from detachment-induced cell death by evading oxidative stress from mitochondria.

Like MCF10A, HMEC and MCF10ACA1.1 cell lines, MDA-MB-231 cells induce PDK4 upon detachment from matrix. But, the abundance of PDK1 is significantly higher than all other three PDK isozyme. Also, PDK1 protein levels are upregulated when detached from the matrix in MDA-MB-231 cells. Therefore, we have decided to examine its role in attenuating mitochondrial oxidation and promoting anoikis resistance and

tumor metastasis *in vivo*. As expected, depletion of PDK1 in MDA-MB-231 enhances mitochondrial PDH activity, decreases lactate levels and increases OCR both under attached and detached culture conditions. However, this metabolic shift does not effect the MDA-MB-231 cells under adherent conditions but markedly promotes anoikis in detached cells. These data help explain why breast cancer cells enhance the Warburg effect upon detachment from the matrix.

Anoikis resistance is an important step during tumor metastasis. For cancer cells to metastasize to distant organs, they need to detach from the primary tumor site, enter the circulatory system or lymphatic system, develop resistance to anoikis to survive through circulation and thus invade the distant organs for secondary site. So, resistance to detachment-induced cell death (anoikis) is a critical step for cancer cells to survive and metastasize. Our work has demonstrated that PDK1 is a key molecule for promoting anoikis resistance in MDA-MB-231 cells. Consistent with our *in vitro* data, depletion of PDK1 in MDA-MB-231 cells markedly reduced lung tumor nodules in an *in vivo* metastatic experimental assay. Altered glucose metabolism is believed to support tumor cell proliferation and our results add new insights into the significance of the Warburg effect in cancer metastasis, and establish PDKs as an important regulator of anchorage-independent cell survival as well as tumor metastasis. The latter may serve as the basis for anti-metastasis therapeutic interventions. Reprogramming tumor metabolism, in particular inhibition of PDKs to stimulate glucose oxidation, should sensitize cancer cells to anoikis, and hence may impede the detachment of cancer cells from the primary site, kill circulating tumor cells, and eradicate disseminated tumor cells at secondary sites before they re-establish conducive cell-matrix interactions.

Increased glucose uptake and glycolysis in cancer cells provides substrates for macromolecular biosynthesis required for cell proliferation. This convincingly explains at least part of the advantage provided by the Warburg effect. However, it is puzzling as to why after the glycolytic process, the end product pyruvate in cancer cells is primarily dispensed as lactate instead of entering the TCA cycle even under normal oxygen tensions. This phenomenon might be attributed to the detrimental consequence of mitochondrial oxidation. Increased glucose consumption through aerobic glycolysis by cancer cells (for the need of biosynthesis) conceivably gives rise to increased pyruvate production. If most pyruvate enters the mitochondrial oxidative pathway as in normal cells, the resultant increased ROS would probably disrupt the cellular redox balance and jeopardize cancer cells' capability to cope with stressful conditions such as loss of matrix attachment. By shunting pyruvate away from mitochondria, the Warburg effect helps cancer cells avoid generation of excessive ROS and resist anoikis. In this regard, increased aerobic glycolysis also stimulates the reactions of the PPP, which is a principal pathway to generate the reducing equivalent, NADPH. By evading production of extra ROS and increasing antioxidant defense, the Warburg effect maintains redox homeostasis, and thus promotes anoikis resistance and metastasis.

It is well established that under hypoxic condition, HIF1α induces PDK1 and PDK3 molecules to promote solid tumor growth and survival[41,43]. DCA is a potential drug available to inhibit PDK enzyme activity by preventing the phosphorylation of PDH enzyme. DCA is a well-studied molecule to prevent lactic acidosis in children[54]. Several recent reports have demonstrated that treatment with DCA activates mitochondrial respiration in cancer cells leading to mitochondrial membrane permeabilization, restores

apoptosis, kills cancer cells *in vitro* and shrinks tumor in rats[53]. Further, Michelakis and group performed phase II clinical trials using DCA to treat glioblastoma patients[132]. DCA successfully regressed the tumor with minimal side effects in all four out of five patients. Although, DCA has been successful in treating certain cancer models, higher dosage of DCA (>25mg/kg/day) causes peripheral neuropathy, neurotoxicity, and gait disturbances. In addition, unlike PDK2, PDK1 and PDK4 are highly resistant to DCA[133]. Therefore, inhibition of PDK1 and PDK4 requires higher amounts of DCA, which might presumably cause severe neuropathic symptoms. Based on our work, it is evident that PDK1 promotes anoikis resistance and tumor metastasis in breast cancer cells. Therefore, it is critical to design additional drugs that can potentially inhibit PDK1 to prevent both cancer growth and metastatic spreading.

Future Directions

The present study focuses mainly on understanding the role of glucose metabolism in regulating anoikis resistance in both normal mammary epithelial cells and metastatic breast cancer cells. We have demonstrated that upon detachment, mammary epithelial cells simultaneously upregulate PDK to attenuate mitochondrial oxidation and MnSOD to evade oxidative stress. This is an important strategy for normal mammary epithelial cells to survive longer under detached conditions. Also, we have established that metastatic breast cancer cells further enhance the Warburg effect upon detachment from matrix by upregulating PDK1 to promote anoikis resistance and tumor metastasis *in vivo*.

Based on our work, it is quite evident that detachment from matrix induces MnSOD in MCF10A cells. Also, MnSOD has been implicated in tumor progression and metastasis. Therefore, it is imperative to identify the molecule that activates MnSOD

during detachment. Several studies have reported that the nuclear factor kappa-light-chain-enhancer of activated B cells (NFκB) is one of the potential regulators of MnSOD[134]. It is well established that detachment activates NFκB, which delays apoptosis in several cell lines[135,136]. So, depleting RelA (p65), an important molecule in the NFκB pathway that induces NFκB-regulated genes is an important future direction. We have obtained the two independent shRNA targeting p65 from Kevin Brown's lab. After depletion of p65 in MCF10A, we will examine the expression of MnSOD in these cells both under attached and detached culture conditions. According to our hypothesis, the depletion of p65 may repress the MnSOD RNA levels in detached cells but not in adherent cells. Thus, we may be able to provide the detailed information of NFkB-MnSOD pathway and how it regulates anoikis resistance in mammary epithelial cells.

Our data provide evidence that normal mammary epithelial cells induce PDK4 upon detachment to prevent anoikis and survive longer. Although MDA-MB-231 induced PDK4 upon detachment, its overall abundance is trivial. Therefore, it will be quite intriguing to examine the expression of PDK4 in different tumor cells other than breast cancer cells. Based on Standford microarray-profiling, A549 (Lung adenocarcinoma) and SKMEL5 (Melanoma cell line) cells show higher PDK4 expression levels. Our preliminary experiments confirm that the expression of PDK4 at RNA level is higher in A549 and SKMEL5 when compared with MCF10A (Figure 6-1). So, future work will include depletion of PDK4 and perform anoikis assay to test its functional significance in these tumor cells.

Finally, the key finding of our work is that PDK1 can be utilized as a potential drug target for breast cancer metastasis. Thus, future work will focus on developing effective

drug inhibiting PDK1 activity. Additionally, since DCA is not effective in inhibiting PDK1 enzyme, it is essential to design potential inhibitors for PDK1 to prevent tumor metastasis *in vivo*.

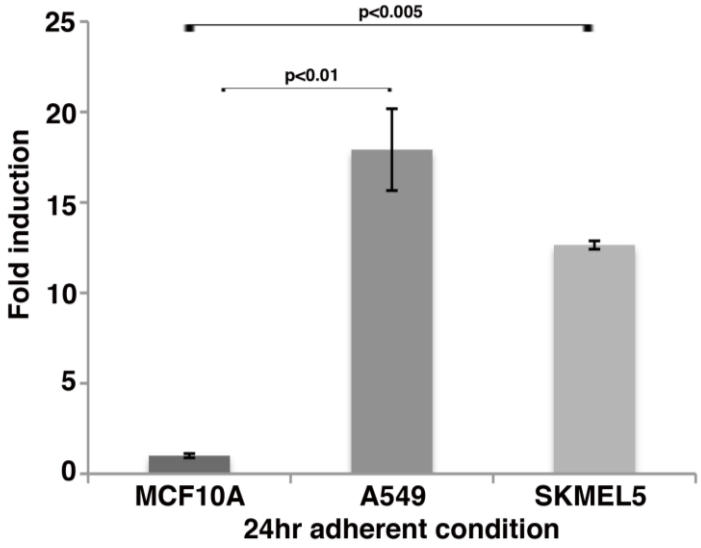

Figure 6-1. Expression of PDK4 in different tumor cells lines. MCF10A, A549 and SKMEL5 cells were grown in 35 mm plates under attached condition for 24 hrs. After 24 hrs of incubation, the cells were collected to extract RNA by Trizol reagent. 2 µg of RNA was used for cDNA synthesis. 1 µL of cDNA was used from each sample to run quantitative RT-PCR. The relative PDK4 RNAL levels were normalized to β-actin. After normalization, the fold induction of PDK4 expression in MCF10A was set to one. The fold induction of PDK4 in A549 and SKMEL5 cells were compared to PDK expression in MCF10A. These data represent n=3. A549= lung adenocarcinoma cells, and SKMEL5= melanoma cells.

LIST OF REFERENCES

1 Frisch, S. M. & Francis, H. Disruption of epithelial cell-matrix interactions induces apoptosis. *Journal of Cell Biology* **124**, 619-626, doi:10.1083/jcb.124.4.619 (1994).

2 Chiarugi, P. & Giannoni, E. Anoikis: A necessary death program for anchorage-dependent cells. *Biochemical Pharmacology* **76**, 1352-1364, doi:10.1016/j.bcp.2008.07.023 (2008).

3 Gilmore, A. P. Anoikis. *Cell Death and Differentiation* **12**, 1473-1477, doi:10.1038/sj.cdd.4401723 (2005).

4 Frisch, S. M. & Screaton, R. A. Anoikis mechanisms. *Current Opinion in Cell Biology* **13**, 555-562, doi:10.1016/s0955-0674(00)00251-9 (2001).

5 Reginato, M. J. *et al.* Integrins and EGFR coordinately regulate the pro-apoptotic protein Bim to prevent anoikis. *Nature Cell Biology* **5**, 733-740, doi:10.1038/ncb1026 (2003).

6 Parsons, J. T. Focal adhesion kinase: the first ten years. *Journal of Cell Science* **116**, 1409-1416, doi:10.1242/jcs.00373 (2003).

7 Frisch, S. M. Evidence for a function of death-receptor-related, death-domain-containing proteins in anoikis. *Current Biology* **9**, 1047-1049, doi:10.1016/s0960-9822(99)80455-2 (1999).

8 Rytomaa, M., Martins, L. M. & Downward, J. Involvement of FADD and caspase-8 signalling in detachment-induced apoptosis. *Current Biology* **9**, 1043-1046, doi:10.1016/s0960-9822(99)80454-0 (1999).

9 Puthalakath, H. *et al.* Bmf: A proapoptotic BH3-only protein regulated by interaction with the myosin V actin motor complex, activated by anoikis. *Science* **293**, 1829-1832, doi:10.1126/science.1062257 (2001).

10 Schmelzle, T. *et al.* Functional role and oncogene-regulated expression of the BH3-only factor Bmf in mammary epithelial anoikis and morphogenesis. *Proceedings of the National Academy of Sciences of the United States of America* **104**, 3787-3792, doi:10.1073/pnas.0700115104 (2007).

11 Hausmann, M. *et al.* BCL-2 modifying factor (BMF) is a central regulator of anoikis in human intestinal epithelial Cells. *Journal of Biological Chemistry* **286**, 26533-26540, doi:10.1074/jbc.M111.265322 (2011).

12 Idogawa, M., Adachi, M., Minami, T., Yasui, H. & Imai, K. Overexpression of bad preferentially augments anoikis. *International Journal of Cancer* **107**, 215-223, doi:10.1002/ijc.11399 (2003).

13 Gilley, J., Coffer, P. J. & Ham, J. FOXO transcription factors directly activate bim gene expression and promote apoptosis in sympathetic neurons. *Journal of Cell Biology* **162**, 613-622, doi:10.1083/jcb.200303026 (2003).

14 Ley, R. *et al.* Extracellular signal-regulated kinases 1/2 are serum-stimulated "Bim(EL) kinases" that bind to the BH3-only protein Bim(EL) causing its phosphorylation and turnover. *Journal of Biological Chemistry* **279**, 8837-8847, doi:10.1074/jbc.M311578200 (2004).

15 Reginato, M. J. *et al.* Bim regulation of lumen formation in cultured mammary epithelial acini is targeted by oncogenes. *Molecular and Cellular Biology* **25**, 4591-4601, doi:10.1128/mcb.25.11.4591-4601.2005 (2005).

16 Whelan, K. A. *et al.* Hypoxia Suppression of Bim and Bmf Blocks Anoikis and Luminal Clearing during Mammary Morphogenesis. *Molecular Biology of the Cell* **21**, 3829-3837, doi:10.1091/mbc.E10-04-0353 (2010).

17 Valentijn, A. J., Zouq, N. & Gilmore, A. P. Anoikis. *Biochemical Society Transactions* **32**, 421-425, doi:10.1042/bst0320421 (2004).

18 Valentijn, A. J. & Gilmore, A. P. Translocation of full-length bid to mitochondria during anoikis. *Journal of Biological Chemistry* **279**, 32848-32857, doi:10.1074/jbc.M313375200 (2004).

19 Ilic, D. *et al.* Extracellular matrix survival signals transduced by focal adhesion kinase suppress p53-mediated apoptosis. *Journal of Cell Biology* **143**, 547-560 (1998).

20 Vitale, M. *et al.* Apoptosis induced by denied adhesion to extracellular matrix (anoikis) in thyroid epithelial cells is p53 dependent but fails to correlate with modulation of p53 expression. *Febs Letters* **462**, 57-60, doi:10.1016/s0014-5793(99)01512-4 (1999).

21 Stromblad, S., Becker, J. C., Yebra, M., Brooks, P. C. & Cheresh, D. A. Suppression of p53 activity and p21(WAF1/CIP1) expression by vascular cell integrin alpha v beta 3 during angiogenesis. *Journal of Clinical Investigation* **98**, 426-433, doi:10.1172/jci118808 (1996).

22 Lu, Y. L. *et al.* The PTEN/MMAC1/TEP tumor suppressor gene decreases cell growth and induces apoptosis and anoikis in breast cancer cells. *Oncogene* **18**, 7034-7045, doi:10.1038/sj.onc.1203183 (1999).

23 Simpson, C. D., Anyiwe, K. & Schimmer, A. D. Anoikis resistance and tumor metastasis. *Cancer Letters* **272**, 177-185, doi:10.1016/j.canlet.2008.05.029 (2008).

24 Liotta, L. A. & Kohn, E. C. The microenvironment of the tumour-host interface. *Nature* **411**, 375-379, doi:10.1038/35077241 (2001).

25 Lopez, D., Niu, G., Huber, P. & Carter, W. B. Tumor-induced upregulation of Twist, Snail, and Slug represses the activity of the human VE-cadherin promoter. *Archives of Biochemistry and Biophysics* **482**, 77-82, doi:10.1016/j.abb.2008.11.016 (2009).

26 Haenssen, K. K. *et al.* ErbB2 requires integrin alpha 5 for anoikis resistance via Src regulation of receptor activity in human mammary epithelial cells. *Journal of Cell Science* **123**, 1373-1382, doi:10.1242/jcs.050906 (2010).

27 Giannoni, E. *et al.* Redox regulation of anoikis: reactive oxygen species as essential mediators of cell survival. *Cell Death and Differentiation* **15**, 867-878, doi:10.1038/cdd.2008.3 (2008).

28 Liu, Z. P. *et al.* Oncogenic Ras inhibits anoikis of intestinal epithelial cells by preventing the release of a mitochondrial pro-apoptotic protein Omi/HtrA2 into the cytoplasm. *Journal of Biological Chemistry* **281**, 14738-14747, doi:10.1074/jbc.M508664200 (2006).

29 Pouyssegur, J., Dayan, F. & Mazure, N. M. Hypoxia signalling in cancer and approaches to enforce tumour regression. *Nature* **441**, 437-443, doi:10.1038/nature04871 (2006).

30 Markert, C. L., Shaklee, J. B. & Whitt, G. S. Evolution of a gene. *Science* **189**, 102-114, doi:10.1126/science.1138367 (1975).

31 Thornburg, J. M. *et al.* Targeting aspartate aminotransferase in breast cancer. *Breast Cancer Research* **10**, doi:R8410.1186/bcr2154 (2008).

32 Giatromanolaki, A. *et al.* Lactate dehydrogenase 5 expression in non-Hodgkin B-cell lymphomas is associated with hypoxia regulated proteins. *Leukemia & Lymphoma* **49**, 2181-2186, doi:10.1080/10428190802450629 (2008).

33 Sugden, M. C. & Holness, M. J. Mechanisms underlying regulation of the expression and activities of the mammalian pyruvate dehydrogenase kinases. *Archives of Physiology and Biochemistry* **112**, 139-149, doi:10.1080/13813450600935263 (2006).

34 Gudi, R., Bowkerkinley, M. M., Kedishvili, N. Y., Zhao, Y. & Popov, K. M. Diversity of the pyruvate-dehydrogenase kinase gene family in humans. *Journal of Biological Chemistry* **270**, 28989-28994 (1995).

35 Huang, B. L., Wu, P. F., Popov, K. M. & Harris, R. A. Starvation and diabetes reduce the amount of pyruvate dehydrogenase phosphatase in rat heart and kidney. *Diabetes* **52**, 1371-1376, doi:10.2337/diabetes.52.6.1371 (2003).

36 Baker, J. C., Yan, X. H., Peng, T., Kasten, S. & Roche, T. E. Marked differences between two isoforms of human pyruvate dehydrogenase kinase. *Journal of Biological Chemistry* **275**, 15773-15781, doi:10.1074/jbc.M909488199 (2000).

37 Roche, T. E. & Hiromasa, Y. Pyruvate dehydrogenase kinase regulatory mechanisms and inhibition in treating diabetes, heart ischemia, and cancer. *Cellular and Molecular Life Sciences* **64**, 830-849, doi:10.1007/s00018-007-6380-z (2007).

38 Hiromasa, Y. & Roche, T. E. Facilitated interaction between the pyruvate dehydrogenase kinase isoform 2 and the dihydrolipoyl acetyltransferase. *Journal of Biological Chemistry* **278**, 33681-33693, doi:10.1074/jbc.M212733200 (2003).

39 Bowker-Kinley, M. M., Davis, W. I., Wu, P. F., Harris, R. A. & Popov, K. M. Evidence for existence of tissue-specific regulation of the mammalian pyruvate dehydrogenase complex. *Biochemical Journal* **329**, 191-196 (1998).

40 Korotchkina, L. G. & Patel, M. S. Site specificity of four pyruvate dehydrogenase kinase isoenzymes toward the three phosphorylation sites of human pyruvate dehydrogenase. *Journal of Biological Chemistry* **276**, 37223-37229, doi:10.1074/jbc.M103069200 (2001).

41 Papandreou, I., Cairns, R. A., Fontana, L., Lim, A. L. & Denko, N. C. HIF-1 mediates adaptation to hypoxia by actively downregulating mitochondrial oxygen consumption. *Cell Metabolism* **3**, 187-197, doi:10.1016/j.cmet.2006.01.012 (2006).

42 Kim, J. W., Tchernyshyov, I., Semenza, G. L. & Dang, C. V. HIF-1-mediated expression of pyruvate dehydrogenase kinase: A metabolic switch required for cellular adaptation to hypoxia. *Cell Metabolism* **3**, 177-185, doi:10.1016/j.cmet.2006.02.002 (2006).

43 Lu, C.-W., Lin, S.-C., Chen, K.-F., Lai, Y.-Y. & Tsai, S.-J. Induction of pyruvate dehydrogenase kinase-3 by hypoxia-inducible factor-1 promotes metabolic switch and drug resistance. *Journal of Biological Chemistry* **283**, 28106-28114, doi:10.1074/jbc.M803508200 (2008).

44 Lu, C.-W. *et al.* Overexpression of pyruvate dehydrogenase kinase 3 increases drug resistance and early recurrence in colon cancer. *The American journal of pathology* **179**, 1405-1414 (2011).

45 Sugden, M. C., Orfali, K. A., Fryer, L. G. D., Holness, M. J. & Priestman, D. A. Molecular mechanisms underlying the long-term impact of dietary fat to increase cardiac pyruvate dehydrogenase kinase: Regulation by insulin, cyclic AMP and pyruvate. *Journal of Molecular and Cellular Cardiology* **29**, 1867-1875, doi:10.1006/jmcc.1997.0425 (1997).

46 Harris, R. A., Huang, B. L. & Wu, P. F. Control of pyruvate dehydrogenase kinase gene expression. *Advances in Enzyme Regulation, Vol 41* **41**, 269-288, doi:10.1016/s0065-2571(00)00020-0 (2001).

47 Ma, K., Zhang, Y., Elam, M. B., Cook, G. A. & Park, E. A. Cloning of the rat pyruvate dehydrogenase kinase 4 gene promoter - Activation of pyruvate dehydrogenase kinase 4 by the peroxisome proliferator-activated receptor gamma coactivator. *Journal of Biological Chemistry* **280**, 29525-29532, doi:10.1074/jbc.M502236200 (2005).

48 Zhang, Y. *et al.* Estrogen-related receptors stimulate pyruvate dehydrogenase kinase isoform 4 gene expression. *Journal of Biological Chemistry* **281**, 39897-39906, doi:10.1074/jbc.M608657200 (2006).

49 Wu, P. F., Peters, J. M. & Harris, R. A. Adaptive increase in pyruvate dehydrogenase kinase 4 during starvation is mediated by peroxisome proliferator-activated receptor alpha. *Biochemical and Biophysical Research Communications* **287**, 391-396, doi:10.1006/bbrc.2001.5608 (2001).

50 Attia, R. R. *et al.* Regulation of Pyruvate Dehydrogenase Kinase 4 (PDK4) by Thyroid Hormone role of the peroxisome proliferator-activated receptor gamma COACTIVATOR (PGC-1 alpha). *Journal of Biological Chemistry* **285**, 2375-2385, doi:10.1074/jbc.M109.039081 (2010).

51 Attia, R. R. *et al.* Regulation of Pyruvate Dehydrogenase Kinase 4 (PDK4) by CCAAT/Enhancer-binding Protein beta (C/EBP beta). *Journal of Biological Chemistry* **286**, 23799-23807, doi:10.1074/jbc.M111.246389 (2011).

52 Mayers, R. M. *et al.* AZD7545, a novel inhibitor of pyruvate dehydrogenase kinase 2 (PDHK2), activates pyruvate dehydrogenase in vivo and improves blood glucose control in obese (fa/fa) Zucker rats. *Biochemical Society Transactions* **31**, 1165-1167 (2003).

53 Bonnet, S. *et al.* A mitochondria-K+ channel axis is suppressed in cancer and its normalization promotes apoptosis and inhibits cancer growth. *Cancer Cell* **11**, 37-51, doi:10.1016/j.ccr.2006.10.020 (2007).

54 Stacpoole, P. W. *et al.* Controlled clinical trial of dichloroacetate for treatment of congenital lactic acidosis in children. *Pediatrics* **117**, 1519-1531, doi:10.1542/peds.2005-1226 (2006).

55 Kato, M., Li, J., Chuang, J. L. & Chuang, D. T. Distinct structural mechanisms for inhibition of pyruvate dehydrogenase kinase isoforms by AZD7545, dichloroacetate, and radicicol. *Structure* **15**, 992-1004, doi:10.1016/j.str.2007.07.001 (2007).

56 Turrens, J. F. Mitochondrial formation of reactive oxygen species. *Journal of Physiology-London* **552**, 335-344, doi:10.1111/j.1469-7793.2003.00335.x (2003).

57 Stowe, D. F. & Camara, A. K. S. Mitochondrial Reactive Oxygen Species Production in Excitable Cells: Modulators of Mitochondrial and Cell Function. *Antioxidants & Redox Signaling* **11**, 1373-1414, doi:10.1089/ars.2008.2331 (2009).

58 Rush, J. D., Maskos, Z. & Koppenol, W. H. Distinction between hyroxyl radical and ferryl species. *Methods in Enzymology* **186**, 148-156 (1990).

59 Gao, S. J. *et al.* Docking of endothelial nitric oxide synthase (eNOS) to the mitochondrial outer membrane - A pentabasic amino acid sequence in the autoinhibitory domain of eNOS targets a proteinase K-cleavable peptide on the cytoplasmic face of mitochondria. *Journal of Biological Chemistry* **279**, 15968-15974, doi:10.1074/jbc.M308504200 (2004).

60 Droge, W. Free radicals in the physiological control of cell function. *Physiological Reviews* **82**, 47-95 (2002).

61 Trachootham, D., Alexandre, J. & Huang, P. Targeting cancer cells by ROS-mediated mechanisms: a radical therapeutic approach? *Nature Reviews Drug Discovery* **8**, 579-591, doi:10.1038/nrd2803 (2009).

62 Thannickal, V. J. & Fanburg, B. L. Reactive oxygen species in cell signaling. *American Journal of Physiology-Lung Cellular and Molecular Physiology* **279**, L1005-L1028 (2000).

63 Tolbert, N. E. & Essner, E. Microbodies-peroxisomes and glyoxysomes. *Journal of Cell Biology* **91**, S271-S283, doi:10.1083/jcb.91.3.271s (1981).

64 Babior, B. M. NADPH oxidase: An update. *Blood* **93**, 1464-1476 (1999).

65 Giannoni, E., Fiaschi, T., Ramponi, G. & Chiarugi, P. Redox regulation of anoikis resistance of metastatic prostate cancer cells: key role for Src and EGFR-mediated pro-survival signals. *Oncogene* **28**, 2074-2086, doi:10.1038/onc.2009.77 (2009).

66 Young, C. D. & Anderson, S. M. Rah, rah, ROS: metabolic changes caused by loss of adhesion induce cell death. *Breast Cancer Research* **11**, doi:30710.1186/bcr2417 (2009).

67 Li, A. E. *et al.* A role for reactive oxygen species in endothelial cell anoikis. *Circulation Research* **85**, 304-310 (1999).

68 Schafer, Z. T. *et al.* Antioxidant and oncogene rescue of metabolic defects caused by loss of matrix attachment. *Nature* **461**, 109-U118, doi:10.1038/nature08268 (2009).

69 Lam, C. R. I. *et al.* TAK1 regulates SCF expression to modulate PKB alpha activity that protects keratinocytes from ROS-induced apoptosis. *Cell Death and Differentiation* **18**, 1120-1129, doi:10.1038/cdd.2010.182 (2011).

70 Hanahan, D. & Weinberg, R. A. Hallmarks of Cancer: The Next Generation. *Cell* **144**, 646-674, doi:10.1016/j.cell.2011.02.013 (2011).

71 Warburg, O. Origin of cancer cells. *Science* **123**, 309-314, doi:10.1126/science.123.3191.309 (1956).

72 Vander Heiden, M. G., Cantley, L. C. & Thompson, C. B. Understanding the Warburg effect: the metabolic requirements of cell proliferation. *Science (New York, N.Y.)* **324**, 1029-1033 (2009).

73 Fantin, V. R., St-Pierre, J. & Leder, P. Attenuation of LDH-A expression uncovers a link between glycolysis, mitochondrial physiology, and tumor maintenance. *Cancer Cell* **9**, 425-434, doi:10.1016/j.ccr.2006.04.023 (2006).

74 Moreno-Sanchez, R., Rodriguez-Enriquez, S., Marin-Hernandez, A. & Saavedra, E. Energy metabolism in tumor cells. *Febs Journal* **274**, 1393-1418, doi:10.1111/j.1742-4658.2007.05686.x (2007).

75 Gillies, R. J., Robey, I. & Gatenby, R. A. Causes and consequences of increased glucose metabolism of cancers. *Journal of Nuclear Medicine* **49**, 24S-42S, doi:10.2967/jnumed.107.047258 (2008).

76 Bartrons, R. & Caro, J. Hypoxia, glucose metabolism and the Warburg's effect. *Journal of Bioenergetics and Biomembranes* **39**, 223-229, doi:10.1007/s10863-007-9080-3 (2007).

77 Boros, L. G. *et al.* Oxythiamine and dehydroepiandrosterone inhibit the nonoxidative synthesis of ribose and tumor cell proliferation. *Cancer Research* **57**, 4242-4248 (1997).

78 Cairns, R. A., Harris, I. S. & Mak, T. W. Regulation of cancer cell metabolism. *Nature Reviews Cancer* **11**, 85-95, doi:10.1038/nrc2981 (2011).

79 McFate, T. *et al.* Pyruvate dehydrogenase complex activity controls metabolic and malignant phenotype in cancer cells. *Journal of Biological Chemistry* **283**, 22700-22708, doi:10.1074/jbc.M801765200 (2008).

80 Koppenol, W. H., Bounds, P. L. & Dang, C. V. Otto Warburg's contributions to current concepts of cancer metabolism. *Nature Reviews Cancer* **11**, 325-337, doi:10.1038/nrc3038 (2011).

81 Flier, J. S., Mueckler, M. M., Usher, P. & Lodish, H. F. Elevated levels of glucose-transport and transporter messenger-RNA are induced by ras or src oncogenes. *Science* **235**, 1492-1495, doi:10.1126/science.3103217 (1987).

82 Shim, H. *et al.* c-Myc transactivation of LDH-A: Implications for tumor metabolism and growth. *Proceedings of the National Academy of Sciences of the United States of America* **94**, 6658-6663, doi:10.1073/pnas.94.13.6658 (1997).

83 Dang, C. V. c-myc target genes involved in cell growth, apoptosis, and metabolism. *Molecular and Cellular Biology* **19**, 1-11 (1999).

84 David, C. J., Chen, M., Assanah, M., Canoll, P. & Manley, J. L. HnRNP proteins controlled by c-Myc deregulate pyruvate kinase mRNA splicing in cancer. *Nature* **463**, 364-U114, doi:10.1038/nature08697 (2010).

85 Robey, R. B. & Hay, N. Is Akt the "Warburg kinase"?-Akt-energy metabolism interactions and oncogenesis. *Seminars in Cancer Biology* **19**, 25-31, doi:10.1016/j.semcancer.2008.11.010 (2009).

86 Zundel, W. *et al.* Loss of PTEN facilitates HIF-1-mediated gene expression. *Genes & Development* **14**, 391-396 (2000).

87 Bensaad, K. *et al.* TIGAR, a p53-inducible regulator of glycolysis and apoptosis. *Cell* **126**, 107-120, doi:10.1016/j.cell.2006.05.036 (2006).

88 Pollard, P. J. *et al.* Accumulation of Krebs cycle intermediates and over-expression of HIF1 alpha in tumours which result from germline FH and SDH mutations. *Human Molecular Genetics* **14**, 2231-2239, doi:10.1093/hmg/ddi227 (2005).

89 Porcelli, A. M. *et al.* The genetic and metabolic signature of oncocytic transformation implicates HIF1 alpha destabilization. *Human Molecular Genetics* **19**, 1019-1032, doi:10.1093/hmg/ddp566 (2010).

90 Reitman, Z. J., Parsons, D. W. & Yan, H. IDH1 and IDH2: not your typical oncogenes. *Cancer Cell* **17**, 215-216, doi:10.1016/j.ccr.2010.02.024 (2010).

91 Gross, S. *et al.* Cancer-associated metabolite 2-hydroxyglutarate accumulates in acute myelogenous leukemia with isocitrate dehydrogenase 1 and 2 mutations. *Journal of Experimental Medicine* **207**, 339-344, doi:10.1084/jem.20092506 (2010).

92 Altekruse, S. F., McGlynn, K. A. & Reichman, M. E. Hepatocellular Carcinoma Incidence, Mortality, and Survival Trends in the United States From 1975 to 2005. *Journal of Clinical Oncology* **27**, 1485-1491, doi:10.1200/jco.2008.20.7753 (2009).

93 Degenhardt, T. *et al.* Three members of the human pyruvate dehydrogenase kinase gene family are direct targets of the peroxisome proliferator-activated receptor beta/delta. *Journal of Molecular Biology* **372**, 341-355, doi:10.1016/j.jmb.2007.06.091 (2007).

94 Edinger, A. L. & Thompson, C. B. Death by design: apoptosis, necrosis and autophagy. *Current Opinion in Cell Biology* **16**, 663-669, doi:10.1016/j.ceb.2004.09.011 (2004).

95 Alves, N. L. *et al.* The Noxa/Mcl-1 axis regulates susceptibility to apoptosis under glucose limitation in dividing T cells. *Immunity* **24**, 703-716, doi:10.1016/j.immuni.2006.03.018 (2006).

96 Chi, M. M. Y., Pingsterhaus, J., Carayannopoulos, M. & Moley, K. H. Decreased glucose transporter expression triggers BAX-dependent apoptosis in the murine blastocyst. *Journal of Biological Chemistry* **275**, 40252-40257, doi:10.1074/jbc.M005508200 (2000).

97 Vander Heiden, M. G. *et al.* Growth factors can influence cell growth and survival through effects on glucose metabolism. *Molecular and Cellular Biology* **21**, 5899-5912, doi:10.1128/mcb.21.17.5899-5912.2001 (2001).

98 Zhao, Y., Wieman, H. L., Jacobs, S. R. & Rathmell, J. C. Mechanisms and methods in glucose metabolism and cell death. *Programmed Cell Death, General Principles for Studying Cell Death, Pt A* **442**, 439-457, doi:10.1016/s0076-0879(08)01422-5 (2008).

99 Patel, M. S. & Korotchkina, L. G. Regulation of the pyruvate dehydrogenase complex. *Biochemical Society Transactions* **34**, 217-222 (2006).

100 Wende, A. R., Huss, J. M., Schaeffer, P. J., Giguere, V. & Kelly, D. P. PGC-1 alpha coactivates PDK4 gene expression via the orphan nuclear receptor ERR alpha: a mechanism for transcriptional control of muscle glucose metabolism. *Molecular and Cellular Biology* **25**, 10684-10694, doi:10.1128/mcb.25.24.10684-10694.2005 (2005).

101 Araki, M. & Motojima, K. Identification of ERR alpha as a specific partner of PGC-1 alpha for the activation of PDK4 gene expression in muscle. *Febs Journal* **273**, 1669-1680, doi:10.1111/j.1742-4658.2006.05183.x (2006).

102 Dufour, C. R. *et al.* Genome-wide orchestration of cardiac functions by the orphan nuclear receptors ERR alpha and gamma. *Cell Metabolism* **5**, 345-356, doi:10.1016/j.cmet.2007.03.007 (2007).

103 Giguere, V. Transcriptional Control of Energy Homeostasis by the Estrogen-Related Receptors. *Endocrine Reviews* **29**, 677-696, doi:10.1210/er.2008-0017 (2008).

104 Eichner, L. J. & Giguere, V. Estrogen related receptors (ERRs): A new dawn in transcriptional control of mitochondrial gene networks. *Mitochondrion* **11**, 544-552, doi:10.1016/j.mito.2011.03.121 (2011).

105 Carroll, V. A. & Ashcroft, M. Targeting the molecular basis for tumour hypoxia. *Expert Reviews in Molecular Medicine* **7**, 1-16, doi:10.1017/s1462399405009117 (2005).

106 Sullivan, R. & Graham, C. H. Hypoxia-driven selection of the metastatic phenotype. *Cancer and Metastasis Reviews* **26**, 319-331, doi:10.1007/s10555-007-9062-2 (2007).

107 Santner, S. J. *et al.* Malignant MCF10CA1 cell lines derived from premalignant human breast epithelial MCF10AT cells. *Breast Cancer Research and Treatment* **65**, 101-110, doi:10.1023/a:1006461422273 (2001).

108 Gatenby, R. A. & Gillies, R. J. Why do cancers have high aerobic glycolysis? *Nature Reviews Cancer* **4**, 891-899, doi:10.1038/nrc1478 (2004).

109 Addabbo, F., Montagnani, M. & Goligorsky, M. S. Mitochondria and Reactive Oxygen Species. *Hypertension* **53**, 885-892, doi:10.1161/hypertensionaha.109.130054 (2009).

110 Chen, Y., Azad, M. B. & Gibson, S. B. Superoxide is the major reactive oxygen species regulating autophagy. *Cell Death and Differentiation* **16**, 1040-1052, doi:10.1038/cdd.2009.49 (2009).

111 Kahl, R., Kampkotter, A., Watjen, W. & Chovolou, Y. Antioxidant enzymes and apoptosis. *Drug Metabolism Reviews* **36**, 747-762, doi:10.1081/dmr-200033488 (2004).

112 Kinnula, V. L. & Crapo, J. D. Superoxide dismutases in the lung and human lung diseases. *American Journal of Respiratory and Critical Care Medicine* **167**, 1600-1619, doi:10.1164/rccm.200212-1479SO (2003).

113 Mates, J. M. Effects of antioxidant enzymes in the molecular control of reactive oxygen species toxicology. *Toxicology* **153**, 83-104 (2000).

114 Mohr, A., Bueneker, C., Gough, R. P. & Zwacka, R. M. MnSOD protects colorectal cancer cells from TRAIL-induced apoptosis by inhibition of Smac/DIABLO release. *Oncogene* **27**, 763-774, doi:10.1038/sj.onc.1210673 (2008).

115 Kiningham, K. K., Oberley, T. D., Lin, S. M., Mattingly, C. A. & St Clair, D. K. Overexpression of manganese superoxide dismutase protects against mitochondrial-initiated poly(ADP-ribose) polymerase-mediated cell death. *Faseb Journal* **13**, 1601-1610 (1999).

116 Li, Y. B. *et al.* Dilated cardiomyopathy and neonatal lethality in mutant mice lacking manganese superoxide-dismutase. *Nature Genetics* **11**, 376-381, doi:10.1038/ng1295-376 (1995).

117 Lebovitz, R. M. *et al.* Neurodegeneration, myocardial injury, and perinatal death in mitochondrial superoxide dismutase-deficient mice. *Proceedings of the National Academy of Sciences of the United States of America* **93**, 9782-9787, doi:10.1073/pnas.93.18.9782 (1996).

118 Van Remmen, H. *et al.* Life-long reduction in MnSOD activity results in increased DNA damage and higher incidence of cancer but does not accelerate aging. *Physiological Genomics* **16**, 29-37, doi:10.1152/physiolgenomics.00122.2003 (2003).

119 Church, S. L. *et al.* Increased manganese superoxide-dismutase expression suppresses the malignant phenotype of human-melanoma cells. *Proceedings of the National Academy of Sciences of the United States of America* **90**, 3113-3117, doi:10.1073/pnas.90.7.3113 (1993).

120 Cullen, J. J. *et al.* Dicumarol inhibition of NADPH: Quinone oxidoreductase induces growth inhibition of pancreatic cancer via a superoxide-mediated mechanism. *Cancer Research* **63**, 5513-5520 (2003).

121 Malafa, M., Margenthaler, J., Webb, B., Neitzel, L. & Christophersen, M. MnSOD expression is increased in metastatic gastric cancer. *Journal of Surgical Research* **88**, 130-134, doi:10.1006/jsre.1999.5773 (2000).

122 Janssen, A. M. L. *et al.* Superoxide dismutases in gastric and esophageal cancer and the prognostic impact in gastric cancer. *Clinical Cancer Research* **6**, 3183-3192 (2000).

123 Kattan, Z., Minig, V., Leroy, P., Dauca, M. & Becuwe, P. Role of manganese superoxide dismutase on growth and invasive properties of human estrogen-independent breast cancer cells. *Breast Cancer Research and Treatment* **108**, 203-215, doi:10.1007/s10549-007-9597-5 (2008).

124 Weinberg, F. & Chandel, N. S. Reactive oxygen species-dependent signaling regulates cancer. *Cellular and Molecular Life Sciences* **66**, 3663-3673, doi:10.1007/s00018-009-0099-y (2009).

125 Saitoh, M. *et al.* Mammalian thioredoxin is a direct inhibitor of apoptosis signal-regulating kinase (ASK) 1. *Embo Journal* **17**, 2596-2606, doi:10.1093/emboj/17.9.2596 (1998).

126 Knebel, A., Rahmsdorf, H. J., Ullrich, A. & Herrlich, P. Dephosphorylation of receptor tyrosine kinases as target of regulation by radiation, oxidants or alkylating agents. *Embo Journal* **15**, 5314-5325 (1996).

127 Sachsenmaier, C. *et al.* Involvement of growth-factor receptors in the mammalian UVC response. *Cell* **78**, 963-972, doi:10.1016/0092-8674(94)90272-0 (1994).

128 Vercesi, A. E., Kowaltowski, A. J., Grijalba, M. T., Meinicke, A. R. & Castilho, R. F. The role of reactive oxygen species in mitochondrial permeability transition. *Bioscience Reports* **17**, 43-52, doi:10.1023/a:1027335217774 (1997).

129 Orrenius, S., Gogvadze, V. & Zhivotovsky, B. Mitochondrial oxidative stress: Implications for cell death. *Annual Review of Pharmacology and Toxicology* **47**, 143-183, doi:10.1146/annurev.pharmtox.47.120505.105122 (2007).

130 Vaughn, A. E. & Deshmukh, M. Glucose metabolism inhibits apoptosis in neurons and cancer cells by redox inactivation of cytochrome c. *Nature Cell Biology* **10**, 1477-U1228, doi:10.1038/ncb1807 (2008).

131 Grassian, A. R., Metallo, C. M., Coloff, J. L., Stephanopoulos, G. & Brugge, J. S. Erk regulation of pyruvate dehydrogenase flux through PDK4 modulates cell proliferation. *Genes & Development* **25**, 1716-1733, doi:10.1101/gad.16771811 (2011).

132 Michelakis, E. D. *et al.* Metabolic Modulation of Glioblastoma with Dichloroacetate. *Science Translational Medicine* **2**, doi:31ra3410.1126/scitranslmed.3000677 (2010).

133 Whitehou.S, Cooper, R. H. & Randle, P. J. Mechanism of activation of pyruvate-dehydrogenase by dichloroacetate and other halogenated carboxylic -acids. *Biochemical Journal* **141**, 761-774 (1974).

134 Morgan, M. J. & Liu, Z.-g. Crosstalk of reactive oxygen species and NF-kappa B signaling. *Cell Research* **21**, 103-115, doi:10.1038/cr.2010.178 (2011).

135 Yan, S. R. *et al.* Activation of NF-kappa B following detachment delays apoptosis in intestinal epithelial cells. *Oncogene* **24**, 6482-6491, doi:10.1038/sj.onc.1208810 (2005).

136 Lin, D.-C. *et al.* PLK1 Is Transcriptionally Activated by NF-kappa B during Cell Detachment and Enhances Anoikis Resistance through Inhibiting beta-Catenin Degradation in Esophageal Squamous Cell Carcinoma. *Clinical Cancer Research* **17**, 4285-4295, doi:10.1158/1078-0432.ccr-10-3236 (2011).

BIOGRAPHICAL SKETCH

Sushama Kamarajugadda was born and brought up in India. She graduated from Holy Mary Girls High School. Her undergraduate degree was in agricultural sciences at Acharya N.G. Ranga Agricultural University. After completion of her bachelor's degree, Sushama Kamarajugadda moved to United States to pursue higher education. In the fall of 2004, she was admitted into master's program in the department of molecular biology & microbiology at University of Central Florida, Orlando. In the summer of 2004, she joined Dr. Henry Daniell's laboratory to conduct her thesis research on the development of malaria vaccine in transgenic plants using chloroplast transformation technique. During her master's program, she also taught microbiology and immunology laboratory courses for undergraduate students. She graduated from her master's degree in the summer, 2006. In the fall of 2006, Sushama Kamarajugadda was admitted into the interdisciplinary program (IDP) in biomedical sciences at the College of Medicine at the University of Florida. She joined Jianrong Lu's lab to conduct her doctoral research project. She worked on breast cancer and her main focus was to understand the role of glucose metabolism in promoting anoikis resistance and tumor metastasis.